TAMPEREEN TEKNILLINEN YLIOPISTO
TAMPERE UNIVERSITY OF TECHNOLOGY

Jenni Rekola

# Factors Affecting Efficiency of LVDC Distribution Network – Power Electronics Perspective

Julkaisu 1340 • Publication 1340

Tampere 2015

Tampereen teknillinen yliopisto. Julkaisu 1340
Tampere University of Technology. Publication 1340

Jenni Rekola

# Factors Affecting Efficiency of LVDC Distribution Network – Power Electronics Perspective

Thesis for the degree of Doctor of Science in Technology to be presented with due permission for public examination and criticism in Tietotalo Building, Auditorium TB103, at Tampere University of Technology, on the 20th of November 2015, at 12 noon.

Tampereen teknillinen yliopisto - Tampere University of Technology
Tampere 2015

ISBN 978-952-15-3606-9 (printed)
ISBN 978-952-15-3622-9 (PDF)
ISSN 1459-2045

# Abstract

The power distribution network will be changed towards the future Smart Grid due to increased number of installed renewable power generation units to fulfill the tightened environmental regulation. The control of the future Smart Grid will be challenging due to increased number of renewable power generation units, which are variable in nature, and at the same time, the customers are highly dependent on uninterruptable, high quality power supply. The Smart Grid control is intensively studied. It can be concluded that the control might be simpler and the grid operation more reliable if the AC grid would be replaced by DC grid. However, the detailed energy efficiency analysis of the DC grid is not thoroughly studied. The efficiency and total lifetime costs are the key parameters when the network owners consider the future grid structure.

This thesis addresses the factors, which affect the energy efficiency of the low voltage DC (LVDC) distribution network from power electronics perspective. The power loss models for the converters and their AC filters are developed and verified by measurements. The impact on the converter topology, used power semiconductor switches, AC filter design and inductor core material, DC network configuration, customer behavior, the need of DC voltage balancing in the bipolar DC network as well as the grounding issues to fulfill the electrical safety standards are treated. For facilitating the design of cost effective LVDC distribution networks, the total power losses of the network with different configurations are evaluated and compared.

It is revealed that the used filter inductor core material has a significant impact on the power losses of the LVDC distribution network. The inductor core material having low high-frequency power loss characteristics, such as amorphous alloy, is recommended. The LVDC distribution network should be grounded to minimize the power losses whenever it is possible according to the local safety standardization and grounding conditions. The three-level NPC converters connected to 1500 VDC should be used to minimize the power losses. The grid-frequency isolation transformer is the main power loss source if the galvanic isolation is needed to isolate the ungrounded LVDC distribution network and the grounded customer electrical installations. In this case, the highest energy efficiency is achieved by using two- or three-level converters connected to 750 VDC if the DC cable length is less than 600 m. Otherwise, slightly higher energy efficiency is achieved by using three-level converters connected to 1500 VDC. Therefore, voltage transformation ratio of the isolation transformer must be 800V/400V instead of 400V/400V. Moreover, the efficiency of the power converters is increased by using SiC MOSFETs instead of conventional IGBTs as power semiconductor switches.

# Preface

The research work was carried out at the Department of Electrical Engineering of Tampere University of Technology (TUT) during the years 2010-2015. The work was mainly funded by Smart Grids and Energy Markets (SGEM) research program, TUT and Fortum Foundation. The grants provided by Finnish Foundation for Technology Promotion, Jenny and Antti Wihuri Foundation and Ulla Tuominen Foundation are greatly appreciated.

First of all, I'm grateful to Professor Teuvo Suntio for his invaluable help and constructive comments regarding to the last publications and the manuscript. It has been a great pleasure to work under his guidance. I express my sincere gratitude to the preliminary examiners, Professor Adrian Ioinovici of Holon Institute of Technology and Sun-Yat Sen University and Professor Pertti Silventoinen of Lappeenranta University of Technology, for their comments on how to improve the manuscript. I'm thankful to emeritus Professor Heikki Tuusa for giving me the opportunity to take part in great research group in the Department of Electrical Engineering.

I would like to thank my colleagues MSc Anssi Mäkinen, MSc Antti Virtanen, MSc Juha Jokipii, MSc Jukka Viinamäki, Dr. Tuomas Messo, MSc Jarno Alahuhtala and MSc Olli Pokkinen for their advice regarding simulation models, laboratory measurements and well written publications. In addition, I wish to thank my colleagues working with the same project in Lappeenranta University of Technology, especially MSc Tero Kaipia and Dr. Pasi Nuutinen. I want to express my gratitude to Terhi Salminen, Mirva Seppänen and Nitta Laitinen for providing valuable assistance regarding practical everyday matters. Pentti Kivinen and Pekka Nousiainen deserve special thanks for their craftsmanship in building experimental devices.

Tampere 21.9.2015

Jenni Rekola

# Contents

APPENDIX C: Simulated and measured voltage and current harmonics

APPENDIX D: Base values

APPENDIX E: Required AC filter parameters depending on the design method

# Nomenclature

Abbreviations

| | |
|---|---|
| AC | alternating current |
| ANPC | active neutral point clamped |
| DC | direct current |
| EV | electric vehicle |
| HVDC | high voltage direct current |
| IEC | International Electrotechnical Commission |
| IEEE | Institute of Electrical and Electronics Engineers |
| IGBT | insulated gate bipolar transistor |
| LCC | line commutated converter |
| LVAC | low voltage alternating current |
| LVDC | low voltage direct current |
| MMC | modular multilevel converter |
| MLT | mean length per turn |
| MOSFET | metal-oxide-semiconductor field-effect transistor |
| MPPT | maximum power point tracking |
| MV | medium voltage |
| NPC | neutral-point clamped |
| PCC | point of common coupling |
| PF | power factor |
| PFC | power factor correction |
| PI | proportional-integral (controller) |
| PLL | phase locked loop |
| PV | photovoltaic |
| PWM | pulse width modulation |
| SHE | single harmonic elimination (modulation method) |
| SiC | silicon carbide |
| SVM | space vector modulation |
| THD | total harmonic distortion |
| UPS | uninterruptable power supply |
| VSC | voltage source converter |
| VSI | voltage source inverter |

Greek characters

| | |
|---|---|
| $\alpha$ | coefficient, Steinmetz parameters and temperature coefficient |
| $\beta$ | coefficient, Steinmetz parameters |
| $\delta$ | skin depth |
| $\eta$ | energy efficiency, porosity factor |
| $\mu$ | permeability |
| $\mu_r$ | relative permeability |
| $\mu_0$ | vacuum permeability |
| $\rho$ | resistivity |

| | |
|---|---|
| $\sigma$ | electrical conductivity |
| $\varphi$ | phase angle |
| $\varphi_s$ | angle of the positive sequence grid voltage |
| $\omega$ | angular frequency |

Latin characters

| | |
|---|---|
| $A_c$ | core effective cross-sectional area |
| $B$ | magnetic flux density |
| $B_{sat}$ | saturation magnetic flux density |
| $C$, C | capacitance, capacitor |
| $C_1$, $C_2$ | upper and lower DC bus capacitors |
| $C_{cust}$ | capacitor of customer converter AC-filter |
| $C_{grid}$ | capacitor of grid converter AC-filter |
| D | diode |
| $d$ | duty cycle, round wire diameter |
| E | electrical energy |
| $E_{on}$ | sum of energy dissipation during turn-on time |
| $E_{off}$ | sum of energy dissipation during turn-off time |
| $E_{rr}$ | reverse recovery energy of diode |
| $f$ | frequency |
| $f_{sw}$ | switching frequency |
| $F_R$ | relationship $R_{DC}/R_{AC}$ |
| $h_{wire}$ | height of the square wire compared to round wire |
| I, i | current, instantaneous current |
| $\hat{\imath}$ | peak value of current |
| $I_c$ | nominal collector current |
| $I_{ref}$ | reference current value of the switching loss measurement |
| $L$, L | inductance, inductor |
| $l_{ag}$ | air gap length in the inductor |
| $l_w$ | width of the copper wire layer |
| $L_{bal}$ | balancing inductor |
| $L_{conv}$ | converter side inductor of grid converter |
| $L_{cust}$ | inductor of customer converter AC-filter |
| $L_{grid}$ | AC-grid side inductor of grid converter |
| $m$ | mass of the inductor core |
| $M$ | number of winding layers in the inductor |
| $m_a$ | modulation index |
| $N$ | number of copper wire turns in the inductor |
| P | active power |
| $P_{cond}$ | conduction power losses |
| $P_{sw}$ | switching power losses |
| R, $R$ | resistor, resistance |
| $R_{ce}$ | IGBT on-state resistance |
| $R_f$ | diode on-state resistance |
| $R_{damp}$ | damping resistor of grid converter AC-filter |
| S | power semiconductor switch, apparent power |
| t | time |
| T | cycle time, temperature |
| U, u | voltage, instantaneous voltage |

| | |
|---|---|
| $U_{ref}$ | reference voltage value of the switching loss measurement |
| $V_f$ | diode forward voltage |
| $V_t$ | IGBT collector-emitter threshold voltage |
| Z | impedance |

Superscripts

| | |
|---|---|
| ref | reference value |

Subscripts

| | |
|---|---|
| 1 | fundamental frequency component |
| b | base value |
| d | variable related to d-component |
| LL | line-to-line |
| n | nominal |
| max | maximum value |
| q | variable related to q-component |
| ref | reference value |
| err | error value |
| rms | root mean square |

# 1 Introduction

This chapter provides the background for the research topics of this thesis and discusses on the motivation of the research. A short introduction to the need to renew the present electricity distribution network towards the future Smart Grid is presented. Especially, the possibility of using DC grid instead of conventional AC grid is discussed and short literature review on the DC grid research topics is presented. Finally, the main scientific contributions of the thesis are summarized and the author's contribution to the published scientific papers, related to this thesis, is specified.

## 1.1 Need to renew electricity distribution network towards the future Smart Grid

The traditional electric power generation is based on large centralized units, where electricity generation is based on fossil fuels, nuclear or hydro power. Nowadays approximately 87 % of the total energy in the world is produced by fossil fuels and only 13 % by renewable energy sources (Bose 2013). Unfortunately, the global fossil fuel reserves are limited and their use is one of the main reasons for global warming and climate change (Bose, 2013).

New power generation forms to replace the use of fossil fuels are extensively researched during the past decades and international protocols, such as UN Kyoto Protocol and Europe 20-20-20, are implemented to increase the use of renewable energy. The renewables are largest new installed power generation source in the world (Karabiber et al, 2013; IEA, 2015). The installed capacity of the renewable energy accounts 80 % of new established generation capacity in OECD countries (IEA, 2015). International Energy Agency IEA estimates that the coal will be replaced by renewables as a largest electric energy production method after 20 years (IEA, 2015).

The renewable power generators are small and distributed within the electricity distribution network and the power generation varies on a large scale depending on the weather conditions. The network inertia will be inherently limited when conventional generation based on synchronously rotating electrical machines will be replaced by inertia-less power electronics interfaced sources. Lack of inertia might lead to frequency stability problems in the electricity distribution network (Justo et al., 2013; Guarnieri, 2013; Patterson, 2012). The challenges related to the reliability, sustainability and overall energy efficiency of the electricity distribution network including renewable power generation, energy storage and controllable loads need to be managed in a future Smart Grid. The proper control methods need to be developed by using information and communication technology. The target is to provide uninterrupted and high quality electric power supply to the end customers.

## 1.2 LVDC distribution network structure

AC power network has been a standard choice since the late 19$^{th}$ century. The first reason to the AC distribution is the use of centralized, synchronously rotating electrical machines to power generation and secondly, the transformer has been a cost-efficient and reliable appliance to transform AC voltage into different voltage levels (Justo et al., 2013; Guarnieri, 2013; Patterson, 2012; Dragicevic et al. 2014). Electric power has been transferred long distances at high voltage level to minimize the power losses and the voltage is decreased to the appropriate voltage level near the electric energy consumption (Justo et al. 2013, Guarnieri 2013, Patterson, 2012).

DC distribution has been used in many applications during these years in spite of the AC distribution dominance. High voltage DC (HVDC) power transmission systems are used for the long-distance electrical power transmission and to connecting unsynchronized AC distribution systems together (Justo et al., 2013; Guarnieri, 2013). HVDC is used, especially, in long undersea cables, where AC is not possible to be used due to cable length-dependent reactive power (Guarnieri, 2013). The capabilities of DC distribution are analyzed also at the medium voltage (MV) level, especially, in large photovoltaic (PV) installation and off-shore windfarms to decrease transmission losses and the complexity of the control systems. Lack of synchronization and reactive power control are the main benefits of the DC distribution (Wang et al., 2014; Wang et al., 2011; Enslin and Heskes, 2004; Kakigano et al., 2010a; Roggia et al., 2011; Gu et al., 2014; Byeon et al., 2013).

The DC distribution is used also for example in vehicles and shipboard systems, aircraft, traction systems and automotive industry (Bose et al., 2012; Justo, 2013; Guarnieri, 2013). The use of DC increases the reliability, survivability and power quality of the shipboard power system (Bose et

al., 2012). An increasing number of AC drives in industrial applications are connected to a common DC bus leading to cost reduction, reduced space requirements, and improved reliability. 48 VDC is used conventionally in the telecommunication systems and data centers (Justo, 2013; Guarnieri, 2013). The efficiency of a DC powered data center is higher compared to AC powered data center due to reduction of required conversion stages, as depicted in Fig. 1.1 (AlLee and Tschudi, 2012; Schneider, 2008). The overall efficiency can be increased by 28 % compared to typical AC equipment found in data centers (Schneider, 2008).

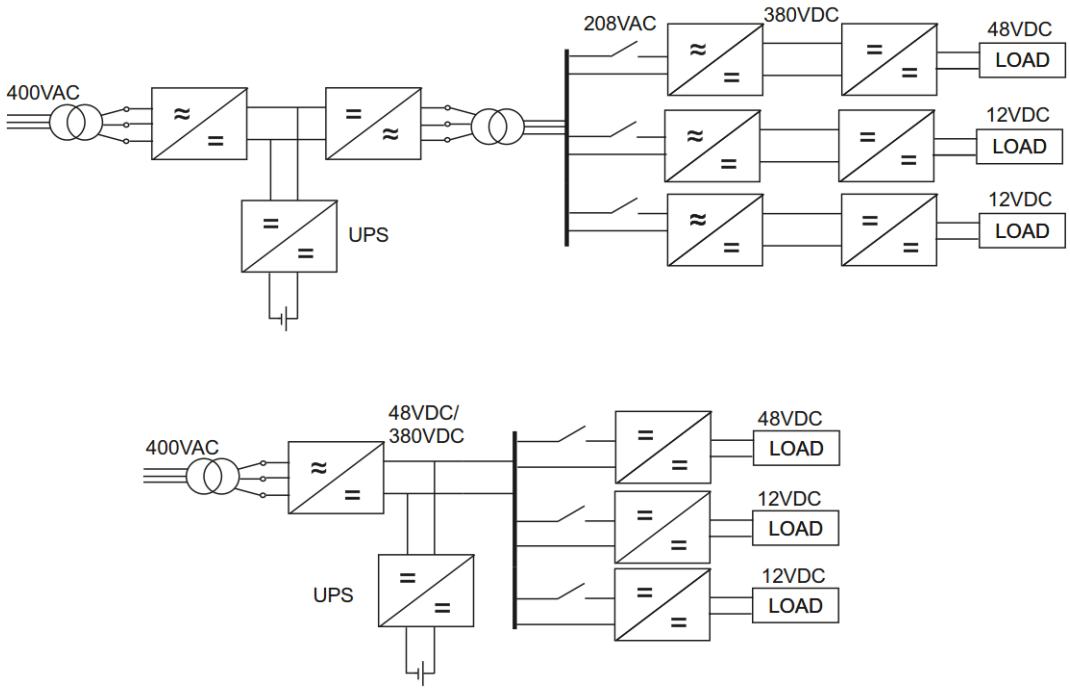


**Fig. 1.1.** a) AC data center and b) DC data center

The possibility to replace part of the present low voltage AC network (LVAC) by using DC distribution is analyzed in this study. The point-to-point type LVDC distribution network, shown in Fig. 1.2, would be the simplest LVDC distribution network configuration. Target is to increase the power quality and network reliability without any changes to the customer power supply.

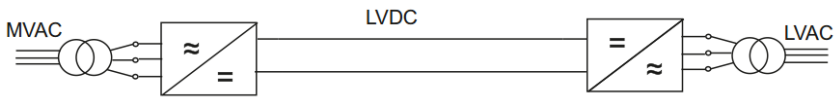


**Fig. 1.2.** Point-to-point LVDC distribution network

The power quality would be possible to be controlled more effectively by power electronic converters compared to voltage step-up transformer (Hakala et al., 2015a). The DC network forms its

own protection area hence it might simplify the network protection and increase reliability (Hakala et al., 2015a).

Approximately 70 % of all generated power passes through a power electronic converter today in US (Reed, 2012; Bose, 2013). It is predicted that nearly 80 % of all power generated would pass through a power electronic converter within the next 15 years and most of this occur at low voltage level (Reed, 2012; Bose, 2013). Multiple AC/DC/AC conversion stages are needed in the future Smart Grid including renewable power generation and energy storages as shown in Fig. 1.3. The amount of DC power generation due to PV power and battery-based DC energy storages will be increased in the future distribution network. Moreover, many of the customer electric appliances, e.g. home electronics and lightning, operate by DC as well (Kakigano et al., 2009; Techakittiroj and Wongpaibool, 2009; Gu et al., 2014, Byeon et al., 2013). The fast charging of electric vehicles is also realized by using DC (Rivera et al. 2015, Byeon et al., 2013).

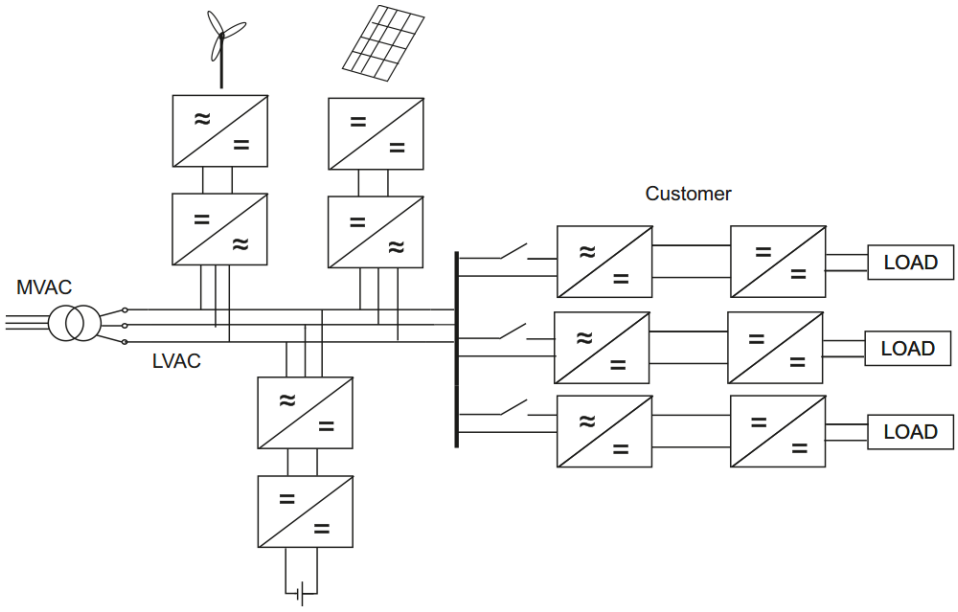


**Fig. 1.3.** AC microgrid

The multi-terminal DC microgrid, shown in Fig. 1.4, would be an interesting option to realize the future Smart Grid. The amount of AC/DC/AC conversion stages will be reduced compared to LVAC grid, shown in Fig. 1.3. (Kim et al., 2013; Kakigano et al, 2010a; Justo, 2013; Guarnieri, 2013; Brenna et al., 2009; Techakittiroj and Wongpaibool, 2009; Gu et al., 2014; Roggia et al., 2011, Byeon et al., 2013; Dragicevic et al. 2014). The DC voltage level transformation has become easier and more cost-efficient during the last years due to development of power semiconductor switches and inductor core materials used in the power electronic converters (Justo, 2013;

Guarnieri, 2013; Brenna et al., 2009). Measuring instruments, protection devices as well as communication devices needed in the future Smart Grid control can be integrated into the power converters as well (Justo, 2013; Mohsenian-Rad and Davoudi, 2014).

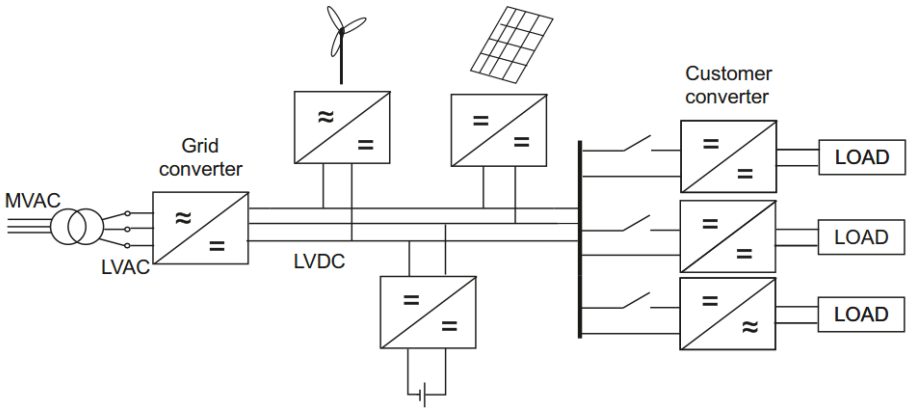


**Fig. 1.4.** DC microgrid

The reliability and power quality of electricity supply experienced by the customer would be increased if every customer or customer group have their own converters, which controls the voltage amplitude and power quality (Brenna et al., 2009; Lago and Heldwein, 2011; Kakigano et al., 2010a). The DC network might operate in island mode during the fault in the AC grid if energy generation or energy storage is connected to the DC network (Kakigano et al., 2010a; Gu et al., 2014).

The DC distribution network might be a cost-efficient and sustainable network configuration to be installed to the rural areas having no access to the present public distribution network. PV generation is already widely installed in the rural areas of South Asia and Africa, and therefore, the DC grid can be implemented based on locally generated electricity (Madduri et al, 2013; Bose, 2013; Sarker et al. 2012). The applicability of a DC grid is also studied for a remote area mine site, where the regenerative brake energy from hoists, draglines and shovels could be reused (Yuan et al., 2014).

### 1.2.1 Control methods of LVDC distribution network

The stable operation of the future Smart Grid is more challenging compared to present network due to the presence of distributed energy generation, energy storage and loads with their power electronic interfaces. A large number of grid connected inverters may cause harmonic instability in an AC power-electronics-based power system, because the harmonic interactions exist between the energy sources, passive filter circuits and cable impedances (Wang et al., 2014; Enslin and Heskes, 2004; Wang et al., 2011; Lago and Heldwein, 201). The converter-based constant power loads have also an impact on the stability, transient behavior and power quality of the network

(Karabiber et al., 2013; Justo, 2013; Chen et al., 2013; Lago et al., 2011; Guerrero et al., 2011; Guerrero et al., 2013; Xu and Chen 2011; Radwan et al., 2012; Brenna et al., 2009; Kakigano et al., 2010; Ahmadi et al., 2014).

One of the main interests of the DC grid research is to analyze the DC grid control. The proposed control methods are designed for the multi-terminal DC grid, consisting of a grid converter, power generation, energy storage and loads as shown in Fig. 1.4 (Karabiber et al., 2013; Justo, 2013; Chen et al., 2013; Lago et al., 2011; Guerrero et al., 2011; Guerrero et al., 2013; Xu and Chen 2011; Radwan et al., 2012; Brenna et al., 2009; Kakigano et al., 2010; Ahmadi et al., 2014, Byeon et al., 2013). The converters connected to the DC grid have two control strategies: regulate the power flow of the local terminal (non-controllable loads or the converters, which operate according to maximum power point tracking (MPPT) algorithm) or to maintain the voltage stability of the DC grid (Gu et al., 2014). The focus of the research is to find the control methods to keep the DC voltage balance of the distribution network and to use the renewable energy generators as efficiently as possible.

The DC grid control seems to be simpler compared to AC grid control due to lack of synchronization requirements, frequency stabilization, and reactive power compensation (Kakigano et al., 2010a; Roggia et al., 2011; Gu et al., 2014; Lago and Heldwein, 2011; Byeon et al., 2013; Dragicevic et al. 2014). The only controlled parameter is the DC voltage amplitude compared to AC grid, where both voltage amplitude and frequency need to be controlled (Kakigano et al., 2010a; Roggia et al., 2011; Gu et al., 2014). The DC network forms its own protection area hence it would be easier to use as an island mode during the fault in the AC network compared to the single AC network branches operating in an island mode.

## 1.3 Motivation of the thesis

The distribution network will be changed towards the future Smart Grid due to tightened environmental regulation. The electric power will be generated locally, changing dramatically the network control principles. At the same time, the customers are dependent on uninterruptable, high quality power supply. The control methods of the future Smart Grid are widely studied and it is proposed that the control might be simpler if the AC would be replaced by DC (Kakigano et al., 2010a; Roggia et al., 2011; Gu et al., 2014; Lago and Heldwein, 2011). However, the detailed energy efficiency analysis of the DC network is not thoroughly studied. The energy efficiency and total lifetime costs are the key parameters when the network owners consider the future grid structure.

The LVDC distribution network energy efficiency is investigated only at general level so far, excluding verified converter and AC filter power loss analyses (Wang et al., 2008; Justo, 2013; Lago et al., 2011; Roggia et al., 2011, Hakala et al., 2015; Hakala et al., 2013; Shenai et al., 2011; Kakigano et al. 2012; Brenna et al., 2009; Roggia et al., 2011; Gu et al., 2014; Anand et al., 2010). The efficiency of the whole DC network is shown to be proportional to the efficiency of the power converters (Kakigano et al., 2012; Lana et al., 2014; Shenai et al., 2011). The energy efficiency of the power converters should be almost as high as the transformers, > 95 %, also at partial load conditions, to increase the energy efficiency of the DC network compared to present AC network (Engelen et al., 2006, Kakigano 2012). However, only the energy efficiency of the converters at nominal power, specified by the manufacturer, is used so far in the power loss calculations of the DC grid. The customer variable load is not taken into account. Moreover, grounding and protection methods of the DC network are not defined.

The transmission losses of the DC cable are lower compared to AC cable due to lack of reactive power and skin effect (Guarnieri, 2013). According to Wang et al. (2008), the transmission losses in the DC cable are 15-50 % lower compared to AC transmission losses at the same voltage level and cable size. Low Voltage Directive 2006/95 enables the use of 1000 VAC and 1500 VDC at maximum in low power transmission. Lower resistive power losses would be achieved due to the use of higher voltage level (Justo, 2013; Lago et al., 2011; Roggia et al., 2011, Anand et al., 2010). Therefore, during the last years, 48 VDC is replaced by 380 VDC in data center to increase the energy efficiency (AlLee and Tschudi, 2012). The network capacity can be increased by replacing LVAC with LVDC network without the need to renew the cables by using the increased voltage level (Hakala et al., 2013; Lago et al., 2011).

The proposed energy efficiency analysis done so far, are concentrated to the use of DC grids in office and residential buildings, where the transmission distance is short and the used DC voltage level is low, 400 VDC at maximum. The overall energy efficiency and power quality of the residential house can be increased by using multi-terminal DC microgrid shown in Fig. 1.4 (Justo, 2013; Kakigano et al. 2010a; Brenna et al., 2009; Roggia et al., 2011; Gu et al., 2014). The number of AC/DC conversion stages will be reduced. However, multiple DC/DC converters are still needed because of various required voltage levels of customer electrical appliances but the energy efficiency of DC/DC converters is higher compared to AC/DC/AC converters (Justo, 2013; Kakigano et al. 2010a; Brenna et al., 2009; Roggia et al., 2011; Gu et al., 2014).

This thesis addresses the factors, which affect the energy efficiency of a 1500 VDC distribution network from power electronics perspective. The analytical calculation and simulation models for the converter power losses and their AC filters are developed and verified by measurements. For facilitating the design of cost effective LVDC distribution networks, the total losses of the network with different configurations are evaluated and the main power loss sources of the LVDC

distribution network are revealed. The use of single-phase loads and the possibility to connect loads asymmetrically to the bipolar DC network are considered. Moreover, the customer loading behavior as well as the grounding issues to fulfil the safety standardization is considered. It would be possible to find the most efficient converter topologies, AC filter design method, inductor core material, and network configuration by using the provided power loss models.

## 1.4 Scientific contribution

The main scientific contributions of this thesis can be summarized as follows:

- The power loss simulation and calculation models for power electronics in an LVDC distribution are developed and verified by measurements. The previous energy efficiency analyses are mainly concentrated to the power losses in the DC cable.
- It is shown that the used filter inductor core material has a significant impact on the overall power losses of the LVDC distribution network. The power losses caused by high frequency current in the inductor core should be minimized by using appropriate core material.
- It is revealed that the LVDC distribution network should be grounded to minimize the overall power losses whenever it is possible according to local safety standardization and grounding conditions. Moreover, the three-level NPC converters with SiC MOSFETs and amorphous core AC filter inductors should be used and connect them to 1500 VDC in the grounded LVDC distribution network to minimize the power losses.
- It can be concluded that the isolation transformer operating at 50 Hz frequency is the main power loss source if the galvanic isolation is needed to isolate the ungrounded LVDC distribution network and the grounded customer electrical installations. The highest energy efficiency is achieved by using two- or three-level converters with SiC MOSFETs and amorphous core AC filter inductors and by connecting the converters to 750 VDC if the length of the DC cable is less than 600 m. Otherwise, slightly higher energy efficiency is achieved by using three-level NPC converters with SiC MOSFETs and amorphous core AC filter inductors and by connecting the converters to 1500 VDC. Therefore, the voltage transformation ratio of the isolation transformer must be 800V/400V instead of 400V/400V.

## 1.5 Published papers

The following publications emanated during the course of this research.

[P1] Rekola J., Jokipii J. and Suntio T. (2014). ”Losses of converters with iron and amorphous core AC-filter inductors in LVDC distribution” in 40th Annual Conference of IEEE Industrial Electronics Society, IECON, pp.1587-1593.

[P2] Rekola J., Jokipii J. and Suntio T. (2014). ”Effect of network configuration and load profile on efficiency of LVDC distribution network”, in 16th European Conference on Power Electronics and Applications, EPE’14-ECCE Europe, pp.1-10.

[P3] Rekola J. and Tuusa H. (2014). “Efficiency of converters and amorphous core AC-filters in an LVDC distribution”, in 29th Annual IEEE Applied Power Electronics Conference and Exposition, APEC, pp. 1827-1834.

[P4] Rekola J., Virtanen A., Jokipii J. and Tuusa H. (2012). ”Comparison of converter losses in an LVDC Distribution”, in 38th Annual Conference of IEEE Industrial Electronics Society, IECON, pp. 1240-1245.

[P5] Rekola J. and Tuusa H. (2011). “Comparison of line and load converter topologies in a bipolar LVDC distribution”, in 14th European Conference on Power Electronics and Applications, EPE, pp. 1-10.

[P6] Rekola J. and Tuusa H. (2011). “Comparison of load inverter topologies in a bipolar LVDC-distribution”, in International Conference on Renewable Energies and Power Quality, ICREPQ’11, pp.1-6.

All of the papers were written and presented by the first author. All the simulations and experiments were carried out by the first author except the impedance measurements by Venable frequency analyzer to analyze the inductance and resistance of the inductors, which were conducted by MSc Juha Jokipii and MSc Jukka Viinamäki. The power loss simulation models of the converters were created in co-operation with MSc Juha Jokipii and the power loss calculation models for the iron core inductors were created in co-operation with MSc Antti Virtanen. The laboratory prototype converters were built by MSc Olli Pokkinen and MSc Jarno Alahuhtala. Professors Teuvo Suntio and Heikki Tuusa, the supervisors of this thesis, gave valuable and inspiring comments regarding to these publications.

## 1.6 Outline of the thesis

The rest of the thesis is organized as follows. Chapter 2 presents the power converter topologies, their control and modulation methods used in this study. Moreover, the AC filter design methods and used AC filter inductor core materials are presented. Next, the LVDC distribution network configurations and network grounding methods are discussed. The need of DC network voltage balancing depending on the network configuration is discussed and the different balancing methods are proposed.

Chapter 3 presents the power loss analytical calculation and simulation models for the power converters and AC filters. Also the power loss simulation models of the balancing circuit, DC cable and isolation transformer are presented. The accuracy of the models is verified by measurements.

Chapter 4 focuses on the impact of power converter to the energy efficiency of the LVDC distribution network. The influence of converter topology, AC filter design method, inductor core material, used power switching devices, converter modulation frequency, power quality limitations and influence of customer load power factor are analyzed.

Chapter 5 focuses on the effect of DC network configuration to the energy efficiency. The influence of grounding methods, DC voltage level, DC cable length and balancing circuit to the overall power losses is studied. In addition, the effect of customer single-phase loads to the energy efficiency and impact on the used converter topology depending on the used power semiconductor switching devises are revealed. Finally, the influence of the customer loading behavior to the energy efficiency is treated by calculating the total power losses of the DC network during one year by using the loading behavior of a typical Finnish customer.

Chapter 6 concludes the thesis and proposes future research topics.

# 2 Analyzed converter topologies and LVDC distribution network configurations

## 2.1 Introduction

The power electronic converters are needed to implement the DC distribution network. The AC/DC grid converter connects AC and DC networks together and, depending on the customer needs, the DC/DC or DC/AC customer converters are needed to transform DC voltage to be appropriate for the customer needs. It is supposed that the customer present electrical installations are not changed in this study, hence three-phase 400 Vrms or single-phase 230 Vrms 50 Hz AC voltage must be delivered to the customer. Therefore, the discussions in this thesis are limited to AC/DC and DC/AC converters.

Section 2.2 gives an overview on the used grid converter topologies in the LVDC distribution network. Also, the control and modulation method of the four-wire, three-level neutral-point-clamped boost rectifier is shortly presented. Section 2.3 provides an overview on the used customer converter topologies. The fundamentals of AC filter sizing and used AC filter inductor core materials are introduced in Section 2.4. Section 2.5 provides an overview on LVDC distribution network configurations including the problems associated to grounding and DC voltage balancing. The required AC filter parameters depending on the used converter topology are compared in Section 2.6. Section 2.7 draws the conclusions.

## 2.2 Grid converters

The grid converter controls the power flow between AC and DC networks and regulates the DC voltage in the AC grid connected operating mode. It can also control the power factor of the point

of common coupling (PCC). The grid converter can be conventional line commutated converter (LCC) or voltage-source converter (VSC).

### 2.2.1 Line commutated converters

The line commutated converters are 6- and 12-pulse diode bridges, thyristor bridges or half-controlled thyristor bridges. Diode rectifier is the simplest and cheapest, robust and high efficient rectifier topology but the output DC voltage is uncontrolled and directly proportional to AC voltage amplitude. Only unidirectional power flow from the AC network to the DC network is possible. The diode rectifier produces high amount of odd low frequency harmonics to the AC network, as shown in Fig. 2.1b-c. The low frequency harmonics, especially $5^{th}$ and $7^{th}$ harmonics, cause additional power losses in the AC transformers and cables. The diode rectifier causes high inrush current which can broke DC capacitors, and therefore, additional inrush-current-limiting circuit is needed.

The thyristor rectifier is conventionally used in HVDC applications. It is almost as simple, reliable, energy efficient and cheap as the diode rectifier. The DC voltage can be fully controlled. The additional inrush-current-limiting circuit is not needed, because the high inrush currents can be limited by delay angle control of thyristors. However, the delay angle control causes additional harmonics to the AC currents decreasing the power factor of the system. Therefore, the thyristor rectifier is used as the diode rectifier in steady state. Reactive power compensation is needed especially at high power and weak networks (Flourenzou et al., 2009). Only unidirectional power flow is possible. The diode and thyristor rectifiers produce $6^{th}$ harmonic (300Hz) to the DC voltages. The power factor correction (PFC) circuit or large DC capacitors can be used to mitigate the DC voltage fluctuation.

The low frequency AC harmonics produced by 6-pulse rectifiers are possible to be decreased by using 12-pulse rectifier, which consists of two series connected 6-pulse rectifiers as illustrated in Fig. 2.1a. The low frequency harmonics, especially $5^{th}$ and $7^{th}$ harmonics are eliminated in the steady state, as shown in Fig. 2.1d-e, due to 30° phase-shift in the transformer (Rekola and Tuusa, 2011). The half-controlled thyristor rectifier is adequate to limit the inrush currents of the DC network (Rekola and Tuusa, 2011).

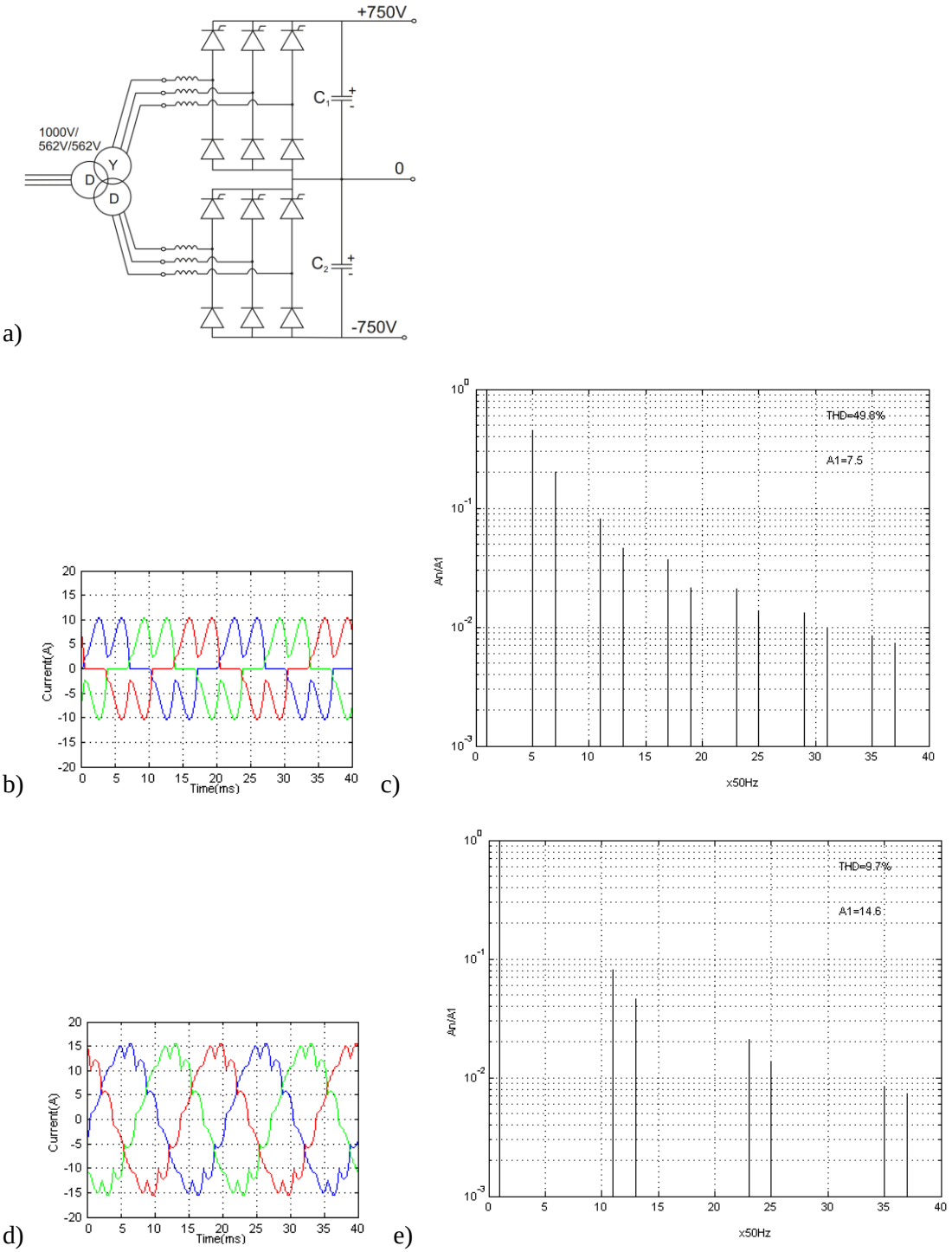


**Fig. 2.1.** a) 12-pulse half controlled thyristor bridge, b) AC current of 6-pulse thyristor bridge, c) AC current spectrum of 6-pulse thyristor bridge, d) AC current of 12-pulse thyristor bridge, e) AC current spectrum of 12-pulse thyristor bridge

12-pulse rectifiers are conventionally used in HVDC transmission due to decreased harmonics and lower required voltage capability of the thyristors. The maximum voltage rating of the thyristors or diodes is half of that required in the 6-pulse rectifier, i.e., $u_{dc}/2$.

### 2.2.2 Voltage source converters

Fully controlled power semiconductor switches are used in VSCs instead of diodes or thyristors. The DC voltage can be fully controlled by a VSC, and therefore, the voltage dips of the AC network do not affect the operation of the LVDC network. Large AC filters, which increase the costs and volume of the converter, are not needed with a VSC, because the AC current does not include low frequency harmonics (Xu et al., 2008; Friedrich, 2010; Flourenzou et al., 2009). The active as well as reactive power can be fully controlled by a VSC, and therefore, the power factor of PCC can be controlled (Mahmoodi et al., 2006; Xu et al., 2008; Friedrich, 2010; Flourenzou et al., 2009). VSC enables bidirectional power flow between AC and DC networks. Therefore, large amount of distributed power generation can be connected to the LVDC network and the surplus power can be supplied to the AC network.

The two-level VSC, shown in Fig. 2.2, is the most used VSC topology so far due to its relatively simple structure and control. The other option is to use multilevel converters. The most common multilevel topologies are the neutral-point-clamped converter (NPC), (i.e., diode-clamped), flying-capacitor converter, (i.e., capacitor clamped) and cascaded multicell H-bridge converter with separate DC sources (Franquelo et al., 2008; Rodriguez et al., 2010). Principle of operation and structure of NPC converter is presented at first time in 1981 by Nabae et al. The NPC topology, shown in Fig. 2.3, is the most commercialized multi-level topology in the market (Franquelo et al., 2008; Rodriguez et al., 2010). The flying-capacitor-multilevel converters are not widely used due to difficulties in the voltage balancing of the cascaded capacitors (Franquelo et al., 2008).

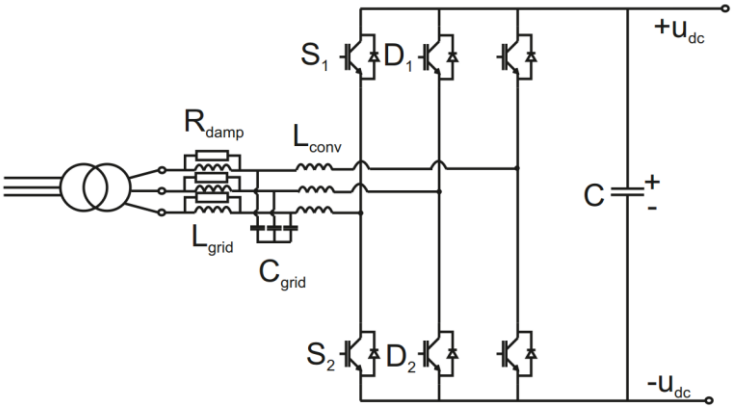


**Fig. 2.2.** Two- level VSC

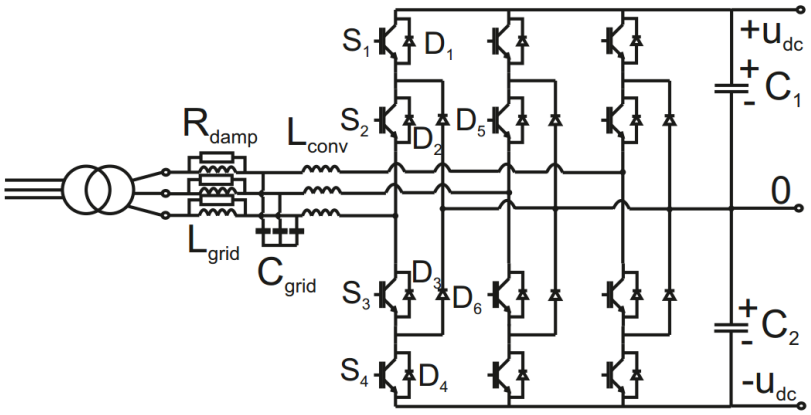


**Fig. 2.3.** Three-wire, three-level NPC

The cascaded multicell converter topologies are used in high power levels in STATCOM and HVDC applications, but these have complex structure and control (Franquelo et al., 2008). The NPC converter (cf. Fig. 2.3) can produce three output voltage levels: $+u_{dc}/2$ by the switches $S_1$, $S_2$, 0 by the switches $S_2$, $S_3$ and the clamping-diodes $D_5$ and $D_6$ and $-u_{dc}/2$ by the switches $S_3$, $S_4$. Always two consecutive switches in each phase leg are conducting.

The drawbacks of the VSCs are more complex structure and control compared to LCCs, which increase the costs and might decrease the reliability. The three-level, so called Vienna rectifier, allows the use of reduced number of power semiconductor switches but still achieves most of the benefits of NPC (Kolar and Zach, 1994). The Vienna rectifier consists of three IGBTs and 18 diodes as illustrated in Fig. 2.4. The output terminal of the Vienna rectifier can be connected to three voltage potentials just as the NPC converter. The phase A of the output terminal is connected to the voltage potential + $u_{dc}$ when the switch $S_1$ is switched off, the diode $D_1$ conducts and the phase current is positive. The output terminal is connected to the voltage potential 0, i.e. to the midpoint of the DC intermediate circuit, when the switch $S_1$ is switched on. Finally, the output terminal is connected to the voltage potential $-u_{dc}$ when the switch $S_1$ is switched off, the diode $D_6$ conducts and the phase current is negative. Low frequency harmonics are not produced into the AC currents and the power factor of the PCC can be controlled. However, only unidirectional power flow is possible.

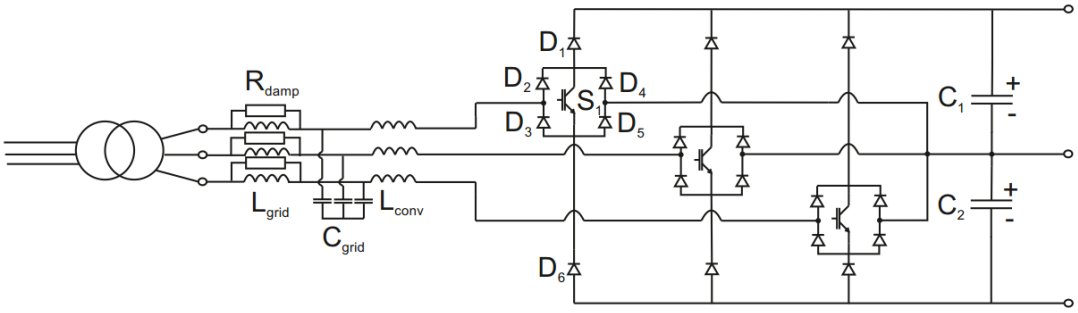


**Fig. 2.4.** Vienna rectifier

**Control and modulation methods of voltage-source converters**

The grid VSC is controlled to produce the desired DC voltage and the grid currents. A control block diagram of the four-wire thee-level NPC grid converter is presented in Fig. 2.5. The control principles are exactly the same for three-wire NPC, Vienna rectifier and two-level VSC but the zero current component $i_{sz}$ does not need to be controlled in three-wire topologies. The vector control scheme is implemented in the grid-voltage-oriented *dq*-reference frame. The angle $\varphi_s$ of the positive-sequence grid voltage is solved by the phase-locked loop (PLL) and used in *abc-dqz* and *dqz-αβ0* transformations. The phase voltages are supposed to be symmetrical when the basic PLL is used (Kim et al., 2013). The fundamental frequency currents and voltages are transformed into DC quantities in the grid-voltage-oriented vector control, and therefore, the steady-state error can be eliminated by using PI-controllers.

The control method is based on cascaded PI-control. The outer control loop regulates the DC voltage and provides the reference $\underline{i}_{sd}^{ref}$ for the d-axis current. The active power can be controlled by grid current *d*-component and the reactive power by grid current *q*-component according to (2.1) and (2.2) when $u_{sq}$ is zero and $u_{sd}$ is constant (Virtanen and Tuusa, 2012).

$$p = \frac{3}{2}\mathrm{Re}\left\{\underline{u}_s \underline{i}_s^*\right\} = \frac{3}{2}(u_{sd}i_{sd} + u_{sq}i_{sq}) = \frac{3}{2}u_{sd}i_{sd} \tag{2.1}$$

$$q = \frac{3}{2}\mathrm{Im}\left\{\underline{u}_s \underline{i}_s^*\right\} = \frac{3}{2}(u_{sq}i_{sq} - u_{sd}i_{sq}) = -\frac{3}{2}u_{sd}i_{sq} \tag{2.2}$$

The inner loop controls the grid current and provides the reference $\underline{u}_r^{ref}$ to the space vector modulator (SVM). The reference value of the current q-component is zero, because the target is to maximize the power factor. The reference value of the zero current component $i_{sz}^{ref}$ is set also to zero. The cross couplings resulting from *abc-dqz* transformation is compensated with the term

$j\omega_r(L_{grid}+L_{conv})$ when the synchronization is supposed to be ideal, i.e. $\omega_s=\omega_r$. The cross couplings do not occur in the control of the zero current component $i_{sz}$. The current feedback is the converter-side current $i_r$ as shown in Fig. 2.5 because it enables overcurrent protection. The grid and converter currents are supposed to be the same but the effect of the LC-filter on the power factor can be compensated by adding an offset value to the current reference $i_{sq}^{ref}$.

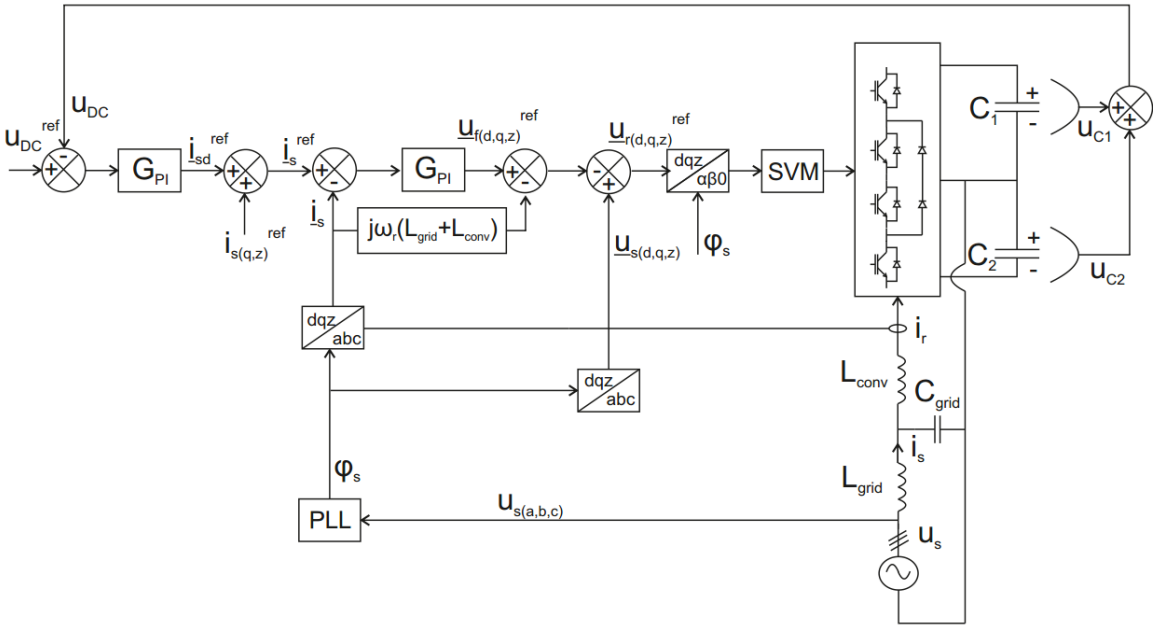


**Fig. 2.5.** Block diagram of the four-wire three-level NPC grid converter control system

The most used modulation methods with the multilevel converters are multilevel sinusoidal pulse width modulation (PWM), multilevel selective harmonic elimination (SHE) and space vector modulation (SVM) (Franquelo et al., 2008; Rodriguez et al., 2010). SHE method is used with low switching frequency to reduce the semiconductor power losses (Rodriguez et al., 2010). Target is to eliminate certain harmonics, e.g. $5^{th}$ and $7^{th}$ from the output voltage. However, high switching frequency is used in this study hence SHE method is not suitable.

Multicarrier PWM is based on traditional PWM technique but multiple carriers are used to control each power switch of the converter. Two carriers are used with three-level converters as illustrated in Fig. 2.6. The amplitude of the carrier signals is $u_{dc}/2$. The carriers are phase-shifted or level-shifted. The level shifted PWM methods can be divided into three different groups: phase disposition PWM (all carriers in phase), opposition disposition PWM (carriers above the reference zero point are out of phase with those below zero by 180°) and alternate opposition disposition PWM (carriers in adjacent bands are phase shifted by 180°) (Franquelo et al., 2008). The output current harmonics are minimized when the carrier signals are co-phasal as in Fig. 2.6 (Brückner et al., 2005).

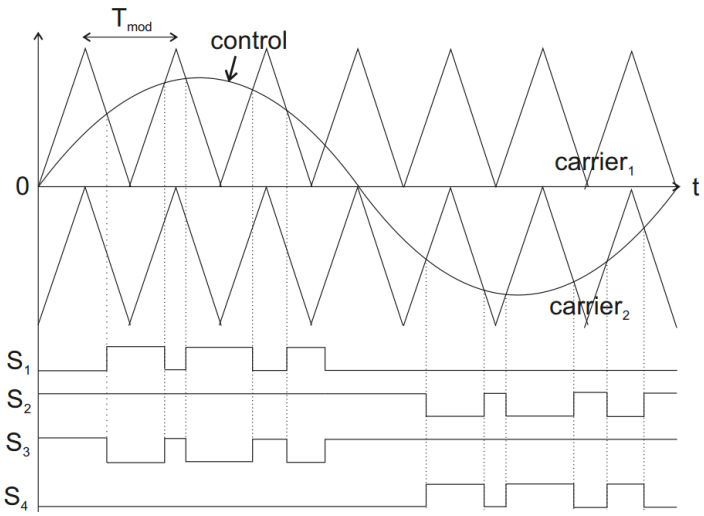


**Fig. 2.6.** Multicarrier PWM

The space-vector quantities are used to calculate the switching instants for a PWM converter in SVM. The principle of the SVM method is the same with the multilevel converters as for the two-level converters. However, 27 feasible switching-state vectors consisting of 24 active states and 3 null states form the switching sequence instead of 8 state vectors of the conventional two-level converter (Franquelo et al., 2008). The modulation of three-level converter is more complex but the redundancy of the switching states (i.e., the same output voltage can be created by using multiple states) can be used to balance the DC voltages, to reduce switching losses, to optimize switching waveforms, and to reduce common mode voltage (Rodriguez et al., 2010). The maximum output voltage can be increased by approximately 15 % in the linear modulation region by the injection of 3$^{rd}$ harmonic to the carriers in the PWM modulation or by using SVM. The output voltage and current THD as well as switching losses are equal in PWM with 3$^{rd}$ harmonic injection and in SVM (Ide et al., 1997). However, the 3$^{rd}$ harmonic injection method is not possible to be used in the four-wire system because the 3$^{rd}$ harmonic current would flow through the neutral wire.

## 2.3 Customer converters

The customer DC/AC power converter can be single-phase or three-phase converter depending on the customer needs. The most simple customer converter would be two-level half-bridge. However, the fundamental frequency current of the half-bridge circulates though the DC capacitors hence the capacitor voltages fluctuate by 50 Hz fundamental frequency. Therefore, the DC ca-

pacitors need to be large to balance the voltage fluctuation or an additional balancing method is needed. Moreover, the half-wave rectifying loads are not possible to be supplied by half bridges, because the voltage balance of the DC capacitors cannot be maintained without an additional balancing circuit. The half bridges are also problematic from the electrical protection point of view. The short circuit current flows through the DC capacitors, and therefore, it is difficult to be limited actively. (Rekola and Tuusa, 2011; Rekola and Tuusa, 2011a)

The problems associated to the DC voltage balance do not exist if the full-bridges are used instead of half-bridges. Half-wave rectifying loads are possible to supply by full bridges. The maximum output voltage amplitude is doubled compared to half bridges. The first current harmonics occur at twice the switching frequency if the unipolar modulation method is used (Rekola and Tuusa, 2011; Rekola and Tuusa, 2011a).

Instead of single-phase converters, three-phase two-level voltage-source inverter (VSI) or three-level NPC, shown in Fig. 2.7, can be used as a customer converter. The single-phase converters generate harmonics into the DC voltage at twice the fundamental frequency of the grid voltage (100 Hz) due to fluctuating power flow. The two-level three-phase VSI do not produce low frequency harmonics into the DC voltage but the three-phase three-level NPC converters produce 3rd harmonic into the DC voltage due to converter connection to the DC-link midpoint. Large DC capacitors can be used to mitigate the harmonics.

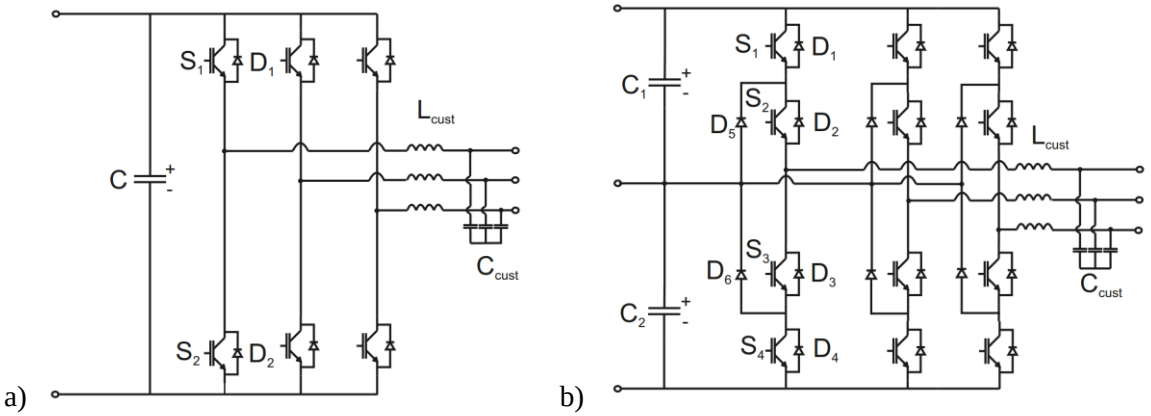


**Fig. 2.7.** Three-phase a) two-level and b) three-level NPC customer converter

The customer converter output voltage is not controlled in this study. Instead, the constant output voltage reference value is given to the modulator of the customer converter. The customer converter control methods are investigated by Peltoniemi et al. (2012, 2012a, 2013). The converter control has to fulfill the standard EN 50160, which defines that the customer AC voltage amplitude should be kept at constant value 230 Vrms (single-phase). 95 % of time the maximum amplitude error is ± 10 % and 100 % of time +10 %/ -15 %. In addition, the AC voltage frequency

should be kept constant at 50 Hz. The allowed maximum frequency error is 50 Hz ± 1 % for 99.5 % of time and +4 %/ -6 % for 100 % of time.

## 2.4 Required AC-filters

The power electronic converters produce high frequency harmonics at their switching frequency and its multiples. The harmonic currents generated by the switching action can be mitigated by using a low-pass filter. Otherwise, the current harmonics causes additional power losses, decrease power capacity, might lead to neutral line overloading and may cause damage or malfunction in other devices connected to the network. Voltage and current harmonics caused by power converters depend on converter topology, modulation method, switching frequency, and the used filters. The harmonics are limited in the standards according to total harmonic distortion (THD), which is defined as (2.3) (EN 50160).

$$THD[\%] = \sqrt{\frac{\sum_{h=2}^{40} U_{G(h)}^2}{U_{G(1)}^2}} \cdot 100 \tag{2.3}$$

where $U_{G(1)}$ is the rms-value of the fundamental frequency voltage and $U_{G(h)}$ is the rms-value of the $h^{th}$ frequency voltage component. The standards limit the maximum voltage THD up to $40^{th}$ harmonic component to be at maximum 8 % (EN 50160) or 5 % (EN 60555, IEC 6100-3-2 (class A), IEC 61727, IEEE 519-1992, IEEE Std 929-2000). The standards limit only the harmonics up to $40^{th}$ harmonic component (i.e., up to 2 kHz), and the EMC standards cover the harmonics above 150 kHz. However, the harmonics caused by the power electronic converters are located between these two frequency values.

The goal of the LVDC distribution network is to ensure better power quality to the customer compared to present AC network. Therefore, the customer voltage THD is limited to be ≤ 2 % at nominal load in this study. In addition, the grid current THD is limited to be ≤ 2 % at nominal load calculated up to three times of the converter modulation frequency.

### 2.4.1 AC-filter sizing

There are various AC filter design methods and multiple issues need to be taken into account in the filter design. These are e.g.

- the maximum allowed current or voltage harmonics in the filter output
- the allowed maximum filter inductor current harmonics
- the filter reactive power consumption
- the filter volume and mass
- the filter power losses
- the filter acquisition costs

The simplest low-pass filter is the inductor (L). The size of the inductor would be very large to sufficiently attenuate the harmonics, as shown in Table 2.1. Required L and LC filters for 10 kVA two-level three-phase customer converter to achieve the target THD $u_{load} \leq 2\%$ with the modulation frequency of 10 kHz are calculated and shown in Table 2.1. The system dynamics would be poor because of the voltage drop across the inductor (Liserre et al., 2005). Therefore, the L-filters are conventionally replaced by LC or LCL filters reducing the filter volume and assuring more effective attenuation compared to L filter. The required inductance value of the LC-filter is 1/6$^{th}$ of the inductance value of the L filter as depicted in Table 2.1.

**Table 2.1.** Required L and LC filters for 10 kVA two-level three-phase customer converter

| $U_{dc}$ | Filter type | $L_{cust}$ [mH (p.u.)] | $C_{cust}$ [μF (p.u.)] | $f_{res}$ [kHz] | $\hat{\imath}_{ripple,Lcust}$ [%] | THD $i_{Lcust}$ [%] |
|---|---|---|---|---|---|---|
| 750V | L | 6 (12 %) | | | 3.5 | 2 |
| | LC | 1.3 (3 %) | 4.5 (2 %) | 2.1 | 17 | 9 |
| 1500V | L | 8 (16 %) | | | 3.5 | 2 |
| | LC | 1.7 (3 %) | 2.8 (1%) | 2.3 | 17 | 10 |

The inductor current harmonics should be limited to reduce the inductor power losses and temperature rise. The harmonics can be limited based on current THD, usually 10 % < THD $i_L$ < 30 % (Wang et al., 2003; Wei et al., 2010). Another option is to limit the harmonics based on the inductor maximum ripple current $\Delta i_{ripple\_max} \leq$ (10 % ~30 %)$\hat{\imath}_{nom1}$ (Wang et al., 2003; Wei et al., 2010). The inductor maximum ripple current can be limited to the required value by choosing the converter side inductor value according to (2.4) for two-level converter and according to (2.5) for three-level converter (Mohan et al., 2003). The magnitude of the voltage pulse, which affect over the inductor is $u_{dc}/2$ in the case of two-level converter and half of that, $u_{dc}/4$, in the case of three-level converter.

$$L_{conv} = \frac{U_{1,rms}}{2\pi f_{sw}\Delta i_{Lconv}} = \frac{\frac{1}{\sqrt{2}} \cdot \frac{4}{\pi} \cdot \frac{u_{dc}}{2}}{2\pi f_{sw}\Delta i_{Lconv}} = \frac{\frac{u_{dc}}{\pi\sqrt{2}}}{\pi f_{sw}\Delta i_{Lconv}} \tag{2.4}$$

where $\Delta i_{Lconv}$ is the current maximum ripple, $f_{sw}$ is the switching frequency of the converter, and $U_{1,rms}$ is the rms-value of the fundamental frequency voltage.

$$L_{conv} = \frac{U_{1,rms}}{2\pi f_{sw}\Delta i_{Lconv}} = \frac{\frac{1}{\sqrt{2}}\cdot\frac{4}{\pi}\cdot\frac{u_{dc}}{4}}{2\pi f_{sw}\Delta i_{Lconv}} = \frac{\frac{u_{dc}}{\pi\sqrt{2}}}{2\pi f_{sw}\Delta i_{Lconv}} \tag{2.5}$$

The capacitance value of the LCL-filter should be limited, because too large capacitive current reduces the power factor and increases capacitive-current induced power losses of the system (Teodorescu et al., 2011; Liserre et al., 2005). The capacitance value $C$ is limited to be ≤ 5 % of the capacitance relative value $C_b$ according to (2.6), where $f_1$ is the fundamental frequency, $U_{LL}$ is the rms-value of the line-to-line voltage and $S_n$ is the nominal power (Liserre et al., 2005).

$$C = 0.05C_b = 0.05\cdot\frac{1}{\omega_1 Z_b} = 0.05\cdot\frac{1}{(2\pi f_1)(U_{LL}{}^2 / S_n)} \tag{2.6}$$

The second inductor of the LCL-filter is chosen typically as a ratio of the converter side filter inductor, e.g. the inductance value is 1/5 of the converter side inductance value. The total inductance value should be ≤ 10 % of the inductance relative value $L_b$, to limit the voltage drop across the inductor (Liserre et al., 2005; Teodorescu et al., 2011). The used base values are shown in Table D.1 in Appendix D.

The resonant frequency of the LC filter and LCL filter are defined according to (2.7) and (2.8). The resonant frequency should be at least ten times higher than the fundamental frequency to avoid resonance phenomena (Liserre et al., 2005). In addition, the resonant frequency should be lower than half of the switching frequency to sufficiently attenuate the switching harmonics (Liserre et al., 2005).

$$f_{res,LC} = \frac{1}{2\pi\sqrt{L_{cust}C_{cust}}} \tag{2.7}$$

$$f_{res,LCL} = \frac{1}{2\pi}\sqrt{\frac{L_{conv}+L_{grid}}{L_{conv}L_{grid}C}} \tag{2.8}$$

The filter capacitor design method might be also based on the resonant frequency of the filter, which is usually 10 % to 20 % of the modulation frequency, i.e. $f_{res,LC} \leq (10\ \% \sim 20\ \%) f_{sw}$. The passive or active damping of the LCL-filter is needed to avoid the resonance phenomena. The passive resistance can be added in series with a capacitor C or in parallel with the grid-side induc-

tor $L_{grid}$. The passive damping is widely used due to its simplicity and reliability. The size of the passive damping resistor is conventionally one third of the filter capacitor impedance at resonant frequency if the resistor is connected in series with the capacitor (Wei et al., 2010).

$$R_{damp} = \frac{1}{3} X_C(f_{res}) = \frac{1}{3} \cdot \frac{1}{2\pi f_{res} C} \tag{2.9}$$

The required AC filter inductance and capacitance values depending on the used design method are shown in Appendix E.

### 2.4.2 AC-filter inductor design

Two filter inductor core materials are treated in this study: EI-shaped laminated iron core (M400-50) and amorphous alloy C-core 2605SA1 by Metglas. Laminated iron core inductors are conventionally used in the AC filters of the power electronic converters. The lamination thickness of the non-oriented magnetic steel inductor core is 500 µm and the amorphous alloy core ribbon thickness is 23 µm. The proper core size is chosen according to the maximum energy ($LI_{rms}^2$). The three-phase inductor consists of three single-phase inductors as shown in Fig. 2.8.

a) 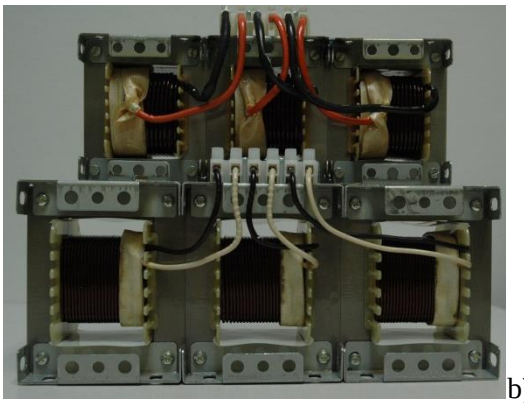 b) 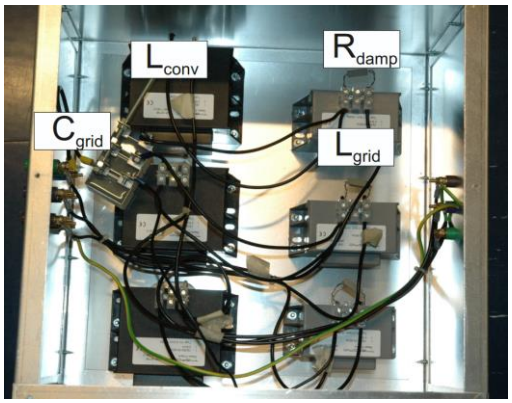


**Fig. 2.8.** a) iron core inductors and b) LCL-filter with the amorphous alloy core inductors

The required number of winding turns to achieve the required inductance value can be calculated according to (2.10)

$$N = \frac{L\hat{\imath}_{\max}}{B_{\max} A_c \cdot 10^{-4}} = \frac{L\hat{\imath}_{\max}}{0.75 B_{sat} A_c \cdot 10^{-4}} \tag{2.10}$$

where $A_c$ is the effective cross sectional area of the inductor core and $B_{max}$ is the maximum allowed magnetic flux density. $B_{max}$ is supposed to be 75 % of the saturation magnetic flux density $B_{sat}$ of the inductor core. Saturation flux density ($B_{sat}$) is for silicon steel 1.5 T and for amorphous

alloy 1.56 T. The permeability of the core is so high that the whole reluctance is supposed to be created in the air gap. Moreover, the permeability of the air gap is supposed to be the same as the permeability of air.

The frequency-dependent impedances of the iron and amorphous core inductors are measured by using Venable Instruments' frequency response analyzer Model 3120. The results have been previously reported in (Rekola et al., 2014). The target is to analyze the inductance value of the iron and amorphous core inductors at the modulation frequency of the converters. The inductors are approximated with a series connection of a resistor and an inductor (i.e., Foster first-order equivalent circuit), whose values are extracted from the measured impedances (de Leon and Semlyen, 1993). The inductance values of the iron core inductor are lower compared to the inductance value defined by the manufacturer at the fundamental frequency (1.6 mH, 1.7 mH and 2 mH instead of the supposed 2.2 mH inductance value) as shown in Fig. 2.9a. Circulating currents exist through three inductors, which are welded together, in spite of their own cores (cf. Fig. 2.8), and therefore, the inductance values differ from each other. The inductance value of the iron core decreases as the frequency increases as depicted in Fig. 2.9a. The inductance values are decreased to 1.2 mH and 1.4 mH at 10 kHz, which is the modulation frequency of the converter. At 20 kHz, the inductance values are decreased to 1.0 mH and 1.2 mH, respectively.

The inductance values of the amorphous cores are the same as the manufacturer defines at the fundamental frequency (0.6 mH). The inductance value stays constant in spite of increased frequency as shown in Fig. 2.9b. The iron core inductor resistance increases exponentially as the frequency increases over 100 Hz. Instead, the amorphous core inductor resistance begins to increase exponentially only > 10 kHz.

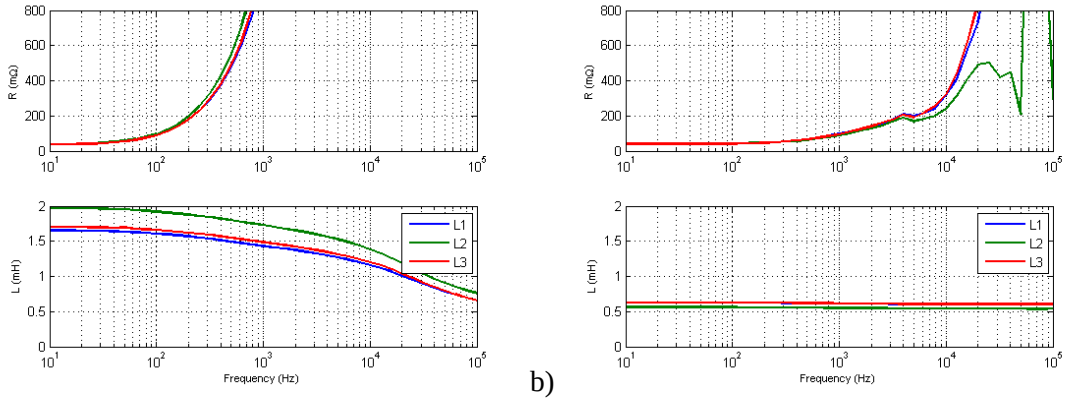


**Fig. 2.9.** The resistance and inductance values of a) the iron core inductor 2.2 mH and b) the amorphous alloy core inductor 0.6 mH

## 2.5 LVDC network configurations

The target of the LVDC distribution network, analyzed in this study, is to use as high voltage as possible to maximize the transmission distance and minimize the transmission cable resistive losses. Low Voltage Directive 2006/95/EC enables the use of 1000 VAC and 1500 VDC at maximum in low-voltage power transmission.

The simplest DC network configuration is a monopolar DC link consisting of one high voltage conductor and a ground- or sea-return. A monopolar link is obviously the most cost-effective solution, and therefore, used in the HVDC links but the ground currents might cause corrosion. It is not possible to be used in the LVDC distribution network because of the safety requirements. The unipolar network consists of two conductors and one voltage level as shown in Fig. 2.10a is the simplest network topology, which is suitable for LVDC application. The grid and customer converters are connected to 1500 VDC in the unipolar network. The bipolar LVDC distribution network consist of three conductors, voltage levels ±750 VDC and the neutral, as illustrated in Figs. 2.10 b-c.

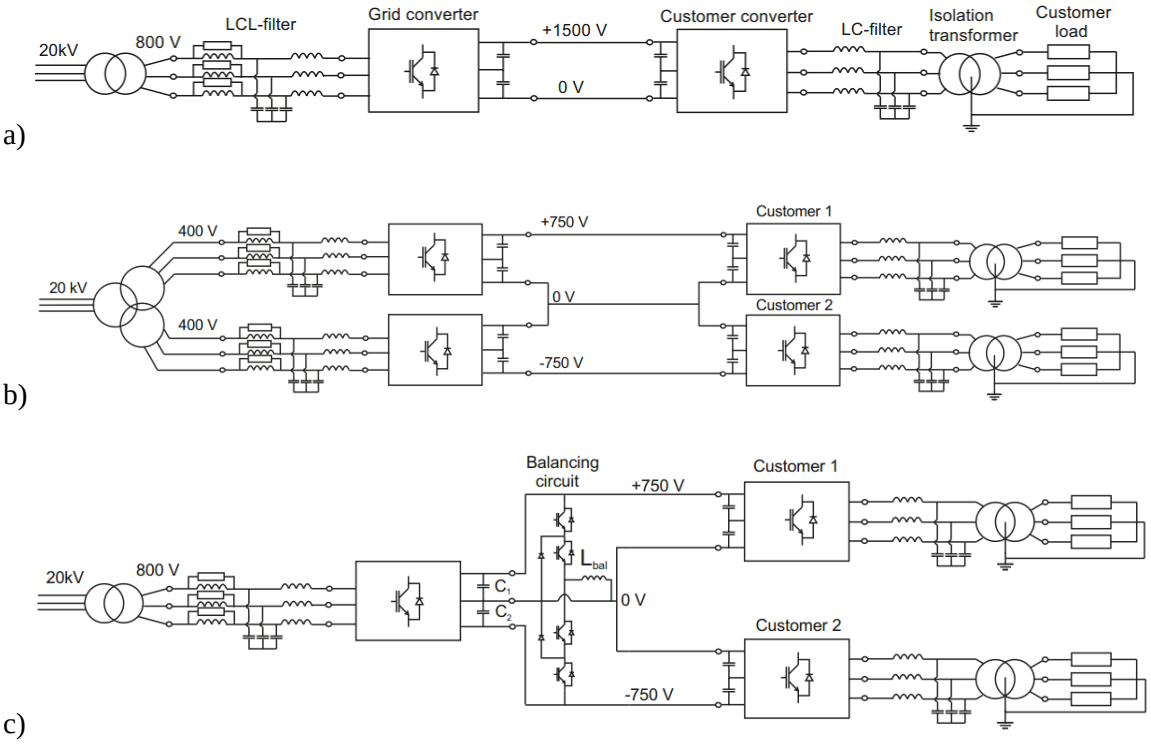


**Fig. 2.10.** a) unipolar LVDC distribution network and bipolar LVDC distribution network supplied by b) two grid converters and c) one grid converter

Bipolar transmission line have higher reliability, because it can operate in unipolar mode if there is a fault in the other pole (Lago et al., 2011; Justo, 2013; Byeon et al., 2013). The converters can be connected between the positive or the negative pole and the neutral, between the positive and negative poles or between the positive and negative poles with the neutral connection in the bipolar DC network. The neutral current equals to zero in the balanced bipolar network.

The maximum transmission distances of AC or DC distribution networks are shown in Fig. 2.11 (Lassila et al., 2009). The cable diameter is limited by maximum temperature of the cable, i.e., the maximum current and the maximum transmission distance is limited by the maximum allowed voltage drop (Lassila et al., 2009; Hakala et al., 2015). The economical sizing of the cables is achieved if the maximum voltage drop is 5-15 % (Lassila et al., 2009). The transmission capacity of ±750 VDC network is four times higher compared to 400 VAC network and the power transfer distance is seven times longer than that of 400 VAC network as depicted in Fig. 2.11. The LVAC cables can be used in DC distribution if the voltage between the conductors and earth is 900 VDC at maximum (IEC 60502-1, IEC 60449).

In addition to the replace of present LVAC distribution network by LVDC, also the length and complexity of the MVAC network can be reduced because of high power transmission capacity and lower construction and cable costs of the DC network (Hakala et al., 2015). The MVAC branch lines having length up to 8 km can be replaced by LVDC distribution network based on the power transfer capacity calculations by Hakala et al. (2015). This would increase the overall reliability of the electricity supply (Hakala et al, 2015).

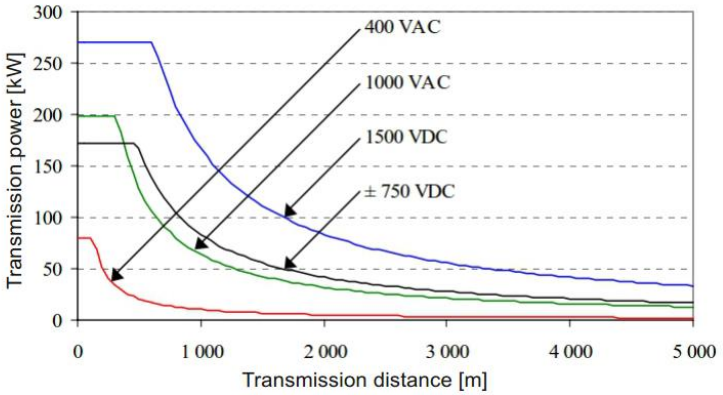


**Fig. 2.11.** Maximum transmission power and transmission distance using 3x35+70 $mm^2$ LV cable in AC and DC distribution systems. Maximum voltage drop 6 %. (Lassila et al., 2009)

The 20 kV medium voltage has to be scaled down by a transformer to low AC voltage (max. 1000 VAC) before rectifying to DC voltage (Low Voltage Directive 2006/95/EC). The voltage

transformation ratio of the front end transformer depends on the DC network topology, grid converter topology as well as the modulation method of the grid converter. The bipolar network can be fed by a two-winding transformer and one grid converter as shown in Fig. 2.10c. The voltage ratio of the two-winding transformer needs to be 1000 V/920 V if the PWM modulation with the 3rd harmonic component injection or SVM is used in the grid converter and 1000 V/800 V in the case of conventional PWM. The bipolar network can be also fed by a three-winding transformer and two grid converters, which are connected between the positive or negative pole and the neutral as shown in Fig. 2.10b. The voltage ratio of transformer needs to be 1000 V/460 V/460 V or 1000 V/400 V/400 V, respectively. With the used turn ratios, the MV voltage can increase by 10 % as it is allowed according to the standard EN-50160, and the DC voltage level can still be kept constant including the controlling tolerance of ± 5%.

The high DC voltage can tolerate a high voltage drop in the DC network due to temporarily fault without any effect on the customer voltage level (Hakala et al., 2013). The voltage can drop by 62 % for the three-phase or by 78 % for the single-phase system from 1500 V DC without any effect to the customer voltage in the unipolar network. In the bipolar network, the DC voltage can drop 24 % or 57 %, respectively.

### 2.5.1 Grounding of LVDC distribution network

The whole LVDC network would be grounded through the neutral conductor, i.e. functionally earthed TN-system, if only one grid converter is used and the neutral conductor is grounded as in Fig. 2.12. The single-phase loads can be connected between the phase and the neutral conductor. The customer electrical installations do not need to be changed. The grounded central conductor of the bipolar DC network requires that the DC network is insulated from an AC system (Kim et al., 2013; Lago et al., 2011; AlLeen, 2012; Kakigano et al., 2010a). The conventional 50 Hz isolation transformer is used in this study. However, the design and control methodology of the bidirectional full-bridge *CLLC* high frequency resonant converter for the galvanic isolation of the DC grid from the AC grid is proposed by Kim et al. (2013).

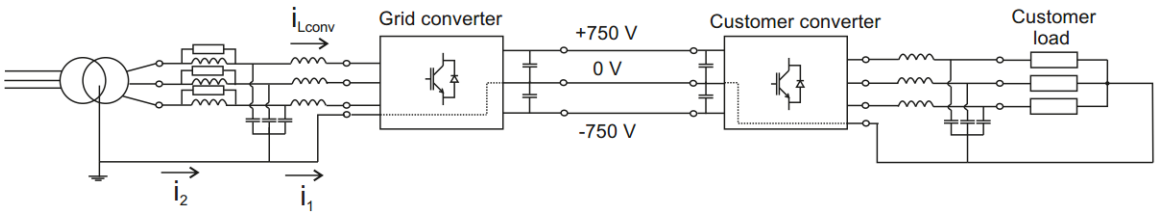


**Fig. 2.12.** Grounded LVDC distribution network

The central conductor is grounded e.g. in the bipolar ±170 VDC network inside the residential house due to Japanese standards and in the bipolar ±190 VDC network in data centres (Kakigano et al., 2012; AlLeen, 2012; Dong et al., 2013).

Dangerous contact voltages could result when the earth resistance is high as in Finland if the whole DC network is grounded (Nuutinen et al., 2013). Therefore, in difficult earth conditions, the customer's network might be grounded and the DC network ungrounded, i.e., a terrain-isolated functionally unearthed IT-system, as shown in Fig. 2.10. The galvanic isolation needs to be added between the DC network and the customer, otherwise the ground faults of the DC network and the grounded TN system would produce dangerous double fault through the ground (Nuutinen et al., 2013). The customer electrical installations do not need to be changed. The isolation transformer provides a neutral connection for single-phase loads. The galvanic isolation is not needed if the customer's network would be also ungrounded IT-system. However, special protections systems would be needed to react for double fault situations and earth fault protection is required.

The LVDC distribution network has to fulfil the local standards concerning electrical safety and it needs to be compatible with the existing protection devices. The main challenges of the DC network protection are related to the customer network faults including converter switch faults and double fault situations between LVDC and customer networks (Nuutinen et al., 2013). The earth faults are short circuits in the grounded network, and therefore, protection against these can be realized by short circuit protection devices (Nuutinen et al., 2013). The power electronics are not allowed to be used as a short-circuit protection according to the existing standards, because a protection device has to include a contact gap (Nuutinen et al., 2013). The fuses and circuit breakers need high, long time overcurrent to react, e.g. 50 A fuse requires at least 250 Arms short-circuit current to operate in five seconds (IEC 60364-4-41; Justo, 2013). The power converter is able to supply only 120 % of its nominal current. Therefore, the converter needs to be sized larger than the power supply capacity would require. The standards for the electrical safety should be updated to permit the protection based on the converter protection algorithms (Dong et al., 2013; Justo et al., 2013). The standardization committees such as Electric Power Research Institute (EPRI), International Electrotechnical Committee (IEC) and Emerge Alliance have started to work with the DC standardization (Dong et al., 2013).

### 2.5.2 DC network voltage balancing

The power generation units, loads and energy storage can be connected asymmetrically to both sides of the bipolar LVDC distribution network as shown in Figs. 2.10b-c. This does not lead to DC voltage unbalance problem if both sides of the bipolar LVDC distribution network are sup-

plied by their own grid converters as in Fig. 2.10b. Instead, if the bipolar LVDC distribution network is supplied by one grid converter as shown in Fig. 2.10c, the network halves are not loaded symmetrically. The DC capacitor voltages do not stay balanced and the DC capacitors can become damaged due to large voltage asymmetry.

The unbalanced loaded LVDC network is problematic if a 12-pulse rectifier is used. The AC grid currents are equal to the AC grid currents of the 6-pulse rectifier if only the other half of the DC network is loaded. The grid current THD varies from 10 % to 50 % depending on the loading conditions as shown in Fig. 2.1 (Rekola and Tuusa, 2011a).

The DC voltage unbalance increase the voltage stress of the VSC grid converter switches as well as the switching losses and thermal loading of the power semiconductor switches (Teichmann et al., 2005; Rodriguez et al., 2002; Franquelo et al., 2008; Von Jouanne et al., 2001; Zhang et al., 2015). The DC voltage unbalance increase also AC grid current and voltage distortion (Teichmann et al., 2005; Rodriguez et al., 2002; Franquelo et al., 2008; Von Jouanne et al., 2001; Zhang et al., 2015).

The simplest way to control the DC voltage balance is to add an offset value ($i_{bias,ref}$) to the grid current references ($i_{ref}$) as depicted in Fig. 2.13. An offset value ($i_{bias,ref}$) is proportional to the DC voltage difference (Rekola and Tuusa, 2011a; Brenna et al., 2009; Agustoni et al., 2005). The voltage of upper capacitor $C_1$ will increase when the current reference is positive. The voltage of lower capacitor $C_2$ will increase, when the added current component is negative, as in Fig. 2.13, respectively.

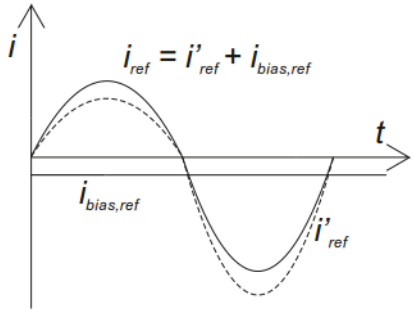


**Fig. 2.13.** Added balancing current component to the current references

Simulation results are presented in Fig. 2.14, where the three-level four-wire NPC grid converter, shown in Fig. 2.4, is used and the unbalanced load (5 kW load is connected to the other half of the network and the other half is unloaded) is controlled with the added DC current component (Rekola and Tuusa, 2011). The DC network is grounded as illustrated in Fig. 2.12. The grid currents are sinusoidal but there are more high frequency harmonics compared to the balanced load due to increased harmonics of the neutral conductor current ($i_2$) (Rekola and Tuusa, 2011a). The

neutral conductor current increases in the unbalanced loading conditions, because $i_N = i_a + i_b + i_c = i_{dc+} + i_{dc-}$. The added current offset value multiplied by three appears in the neutral conductor (Brenna et al., 2008). Therefore, this method is not possible to be used if the DC network is grounded (Kakigano et al., 2010a; Brenna et al., 2009).

The DC current is harmful in distribution networks because it can saturate the distribution transformers, which can lead to overheating or tripping (Teodorescu et al., 2011). The lifetime of the transformers would reduce because of increased hysteresis and eddy current losses due to unidirectional saturation and larger excitation current. The DC component might also affect the operation of the other loads connected to the grid, causing torque ripple and increased power losses in the motors (Teodorescu et al., 2011). Therefore, the maximum grid current DC component is limited in the standards to be under 1.0 % (IEC 61727) or 0.5 % (IEEE 1547-2003) of the rated rms AC current.

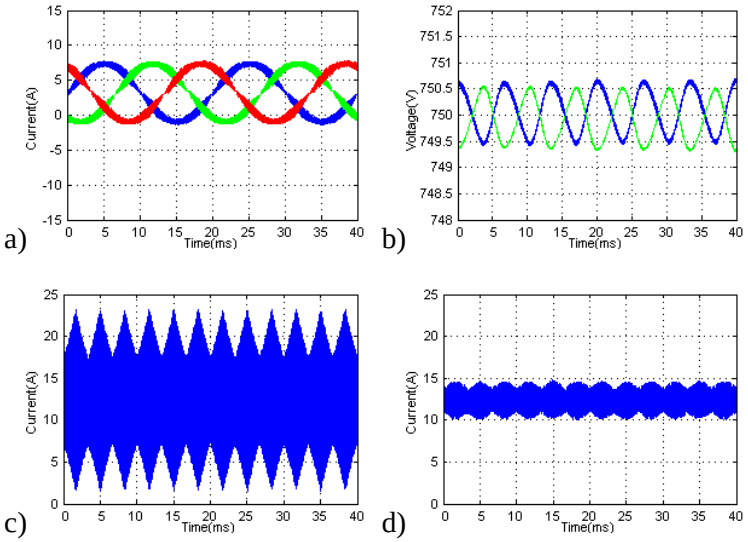


**Fig. 2.14.** a) AC grid currents, b) partial DC voltages, c) converter side neutral conductor current $i_1$, d) grid side neutral conductor current $i_2$

The other method to realize the DC voltage balancing is to use the redundancy of the switching vectors when space vector modulation is used with multilevel converters (Rodriguez et al., 2010). Additional hardware is not needed but the balancing algorithm cannot fully compensate the neutral-point voltage variation. The balancing schemes consider that the system is used as a unipolar DC network hence these are not suitable to the bipolar DC network voltage balancing, whose unbalance is inherent to the system (Rivera et al., 2015).

The third balancing method is to add the balancing circuit to the bipolar network (Kakigano et al., 2010a). The balancing circuit consists of an additional two- or three-level converter leg, depending on the grid converter structure, and the balancing inductor $L_{bal}$ as shown in Fig. 2.10c (von Jouanne et al., 2001; Kakigano et al., 2010a; Zhang et al., 2015; Rivera et al., 2015). The target of the balancing circuit is to control the voltage unbalance $u_{Lbal}$ of the DC capacitor voltages to zero (Rekola et al., 2014a; Rekola and Tuusa, 2011). The control scheme of the four-wire three-level NPC grid converter with the balancing circuit control is shown in Fig. 2.15. The inductor $L_{bal}$ current is controlled by changing the voltage across the inductor, $u_{Lbal}$. The proportional unbalance $u_{bal}$ is controlled by a PI-controller, whose output is the current reference ($\underline{i}_{Lbal}^{ref}$). The error between the measured current ($\underline{i}_{Lbal}$) and the reference value ($\underline{i}_{Lbal,}^{ref}$) is controlled by a second PI-controller, whose output is the voltage reference ($u_{Lbal}^{ref}$) of the modulator. The control system is not allowed to react to the 3rd harmonic component, which occurs in the DC voltages due to three-level converter topology. The modulation method of the balancing circuit differs from the modulation method of the converters, because the balancing circuit is always connected to the positive or negative pole of the DC link but not to the midpoint. The duty cycle of the balancing circuit can be defined according to (2.11)

$$u_{Lbal} = dU_{C1} - (1-d)U_{C2} \Rightarrow d = \frac{u_{Lbal}^{ref} + U_{C2}}{U_{dc}} \tag{2.11}$$

The duty cycle defines, how long time of during one period the inductor ($L_{bal}$) is connected to the positive pole of the DC link.

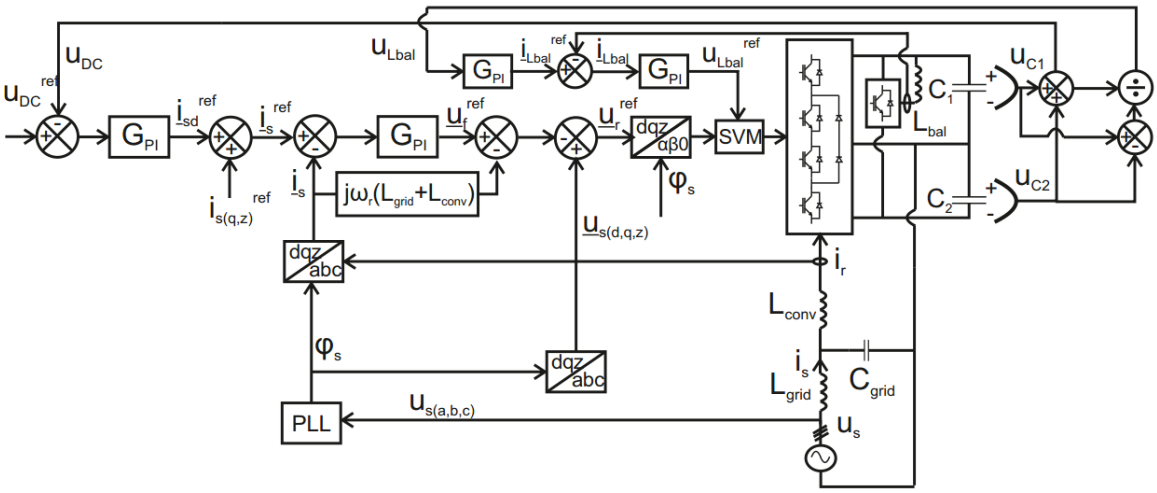


**Fig. 2.15.** Control scheme of grounded LVDC network with balancing circuit

The simulated current of the balancing inductor, DC voltages, DC currents, grid current and customer load currents are shown in Fig. 2.16 when three-level NPC customer converter with

10 kW load is connected between the negative pole and the neutral and the other half of the DC network is unloaded. The DC voltages are balanced despite of the asymmetrical load as shown in Fig. 2.16b. The unloaded DC positive pole current is zero as shown in Fig. 2.16c. THD of the AC grid currents is exactly the same with balanced or unbalanced load (Rekola et al., 2014a; Rekola and Tuusa, 2011a; von Jouanne et al., 2011; Zhang et al., 2015). Therefore, this DC voltage balancing method is suitable to LVDC distribution network (Kakigano et al., 2010a; Brenna et al., 2009).

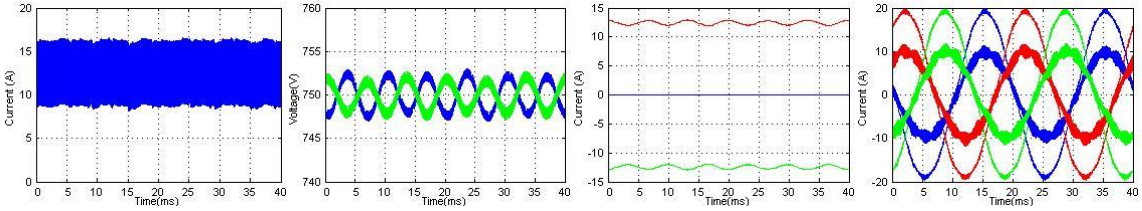


a) b) c) d)

**Fig. 2.16.** Simulated a) current of the balancing inductor $i_{Lbal}$, b) partial DC voltages, c) DC currents (blue positive pole, red midpoint and green negative pole current), d) input current of the grid converter and load current with 10 kW load in the other half of the network

The balancing inductor should be as large as possible to minimize the current ripple. However, the modulation frequency and dead time of the power semiconductor switches limits the inductance value according to (2.12)

$$L_{bal,\max} = \frac{(T/2 - T_d)U_{dc}}{2\Delta i_{Lbal}} \tag{2.12}$$

where $T$ is the cycle time ($1/f_{sw}$), $T_d$ is the dead time of the power semiconductor switches, and $\Delta i_{Lbal}$ is the maximum current ripple of the balancing inductor (Zhang et al., 2015). The drawback of the balancing circuit is the need to install extra converter leg and an inductor to the grid converter, the need of additional control hardware and the possibility of oscillations.

## 2.6 Required AC-filter parameters depending on the converter topology

The required AC filter inductor and capacitor values depending on the converter topology are shown in Fig. 2.17. It is assumed that the nominal power of three-phase converter is 10 kVA, the nominal power of the single-phase converters 3.3 kVA and the modulation frequency is 10 kHz.

The DC network is assumed to be ungrounded and the converters are connected to 750 VDC or 1500 VDC. The same AC filters can be used with three-level NPC and with Vienna rectifier. The AC filter design targets are that THD $i_{grid} \leq 2$ % and THD $u_{load} \leq 2$ % calculated up to 25 kHz. The inductor current harmonics are limited to $\Delta i_{Lconv\_ripple} \leq 10$ % $\hat{\imath}_{nom1}$.

a)

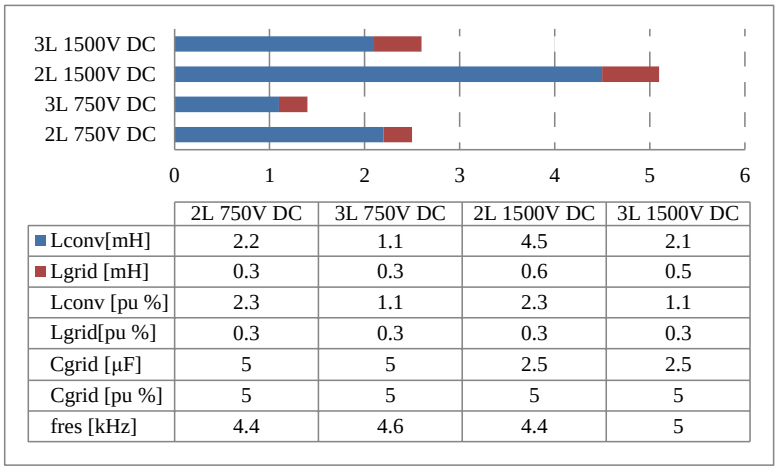


| | 2L 750V DC | 3L 750V DC | 2L 1500V DC | 3L 1500V DC |
|---|---|---|---|---|
| Lconv[mH] | 2.2 | 1.1 | 4.5 | 2.1 |
| Lgrid [mH] | 0.3 | 0.3 | 0.6 | 0.5 |
| Lconv [pu %] | 2.3 | 1.1 | 2.3 | 1.1 |
| Lgrid[pu %] | 0.3 | 0.3 | 0.3 | 0.3 |
| Cgrid [µF] | 5 | 5 | 2.5 | 2.5 |
| Cgrid [pu %] | 5 | 5 | 5 | 5 |
| fres [kHz] | 4.4 | 4.6 | 4.4 | 5 |

b)

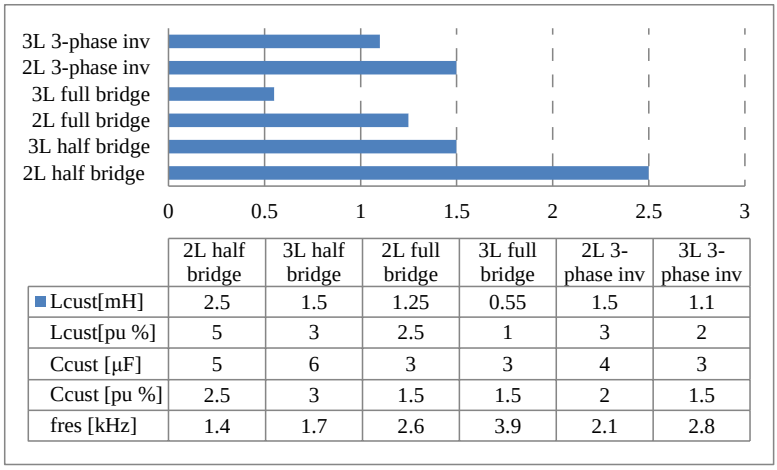


| | 2L half bridge | 3L half bridge | 2L full bridge | 3L full bridge | 2L 3-phase inv | 3L 3-phase inv |
|---|---|---|---|---|---|---|
| Lcust[mH] | 2.5 | 1.5 | 1.25 | 0.55 | 1.5 | 1.1 |
| Lcust[pu %] | 5 | 3 | 2.5 | 1 | 3 | 2 |
| Ccust [µF] | 5 | 6 | 3 | 3 | 4 | 3 |
| Ccust [pu %] | 2.5 | 3 | 1.5 | 1.5 | 2 | 1.5 |
| fres [kHz] | 1.4 | 1.7 | 2.6 | 3.9 | 2.1 | 2.8 |

c)

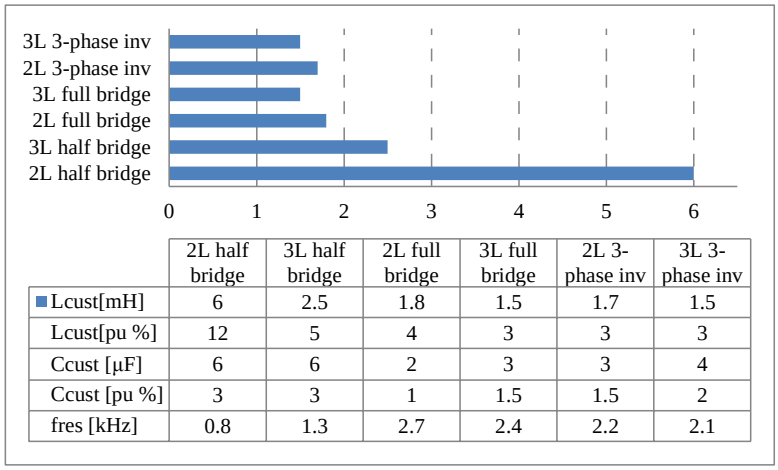


| | 2L half bridge | 3L half bridge | 2L full bridge | 3L full bridge | 2L 3-phase inv | 3L 3-phase inv |
|---|---|---|---|---|---|---|
| Lcust[mH] | 6 | 2.5 | 1.8 | 1.5 | 1.7 | 1.5 |
| Lcust[pu %] | 12 | 5 | 4 | 3 | 3 | 3 |
| Ccust [µF] | 6 | 6 | 2 | 3 | 3 | 4 |
| Ccust [pu %] | 3 | 3 | 1 | 1.5 | 1.5 | 2 |
| fres [kHz] | 0.8 | 1.3 | 2.7 | 2.4 | 2.2 | 2.1 |

**Fig. 2.17.** Required LCL filters with a) grid converters and LC filters with b) customer converters connected to 750 V DC and c) customer converters connected to 1500 V DC

The inductor harmonics can be limited based on current THD or based on the inductor maximum ripple current as discussed in Section 2.4.1. The required inductance and capacitance values by using the different limitations are shown in Appendix E. The LCL-filter is connected in front of the grid converters to achieve lowest total inductance value. The LC-filter is adequate after the customer converter, because according to the used filter design method, the customer side inductance value would be negligible. The required LC-filter values for all the analyzed customer converter topologies depending on the output voltage power quality are shown in (Rekola and Tuusa, 2011; Rekola and Tuusa, 2011a).

According to Fig. 2.17a, the filter inductance value required with three-level NPC grid converter is half of that with the comparable two-level converter because of multiple output voltage levels. The required inductance value is doubled if the voltage level is doubled from 750 VDC to 1500 VDC. The smaller filter inductance is sufficient also with three-level customer converter connected to 750 VDC compared to two-level converter as depicted in Fig. 2.17b. However, significant difference does not occur in the required filter inductance when customer converters are connected to 1500 VDC, because the modulation index of the converters is lower than 0.5. The modulation index $m_a$ is defined in (2.13).

$$m_a = \frac{\hat{u}_1}{U_{dc} / 2} \tag{2.13}$$

All the potential three-level converter output voltage levels are not used. The required inductance value is increased if the customer converters are connected to 1500 V DC instead of 750 V DC.

The first current and voltage high frequency harmonics occur at twice the switching frequency if the unipolar modulation method is used with the single-phase full-bridge converter. Therefore, the filter inductors required with full-bridges are smaller compared to filters with half-bridges. The output voltage of two-level full-bridge includes three voltage levels ($\pm u_{dc}/2$ and 0) whereas the output voltage of three-level full-bridge includes five voltage levels ($\pm u_{dc}/2$, $\pm u_{dc}/4$ and 0). Therefore, smaller filter inductors are required with three-level full-bridges.

The maximum voltage stresses of power semiconductor switches in three-level converter and in Vienna rectifier are half of those with the comparable two-level converters, $u_{dc}/2$, which is an important advantage especially at higher voltage levels because of limited voltage capability of IGBTs (Teichmann et al., 2005; Brückner et al., 2005).

## 2.7 Conclusions

The applicability of the different converter topologies to the 1500 VDC LVDC distribution network is analyzed by taking into account the controllability of AC current and DC voltage, size of the required AC filter and capability to operate with bidirectional power flow. Two- and three-level VSCs offer multiple advantages compared to LCCs (6- and 12-pulse diode-, thyristor- and half-controlled thyristor bridges) in spite of higher acquisition costs, more complex structure and control. The DC voltage is possible to be fully controlled, the bidirectional power flow is possible and the power factor of PCC can be controlled. Unity power factor and lack of low frequency harmonics ensures high utilization factor of the transformers and AC cables. The Vienna rectifier enable DC voltage and power factor control and lack of low frequency harmonics but only unidirectional power flow is possible.

It can be concluded that the customer converters should be connected to 750 VDC instead of 1500 VDC if 230 VAC rms phase voltage is produced to the customer, to maximize the modulation index, and minimize the required AC filter inductance value. The required AC filter inductance value with three-level converter is half of that with two-level converter when the modulation index is > 0.5. Moreover, the required maximum voltage rating of the used power semiconductor switches is half of that with the two-level converters. The full-bridge is the most suitable customer converter topology if the single-phase supply is adequate because smaller required passive components, both at the DC and AC side, compared to half-bridges.

The maximum transmission power capability and transmission distance increase when the 400 V LVAC distribution network would be replaced by 1500 V LVDC distribution network. The whole LVDC distribution network and the customer electrical installations can be grounded in good grounding conditions. Otherwise the LVDC distribution network needs to be ungrounded, and the galvanic isolation is needed between the ungrounded network and the customer grounded electrical installations.

The need of DC voltage balancing in the asymmetrically loaded bipolar LVDC distribution network is taken into account. Three DC voltage balancing methods are compared. It can be concluded that the balancing circuit should be added to the DC network if the asymmetrically loaded bipolar LVDC distribution network is supplied by one grid converter.

# 3 Power loss simulation models

## 3.1 Introduction

The advantages of LVDC distribution over conventional AC distribution have been analyzed using theoretical means over the past few years but experimental results, which prove the high energy efficiency and power quality, or otherwise, have not yet been presented (Nilsson et al., 2004; Engelen et al., 2006; Anand et al., 2010; Sannino et al., 2003; Kakigano et al., 2010; Kakigano et al., 2012; Shenai et al., 2011). Section 3.2 describes the two-level VSC and three-level NPC as well as Vienna rectifier analytical power loss calculation and simulation methods. The AC filter power loss calculation methods are discussed in Section 3.3. The simulation and calculation methods for the other power loss sources in the LVDC distribution network are presented in Section 3.4. Finally, the developed power loss models are verified by measurements and the accuracy of the models is discussed in Section 3.5. The measured power loss results have been previously reported in (Rekola et al., 2014; Rekola and Tuusa, 2014b). The conclusions are drawn in Section 3.6.

## 3.2 Converter power losses

The power losses of the power electronic converter include switching and conduction losses of power semiconductor switches as well as conduction and reverse recovery losses of diodes. IGBTs are used as a power semiconductor switches in this study. The average conduction losses of the IGBTs and diodes are calculated according to the equations (3.1) and (3.2)

$$P_{cond,IGBT} = \frac{1}{T}\int_0^T \left(i_{IGBT}R_{ce} + V_t\right) i_{IGBT}\,dt \tag{3.1}$$

$$P_{cond,D} = \frac{1}{T}\int_0^T \left(i_D R_f + V_f\right) i_D\,dt \tag{3.2}$$

where $R_{ce}$ and $R_f$ are the on-state resistances, $V_t$ and $V_f$ are the zero-current voltage drops for the IGBTs and diodes, i.e. the collector-emitter threshold voltage and the diode forward voltage (Dieckerhoff et al., 2005; Rekola et al., 2014; Virtanen et al., 2013). The parameters can be obtained from the datasheets of IGBTs and diodes. The converter switching losses consist of the turn-on and turn-off losses of the IGBTs and the reverse recovery losses of the diodes. The average switching losses are calculated according to (3.3), (3.4) and (3.5)

$$P_{sw,on\_IGBT} = \frac{1}{T}\sum \frac{U_{dc}}{U_{ref}} E_{on}(i_{igbt}) \tag{3.3}$$

$$P_{sw,off\_IGBT} = \frac{1}{T}\sum \frac{U_{dc}}{U_{ref}} E_{off}(i_{igbt}) \tag{3.4}$$

$$P_{sw,rr\_D} = \frac{1}{T}\sum \frac{U_{dc}}{U_{ref}} E_{rr}(i_D) \tag{3.5}$$

where $U_{dc}$ is the DC voltage and $U_{ref}$ is the IGBTs and diodes loss energy determination voltage. $E_{on}(i_{IGBT})$, $E_{off}(i_{IGBT})$ are the IGBTs turn-on and turn-off energies and $E_{rr}(i_D)$ is the reverse recovery energy of the diodes as a function of current (Rekola et al., 2014; Virtanen et al., 2013). The parameters are found in the manufacturer's datasheets. Temperature coefficients are not taken into account in the converter power loss calculation models but the worst case values are used, i.e., the values measured at 125°C. The total losses of the converter can be calculated according to (3.6)

$$P_{loss\_total} = n(P_{cond,IGBT} + P_{cond,D} + P_{sw,on\_IGBT} + P_{sw,off\_IGBT} + P_{sw,rr\_D}) + P_{add} \tag{3.6}$$

where $n$ is the number of switching devices in the converter. The additional cooling and control losses are denoted by $P_{add}$.

### 3.2.1 Analytical power loss calculation method

The average power losses of the converter can be calculated analytically. The average conduction losses for one active switching device and for one antiparallel diode in two-level converter can be calculated according to (3.7.) and (3.8.). SVM or PWM modulation method with 3rd harmonic injection is supposed to be used. The currents are supposed to be sinusoidal and the calculated power losses are an average over the 50 Hz fundamental period.

$$P_{cond,IGBT} = V_t i_{ave} + R_{ce} {i_{rms}}^2 = V_t \hat{i}_{conv} \left( \frac{1}{2\pi} + \frac{m_a \cos\varphi}{8} \right) + R_{ce} {\hat{i}_{conv}}^2 \left( \frac{1}{8} + \frac{m_a \cos\varphi}{3\pi} \right) \quad (3.7)$$

$$P_{cond,D} = V_f i_{ave} + R_f {i_{rms}}^2 = V_f \hat{i}_{conv} \left( \frac{1}{2\pi} - \frac{m_a \cos\varphi}{8} \right) + R_f {\hat{i}_{conv}}^2 \left( \frac{1}{8} - \frac{m_a \cos\varphi}{3\pi} \right) \quad (3.8)$$

where $\hat{i}_{conv}$ is the sinusoidal converter current peak-value, $i_{ave}$ is the current average value, $i_{rms}$ is the current rms value, $cos\varphi$ is the power factor and $m_a$ is the modulation index, defined in (2.13) (Dieckerhoff et al., 2005; Moia et al., 2012).

The current stresses of the power semiconductors in three-phase and single-phase half-bridge are the same when the load per phase is the same. However, the current stresses of the semiconductors of the single-phase full-bridge are half of that (Rekola and Tuusa, 2011a). The converter average switching losses are calculated as follows

$$P_{sw,IGBT} = f_{sw} \frac{1}{\pi} \frac{U_{dc}}{U_{ref}} (E_{on}(\hat{i}_{conv}) + E_{off}(\hat{i}_{conv})) \quad (3.9)$$

$$P_{sw,D} = f_{sw} \frac{1}{\pi} \frac{U_{dc}}{U_{ref}} E_{rr}(\hat{i}_{conv}) \quad (3.10)$$

where $f_{sw}$ is the converter modulation frequency (Dieckerhoff et al., 2005). Finally, the total power losses for the two-level converter including six IGBTs and diodes can be calculated according to (3.6.). The average conduction losses of three-level NPC converter can be calculated analytically according to eq. (3.11) - (3.14)

$$P_{cond,S1,S4} = m_a \left( \frac{V_t \hat{i}_{conv}}{4\pi} ((\pi - \varphi)\cos(\varphi) + \sin(\varphi)) + \frac{R_{ce} {\hat{i}_{conv}}^2}{6\pi} (1 + 2\cos(\varphi) + \cos(\varphi)^2) \right) \quad (3.11)$$

$$P_{cond,S2,S3} = \frac{1}{12\pi} \left( \begin{array}{l} V_t \hat{i}_{conv} (12 + 3m_a (\varphi \cos(\varphi) - \sin(\varphi))) \\ + R_{ce} {\hat{i}_{conv}}^2 (3\pi - 2m_a (1 - 2\cos(\varphi) + \cos(\varphi)^2)) \end{array} \right) \quad (3.12)$$

$$P_{cond,D1,D2,D3,D4} = m_a \left( \frac{V_f \hat{i}_{conv}}{4\pi} (\sin(\varphi) - \varphi \cos(\varphi)) + \frac{R_f {\hat{i}_{conv}}^2}{6\pi} (1 - 2\cos(\varphi) + \cos(\varphi)^2) \right) \quad (3.13)$$

$$P_{cond,D5,D6} = \left( \frac{V_f \hat{i}_{conv}}{\pi} + \frac{R_f \hat{i}_{conv}{}^2}{4} \right) + m_a \left( \frac{V_f \hat{i}_{conv}}{4\pi} ((2\varphi - \pi)\cos(\varphi) - 2\sin(\varphi)) - \frac{R_f \hat{i}_{conv}{}^2}{3\pi} (1 + \cos(\varphi)^2) \right) \quad (3.14)$$

where $\varphi$ is the phase angle (Staudt et al., 2011; Bendre et al., 2009; Wang et al., 2007; Dieckerhoff et al., 2005; Moia et al., 2012). The IGBTs and diodes are marked in Fig. 2.3. The average switching losses of three-level NPC converter are calculated as follows

$$P_{sw,S1,S4} = f_{sw}(E_{on} + E_{off}) \left( \frac{\hat{i}_{conv}}{I_{ref}} \right) \left( \frac{U_{dc}}{U_{ref}} \right)^{1.4} \left( \frac{1}{2\pi} \right) (1 + \cos(\varphi)) \quad (3.15)$$

$$P_{sw,S2,S3} = f_{sw}(E_{on} + E_{off}) \left( \frac{\hat{i}_{conv}}{I_{ref}} \right) \left( \frac{U_{dc}}{U_{ref}} \right)^{1.4} \left( \frac{1}{2\pi} \right) (1 - \cos(\varphi)) \quad (3.16)$$

$$P_{sw,D1,D4} = f_{sw} E_{rr} \left( \frac{\hat{i}_{conv}}{I_{ref}} \right)^{0.6} \left( \frac{U_{dc}}{U_{ref}} \right)^{0.6} \left( \frac{1}{2\pi} \right) (1 - \cos\varphi)^{0.4} \cdot 1.15 \quad (3.17)$$

$$P_{sw,D2,D3} \approx 0 \quad (3.18)$$

$$P_{sw,D5,D6} = f_{sw} E_{rr} \left( \frac{\hat{i}_{conv}}{I_{ref}} \right)^{0.6} \left( \frac{U_{dc}}{U_{ref}} \right)^{0.6} \left( \frac{1}{2\pi} \right) (1 + \cos\varphi)^{0.4} \cdot 1.15 \quad (3.19)$$

where $I_{ref}$ is the current used in determining the loss energies $E_{on}$, $E_{off}$ and $E_{rr}$ (Semikron Application Note, 2015). The three-level NPC converter is supposed to be symmetrically loaded. Antiparallel diodes $D_2$ and $D_3$ conducts the whole positive or negative half cycle in the rectifier operation mode, hence the switching frequency is 50 Hz and the switching losses are supposed to be negligible. Antiparallel diodes $D_2$ and $D_3$ do not conduct in the inverter operation mode hence the switching losses are negligible in this case. Finally, the total power losses for the three-level converter can be calculated according to (3.6.).

The current average and rms values of Vienna rectifier are calculated according to (3.20)–(3.27). The IGBT and diodes are marked in Fig. 2.4. The current stresses of the IGBTs and diodes are unbalanced in the Vienna rectifier. The average currents of IGBT $S_1$ is doubled compared to the average current of diodes $D_4$ and $D_5$. The average currents stresses of diodes $D_2$ and $D_3$ are the highest, because either of them is always conducting. Diode $D_2$ conducts during the whole positive half cycle and diode $D_3$ conducts during the negative half cycle (Rekola and Tuusa, 2011).

$$I_{ave,S1} = \left( \frac{2}{\pi} - \frac{1}{\sqrt{3} m_a} \right) \hat{i}_{conv} \tag{3.20}$$

$$I_{rms,S1} = \sqrt{\frac{1}{2} - \frac{8}{3\sqrt{3}\pi} \cdot \frac{1}{m_a}} \hat{i}_{conv} \tag{3.21}$$

$$I_{ave,D1,D6} = \frac{1}{2\sqrt{3} m_a} \hat{i}_{conv} \tag{3.22}$$

$$I_{rms,D1,D6} = \sqrt{\frac{4}{3\sqrt{3}\pi} \cdot \frac{1}{m_a}} \hat{i}_{conv} \tag{3.23}$$

$$I_{ave,D2,D3} = \frac{1}{\pi} \hat{i}_{conv} \tag{3.24}$$

$$I_{rms,D2,D3} = \frac{1}{2} \hat{i}_{conv} \tag{3.25}$$

$$I_{ave,D4,D5} = \left( \frac{1}{\pi} - \frac{1}{2\sqrt{3} m_a} \right) \hat{i}_{conv} \tag{3.26}$$

$$I_{rms,D4,D5} = \sqrt{\frac{1}{4} - \frac{4}{3\sqrt{3}\pi} \cdot \frac{1}{m_a}} \hat{i}_{conv} \tag{3.27}$$

where $m_a$ is the modulation index (Kolar et al., 1996). The calculated current average and rms values are used to calculate the average conduction losses of the IGBTs (3.28) and diodes (3.29).The average switching losses of IGBTs and diodes are calculated according to (3.9) and (3.10).

$$P_{cond,igbt} = V_t I_{avg} + R_{ce} {I_{rms}}^2 \tag{3.28}$$

$$P_{cond,diode} = V_f I_{avg} + R_f I_{rms}^2 \tag{3.29}$$

Finally the total power losses for the Vienna rectifier can be calculated according to (3.6.).

### 3.2.2 Power loss simulation models

In addition to the previous average power loss calculation, the converter power loss analysis is made also by computer simulations using Matlab Simulink software. The target is to create more detailed converter power loss models compared to the average power loss calculation but at the same time, the models are general hence the parameters from the manufacturer's datasheets can be used. In addition, the target is to keep the model as simple as possible in order to keep the simulation time short. The simulation model calculates the conduction and switching losses as a function of the instantaneous IGBT and diode currents and voltages by taking into account every switching occasion from the modulator by using (3.1) - (3.6) . Therefore, the non-linear behavior of the switching losses depending on the current, shown in Fig. 3.1, is taken into account in the simulation models (Semikron, 2015b; Semikron, 2015e). The total power losses are summed and averaged over the fundamental cycle.

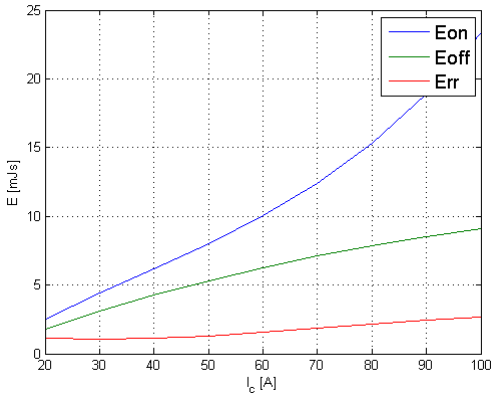


**Fig. 3.1.** The switching energy loss curve of SKM75GB123D ($E_{on}$ and $E_{off}$) and SKKD 40F10 ($E_{rr}$)

## 3.3 AC-filter power losses

The AC filter power losses consist of the filter inductor losses, capacitor losses and losses of damping resistor. The filter inductor power losses are caused by hysteresis and eddy currents in the inductor core and the resistance and eddy currents in the copper windings (Erickson and Maksimovic, 2001).

### 3.3.1 Inductor core power losses

Hysteresis loss is due to the energy consumed to redirecting of the magnetic domains of the material during every flux direction reversal. The fundamental frequency core losses are mainly caused by the hysteresis phenomenon in the core. Eddy current is the circulating current induced in the

material by changing magnetic flux as a consequence of the electromagnetic induction. High frequency core losses are mainly caused by the high frequency eddy currents induced into the core material. (Erickson and Maksimovic, 2001)

The inductor current harmonics need to be calculated to analyzing the inductor core power losses. Majority of the harmonics occur at the modulation frequency (10 kHz) and its multiples, mostly at 20 kHz. The harmonics located around 10 kHz are squared, summed and the square root of the sum is calculated hence the harmonics located around 10 kHz are all supposed to be located at 10 kHz frequency. The same method is used around 20 kHz. The amplitude of the current harmonics at 10 kHz is 10 % to 20 % of the fundamental frequency current value depending on the filter design and the amplitude of the 2$^{nd}$ multiples is about 2 % of that with half bridges and three-phase converters. Most of the harmonics are located at 20 kHz in the case of single-phase full-bridges when the unipolar PWM modulation is used.

The peak magnetic flux densities in the core at 50 Hz fundamental frequency, around 10 kHz modulation frequency and around 20 kHz are calculated according to (3.30) or by using (2.10) in order to analyze the losses caused by these frequencies in the filter inductor core

$$\hat{B} = \frac{\mu_0 \mu_r N \hat{\imath}}{l_{ag}} \tag{3.30}$$

where $\mu_0$ is the vacuum permeability, $\mu_r$ is the relative permeability of the air gap, $N$ is the number of winding turns, $\hat{\imath}$ is the current peak value at the calculated frequency and $l_{ag}$ is the inductor air gap length (Erickson and Maksimovic, 2001; Rekola et al., 2014; Virtanen et al., 2013).

The most used equation that characterizes core losses as a function of frequency is the Steinmetz equation

$$P_{core} = mk\hat{B}^{\alpha} f^{\beta} \tag{3.31}$$

where $m$ is the mass of the inductor core and $\hat{B}$ is the peak value of magnetic flux density in the core in the analyzed frequency $f$ (Steinmetz, 1984). Three coefficients $k$, $\alpha$ and $\beta$ are determined by fitting the model for the measured data. The manufacturer of the electrical steel for laminated iron cores gives the core losses per core mass only at the frequencies from 50 Hz to 2 kHz. Therefore, the coefficients for higher frequencies are found by using the measured power losses. The parameters are valid only for a limited frequency and flux density range hence different parameters are used with different inductor cores. The manufacturer gives the coefficients needed for the Steinmetz equation for the amorphous alloy core up to 100 kHz

$$P_{loss,core} = m6.5\hat{B}^{1.74} f^{1.51} \tag{3.32}$$

where $f$ is in kHz (Hitachi, 2015). Fig. 3.2 presents the loss curve for M400-50 electrical steel and for amorphous alloy with the respective frequencies 50 Hz, 10 kHz and 20 kHz as a function of the magnetic flux density.

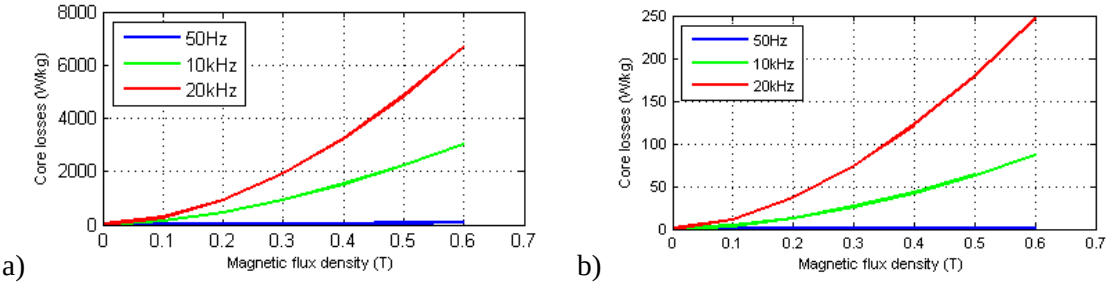


**Fig. 3.2.** Loss curves of a) iron core (1.1 mH) M400-50 electrical steel and b) amorphous alloy core 2605SA1

The losses in the iron core are huge at high frequencies as shown in Fig. 3.2., but still iron core inductors are widely used in the industrial converters. The BH-loop behavior and frequency dependence of the eddy current losses has an impact on the inductor core power losses (Hasegawa, 2004). The edges of the BH-loop are rounded for the amorphous alloy, i.e. flux reversal is faster than for the silicon steel (Hasegawa, 2004). Eddy current loss is generally proportional to $f^2$ with the soft magnetic materials but for the amorphous alloy $f^{1.5}$, which leads to lower high-frequency harmonic losses than in conventional electrical steels (Hasegawa, 2004). Moreover, eddy current loss is small in amorphous alloy, because the foil thickness (23 µm) is approximately 1/20 compared with the used silicon steel (500 µm) (Hitachi, 2015; Wang et al., 2010; Hasegawa and Azuma, 2008). There is no rule of atomic arrangement in the amorphous metal and the coercive force is low compared to silicon steel thus the hysteresis loss is small (Hasegawa and Azuma, 2008; Wang et al., 2010). The power losses caused by hysteresis and eddy currents in the inductor core made of electrical steel can be represented as shown in (3.33)

$$\begin{aligned} P &= P_{hyst} + P_{eddy} \\ &= W_h(\hat{\imath}) f_{sw} + \sigma(\pi d\hat{\imath} f_{sw})^2 / 6 + 8\sqrt{\sigma G S V_o}(\hat{\imath} f_{sw})^{3/2} \\ &= V_{core} \int_0^B H dB + \frac{\sigma(d\omega\hat{B})^2}{24} + 8,76\sqrt{\sigma G S V_o}\hat{B}^{1.5} f_{sw}^{1.5} \end{aligned} \tag{3.33}$$

The material parameter $V_{core}$ is defined by the material's microstructure and texture. The electrical conductivity σ and the lamination thickness $d$ are the parameters, which the steel producer can change for reducing the eddy current. The parameters $G$ and $V_o$ are related to metallurgical properties of the material and $S$ is the cross-section of the iron sheet (Bertotti, 1988). The thickness of

the laminated steel sheet has an effect to the power losses of the iron core inductor as shown in Fig. 3.3. The power loss curves of the silicon steels at 50 Hz and at 2500 Hz frequencies are shown in Fig. 3.3 (Perso, 2015).

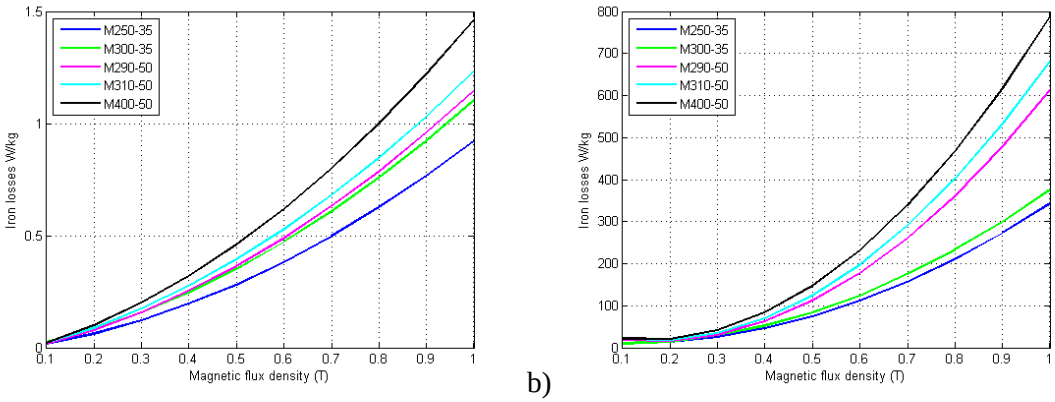


**Fig. 3.3.** The power losses of laminated silicon steel a) at 50 Hz and b) at 2500 Hz frequencies

The power loss curves are given to the silicon steels only up to 2500 Hz. Therefore, the accurate comparison of the power losses caused by current harmonics at 10 kHz and 20 kHz are not possible to do without measurements in the laboratory. However, it can be concluded that the power losses of the iron core inductors would be somewhat lower if the thickness of the silicon steel would be reduced from 500 µm (M400-50) used in this study.

In addition to amorphous alloy, there are other new magnetic materials, which have low no-load losses at high frequencies. Ferrite cores are widely used in low power applications. However, multiple ferrite cores should be connected in parallel in LVDC distribution network application due to low saturation flux density. The saturation magnetic flux density of the ferrite is 0.4 T whereas the saturation flux density of amorphous core is 1.56 T and iron 1.5 T (Wang et al., 2010).

### 3.3.2 Inductor copper winding power losses

The inductor copper losses consist of resistive losses caused by fundamental frequency current as well as eddy current losses caused by skin and proximity effect. The copper losses are calculated as the core losses at the fundamental frequency, the modulation frequency and twice of the modulation frequency. The resistive losses at the fundamental frequency are calculated according to (3.34), where $\rho_{Cu}$ is copper resistivity and $A_w$ is wire cross-sectional area. Winding wire length $l_{wire}$ can be calculated by multiplying mean length per turn ($MLT$) and number of wire turns ($N$) (Rekola et al., 2014; Virtanen et al., 2013).

$$P_{w,50Hz} = R_{50Hz} I_{rms,50Hz}^2 = \rho_{Cu} \frac{l_{wire}}{A_w} I_{rms,50Hz}^2 = \rho_{Cu} \frac{MLT \cdot N}{A_w} I_{rms,50Hz}^2 \quad (3.34)$$

The copper resistivity is dependent on temperature according to

$$\rho_{Cu} = \rho_{Cu,0} - (1 + \alpha(T - T_0)) \quad (3.35)$$

where $\rho_{Cu,0}$ is $1.724*10^{-8}$ Ω/m at 20°C temperature and the temperature coefficient α is 0.003862°C. The losses at high frequencies, caused by the combined influence of skin and proximity effects, are calculated by using the Dowell equation (3.36) defining the relationship $F_R$ of the high frequency resistance compared to fundamental frequency resistance (Dowell, 1966). The skin effect increases the current density in a wire exponentially as a function of frequency leading to reduction of the wire effective cross-sectional area, and hence increased wire resistance. The proximity effect increases the eddy currents, and hence the winding power losses within closely wound inductor wires.

$$F_R = \varphi' \left[ G_1(\varphi) + \frac{2}{3}(M^2 - 1)(G_1(\varphi) - 2G_2(\varphi)) \right] \quad (3.36)$$

where $M$ is number of winding layers. Moreover, the factor $\varphi$ is defined in (3.37)

$$\varphi = \frac{h_{wire}}{\delta} = \frac{h_{wire}}{\sqrt{\frac{\rho_{Cu}}{\pi \mu_0 \mu_r f}}} \quad (3.37)$$

where δ is skin depth of the wire, $\mu_0\mu_r$ is the permeability of the air gap and $f$ is the analyzed frequency . The porosity factor needs to be considered, and therefore, the factor $\varphi'$ is defined as

$$\varphi' = \frac{\sqrt{\eta\pi}}{2} \cdot \frac{d}{\delta} = \frac{\sqrt{h_{wire}(M / l_w)\pi}}{2} \cdot \frac{d}{\delta} = \frac{\sqrt{\frac{\sqrt{\pi}}{2} d(M / l_w)\pi}}{2} \cdot \frac{d}{\delta} \quad (3.38)$$

where $h_{wire}$ is defined as height of the square wire compared to round wire diameter $d$ and $l_w$ is the width of the copper wire layers in the inductor. The functions $G_1(\varphi)$ and $G_2(\varphi)$ are defined as

$$G_1(\varphi) = \frac{\sinh(2\varphi) + \sin(2\varphi)}{\cosh(2\varphi) - \cos(2\varphi)} \quad (3.39)$$

$$G_2(\varphi) = \frac{\sinh(\varphi)\cos(\varphi) + \cosh(\varphi)\sin(\varphi)}{\cosh(2\varphi) - \cos(2\varphi)} \quad (3.40)$$

Finally, the total copper wire power losses can be calculated according to (3.41) (Erickson and Maksimovic, 2001; Rekola et al., 2014; Virtanen et al., 2013).

$$P_{loss,w} = n(R_{50Hz} I_{rms,50Hz}^2 + F_{R,50Hz} R_{50Hz} I_{rms,50Hz}^2 + F_{R,10kHz} R_{50Hz} I_{rms,10kHz}^2 + F_{R,20kHz} R_{50Hz} I_{rms,20kHz}^2) \quad (3.41)$$

where $n$ is the number of single-phase inductors in the filter.

### 3.3.3 Capacitor power losses and power losses in damping resistors

The power losses of capacitors in an LCL-filter are defined as

$$P_{loss,C} = nR_{ESR,C} {I_{Crms}}^2 \quad (3.42)$$

where $n$ is the number of the capacitors, $R_{ESR,C}$ is the equivalent series resistance of the capacitor and $I_{Crms}$ is the rms value of the capacitor current (Mohan et al., 2003). Moreover, the temperature and frequency dependency of the equivalent series resistance should be taken into account in the very detailed power loss models.

The passive damping method is used to guarantee the stability of the LCL-filter-based grid converter. The passive damping resistors are connected in parallel with the grid side inductor in this study. The fundamental frequency losses in the damping resistors were calculated according to (3.43), where $I_s$ is the rms-value of the phase current (Rekola et al., 2014).

$$P_{loss,Rdamp} = 3R_{damp} \left( \frac{I_s X_{L,grid}}{R_{damp} + X_{L,grid}} \right)^2 = 3R_{damp} \left( \frac{I_{rms,50Hz} \cdot 2\pi \cdot 50Hz \cdot L_{grid}}{R_{damp} + 2\pi \cdot 50Hz \cdot L_{grid}} \right)^2 \quad (3.43)$$

The power losses of damping resistor and capacitors are lower than 2 W. Therefore, the power losses of the filter capacitors and damping resistors are not taken into account in the power loss calculation models, because these are considered insignificant compared to the inductor losses. Thus, in the simulation model, the AC filter power losses are supposed to be inductor power losses.

## 3.4 Other power loss sources in the LVDC distribution network

### 3.4.1 Balancing circuit power losses

The power losses of the balancing circuit are calculated by using the converter power loss simulation model shown in Section 3.2.2. The three-level balancing circuit is always connected to the positive or negative pole of the DC link, not to the midpoint. Therefore, the analytical power loss calculation models are not possible to be used in the case of the balancing circuit. The power losses of the balancing circuit are higher compared to conventional three-level converter leg due to lack of the midpoint connection. The inductor power loss calculation model is used to calculate the power losses of the balancing inductor.

### 3.4.2 DC capacitor power losses

The DC capacitors are connected after the grid converter and in front of the customer converters to balance the DC voltage. The required DC capacitor value is dependent on the chosen voltage level, converter topology and the control method of the converters. The well designed control of the DC network decreases the required DC capacitance value (Mahmoodi et al., 2006; Lana et al., 2011a). The power losses of DC capacitor are defined as

$$P_{loss,C} = nR_{ESR,C}I_{C,rms}{}^{2} \tag{3.44}$$

where $n$ is the number of the capacitors, $R_{ESR,C}$ is the equivalent series resistance of the capacitor, which is the sum of the frequency-sensitive resistance of the oxide dielectric, the temperature-sensitive resistance of the electrolyte and the resistance of the foil, the tabs and the terminals and $I_{C,rms}$ is the rms value of the capacitor current (Kolar and Round, 2006).

### 3.4.3 DC cable power losses

The DC cable is modeled by using the standard short-line π-equivalent model of the cable shown in Fig. 3.4. The typical low voltage underground cable is used in the analysis.

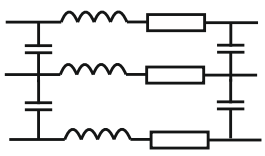

**Fig. 3.4.** The standard short-line π-equivalent model of the cable

The resistance of the used 4*16mm$^2$ AXMK-cable is 1.91 Ω/km at 20°C with DC current, the inductance is 0.29 mH/km and the capacitance is 0.30 μF/km (Pysmian, 2015).

### 3.4.4 Isolation transformer power losses

The isolation transformer is needed between the DC network and the customer electrical installations if the DC network is ungrounded and the customer electrical installation are not changed as mentioned in Section 2.5.1. Transformer power losses include iron core losses and copper winding losses just as with the iron core inductors (Erickson and Maksimovic, 2001). However, the current harmonics in the transformer current are negligible because of the AC filter design that limits THD $u_{load} \leq 2$ %. Therefore, the power losses caused by high frequency current harmonics do not need to be taken into account. The resistive power losses in the transformer copper wires are calculated according to (3.34). The iron core losses consist of no-load losses defined by the manufacturer and the power losses which depend on the current fundamental component (Eaton, 2015; Lana et al., 2014).

## 3.5 Accuracy of the created simulation models

The accuracy of the presented calculation and simulation models is verified by laboratory measurements (Rekola et al., 2014; Rekola and Tuusa, 2014b). The structure of the bipolar LVDC distribution network, assessed in this work is shown in Fig. 2.12. The DC voltage level is half of the maximum allowed by the standard, ± 375 VDC and the supply AC voltage is 400 V due to limited laboratory facilities. The laboratory prototype is presented in Appendix A. The 10 kVA three-level NPC converters are designed for 1500 VDC voltage level even if these are used 750 VDC voltage level hence the voltage capability of these IGBT modules is 1200 V. The converters use space vector modulation with the modulation frequency of 10 kHz. Power losses of an LCL-filter of the grid converter and an LC-filter of customer converter are measured by the air-cooled open type balance calorimeter, which operation principle is presented in Appendix B. The used filter inductance and capacitance values as well as resonant frequencies of the AC filters used in the power loss measurements are shown in Table 3.1. The current capability of all the inductor cores is the same, 16 Arms/25 Apeak.

LC-filters numbered 1 to 4 include iron core inductors. LC-filters 5 and 6 include amorphous core inductors. LCL-filter 7 includes iron core inductors and LCL-filter 8 amorphous core inductors. Multiple iron core inductors are tested due to nonlinear behavior of the core to achieve as reliable results as possible. The parameters for the Steinmetz power loss equation for the iron core inductors are found by fitting the measured results to (3.31) as mentioned in the previous Section 3.3.1.

**Table 3.1.** Properties of studied AC-filters

| Number of filter | LCL-filter | | | LC-filter | | $f_{res}$ [kHz] |
|---|---|---|---|---|---|---|
| | $L_{grid}$ [mH (p.u.)] | $C_{grid}$ [µF (p.u.)] | $L_{conv}$ [mH (p.u.)] | L [mH (p.u.)] | C [µF (p.u.)] | |
| 1 iron | | | | 2.2 (4 %) | 2.5 (1%) | 2.15 |
| 2 iron | | | | 2.2 (4 %) | 5 (3%) | 1.52 |
| 3 iron | | | | 1.1 (2 %) | 5 (3%) | 2.15 |
| 4 iron | | | | 3.0 (6 %) | 5 (3 %) | 1.30 |
| 5 amor | | | | 0.6 (1 %) | 5 (3 %) | 2.91 |
| 6 amor | | | | 1.5 (3 %) | 5 (3 %) | 1.84 |
| 7 iron | 0.6 (0.6 %) | 10 (10 %) | 5 (5 %) | | | 2.17 |
| 8 amor | 0.3 (0.3 %) | 10 (10 %) | 2.5 (2.5 %) | | | 3.08 |

The THD of the measured and simulated inductor current and load voltage with resistive loads are calculated up to 25 kHz and presented in Appendix C. The LC-filters 1-3 and 5 fulfill the requirement THD of $u_{load} \leq 2$ % in the laboratory prototype network when the DC network is ungrounded. Instead, in the grounded LVDC network the filters 2, 4 and 6 need to be used to fulfill the requirement.

The inductance value given by the manufacturer at 50 Hz frequency, is used in the simulations to obtain the same amorphous core inductor current THD as in the measurements. The inductance value of the iron core inductor is decreased to 70 % at 10 kHz and to 60 % at 20 kHz of the inductance value at 50 Hz frequency according to measurements shown in Section 2.4.2. Therefore, the filter current THD value is almost the same in the measurement and in the simulations and it is possible to analyze the losses in the inductor caused by the same current as presented in Appendix C. However, the simulated voltage THD is slightly smaller in comparison with the measured voltage THD, because low frequency harmonics occur in the measurements as shown in Appendix C.

The measured, analytically calculated and simulated power losses of the four-wire three-level NPC grid converter are shown in Fig. 3.5. The customer's electricity consumption varies extensively and therefore, the converter efficiencies have been analyzed at partial loading conditions. The purely resistive loads are used to simplify the measurements.

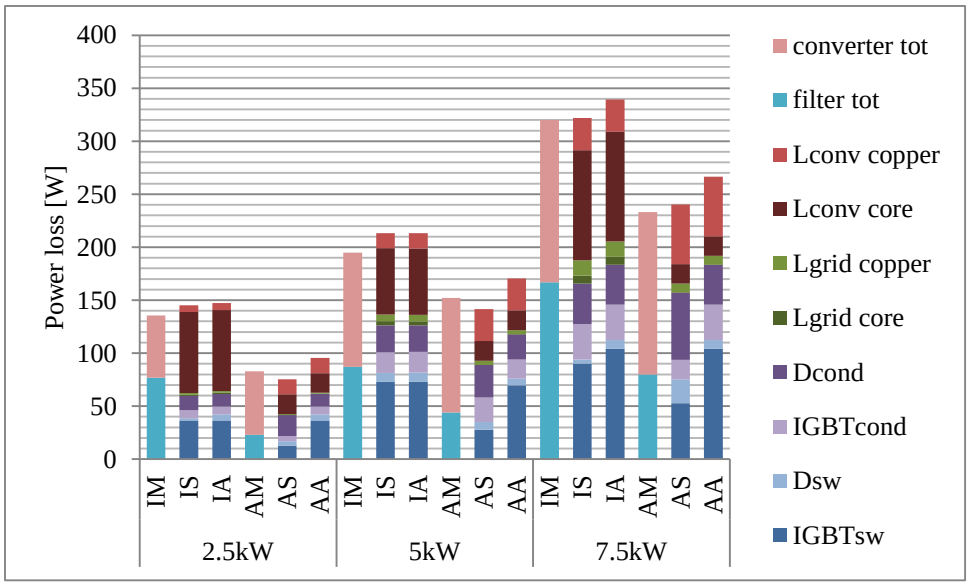


**Fig. 3.5.** The total losses of the four-wire three-level NPC grid converter are measured (M), simulated (S) and calculated analytically (A) with purely resistive 2.5 kW, 5 kW and 7.5 kW loads and with iron core (I) or amorphous core (A) LCL-filter inductors

The maximum grid converter power loss error between measured and simulated results is 10 %. The maximum relative error is achieved with the lowest power losses (2.5 kW load and amorphous core). It should be noted that the absolute error is only 10 W. The inductor current THD is at its maximum value (20 %) in this case, which might cause inaccuracy to the electrical power measurements. Otherwise the inductor current THD is ≤ 10 % and the maximum error is 7 %.

The maximum grid converter power loss error between measured and analytically calculated results is 15 %. The maximum relative error is achieved also with the lowest power losses (2.5 kW load and amorphous core), and the absolute error is 13 W. The accuracy of the analytically calculated power losses is slightly lower compared to simulated results in all loading conditions as depicted in Fig. 3.5.

The majority of the filter power losses are caused by the converter side inductor $L_{conv}$. The losses of the grid side inductor $L_{grid}$ are small because the harmonic content of the inductor current is small and a small inductor can be used. The filter causes approximately half of the overall power losses if the iron core inductors are used and 1/3 of the power losses when the amorphous inductor core is used.

The analytically calculated, simulated and measured customer converter power losses are shown in Figs. 3.6 – 3.8. The power losses of the customer converters are measured by using grounded

(marked as N in Figs. 3.6- 3.8) as well as ungrounded network. The maximum customer converter power loss error between measured and analytically calculated results is 20 % in Fig. 3.6. The accuracy achieved with the simulations is slightly higher. The maximum relative error is achieved with the lowest load (2.5 kW) just as with the grid converters. The maximum overall power loss error between the measured and simulated power losses is < 10 % except the filters 1N and 2N. The error occurs in the converter electric measurements with filters 1N and 2N due to high current harmonics shown in Appendix C. The current harmonics are almost constant despite the loading condition hence the proportional share of the current harmonics is at its maximum with low load.

The maximum customer converter power loss error between measured and analytically calculated results is decreased to 15 % when the load is increased to be half of the nominal load as illustrated in Fig. 3.7. The maximum error achieved with the simulation model is 10 %. The error occurs in the converter electric measurements with filter 3 due to high current harmonics. The smallest inductor (3) saturates and temperature rise is high due to large amount of current harmonics causing inaccuracy to the measured losses. The most accurate results are achieved with the largest load as depicted in Fig. 3.8. The highest current fundamental component increases the accuracy of the electrical power loss measurements. The maximum converter power loss error is 5 % except the use of the filter 1N. The accuracy of the power loss simulations and average power loss equations is almost the same. The error between the measured, simulated and analytically calculated power losses is < 10 % except the saturated inductor 3. The error occurs in the filter power loss measurements with the filter 3 and 1N but otherwise the error between the calculated and measured filter losses is 10 W at maximum.

The AC filter inductor core material has a significant impact on the overall customer converter power losses. The AC filter power losses with amorphous core inductors are at least half of those with the iron core filter inductors. The AC filter losses are 20 % to 30 % of the total losses if amorphous filter inductor core is used. The majority of the iron core inductor power losses are core losses caused by high frequency current harmonics. The proportional part of the filter losses from the total losses is in its maximum value with lowest load because most of the filter losses are caused by current harmonics. The power losses are significantly higher if the converter is grounded with iron core inductors whereas the power losses of the grounded and ungrounded converter are almost the same with the amorphous core inductors.

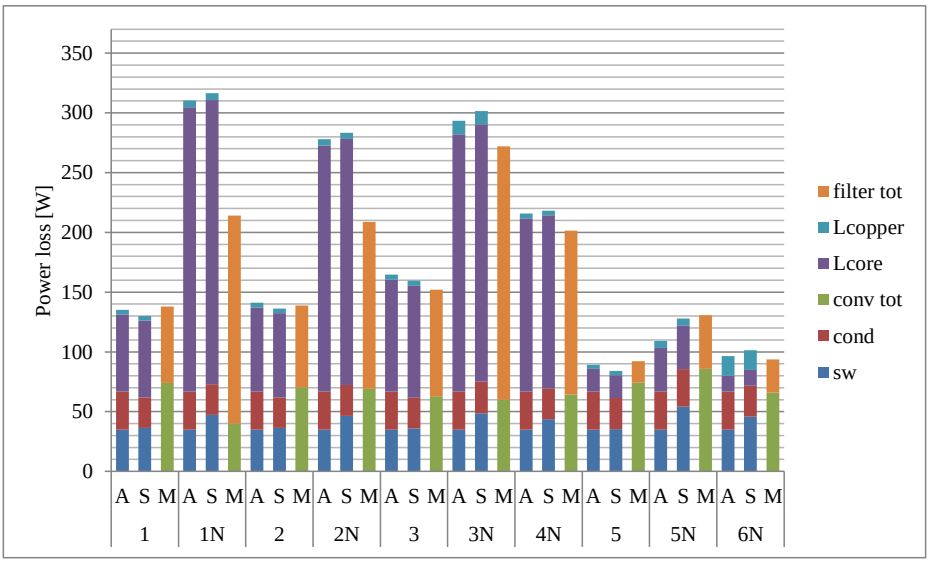


**Fig. 3.6.** Analytically calculated (A), simulated (S) and measured (M) three-level NPC customer converter power losses in ungrounded and grounded (N) network with resistive 2.5 kW load

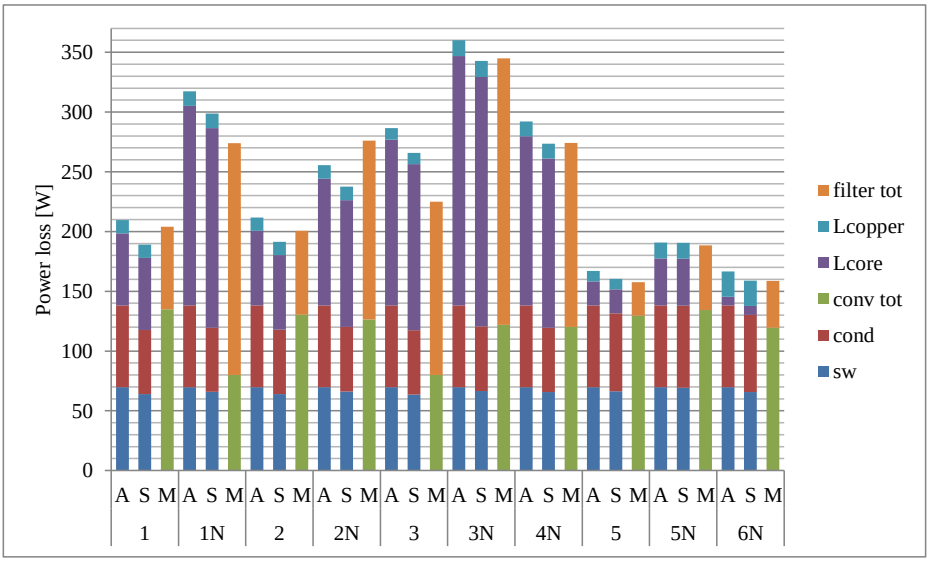


**Fig. 3.7.** Analytically calculated (A), simulated (S) and measured (M) three-level NPC customer converter power losses in ungrounded and grounded (N) network with resistive 5kW load

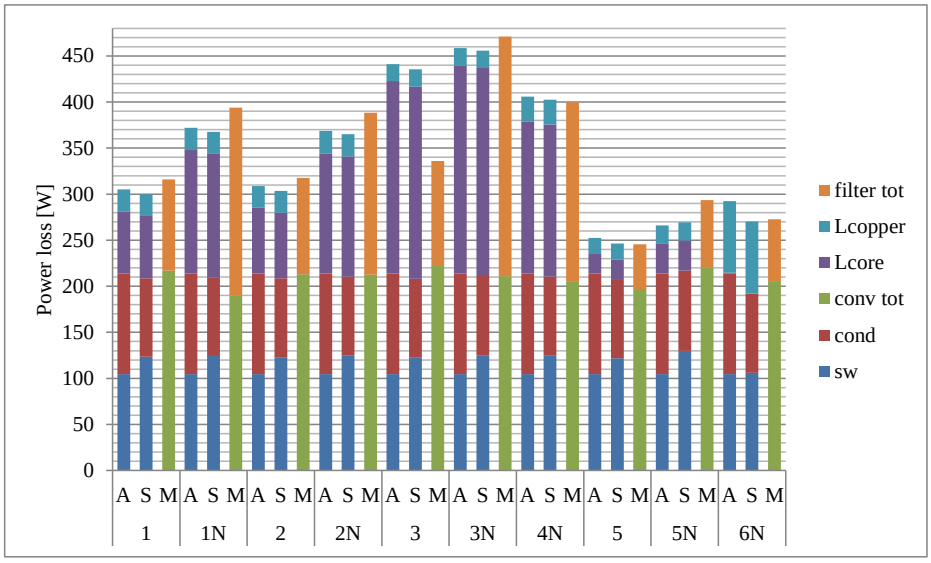


**Fig. 3.8.** Analytically calculated (A), simulated (S) and measured (M) three-level NPC customer converter power losses in ungrounded and grounded (N) network with resistive 7.5kW load

The overall measured and calculated power losses and energy efficiency of three-level grid and customer converters are shown in Fig. 3.9. The 200-metre long 4*16mm$^2$ AXMK underground cable is connected between the grid and the customer converters in the laboratory as shown in Appendix A. The DC network is grounded. The largest total power loss error between the measured and simulated power losses, 20 %, is achieved with the lowest load and with the amorphous alloy inductor cores. Otherwise the power loss error is 10 % at maximum.

It was depicted in Figs. 3.6- 3.8 that the power losses of the grounded converter are higher compared to ungrounded one when the power losses of the isolation transformer were not considered. However, the energy efficiency of the ungrounded DC network including isolation transformer is lower compared to grounded network especially at low load as shown in Fig. 3.9. The power losses of the customer converter and its AC filter are higher in the grounded network but the isolation transformer with large no-load losses is not needed.

It should be noted that the voltage rating of the IGBTs used in this study is 1200 V, i.e., they are rated for 1500 VDC. However, the used DC voltage is 750 VDC hence the IGBTs and diodes with lower voltage rating could be used. The converter losses would be approximately 30 % lower at nominal load with the IGBTs, whose voltage range is 600 V (Rekola and Tuusa, 2014b). Both the switching as well as conduction losses would be lower with the lower-voltage-rated IGBTs.

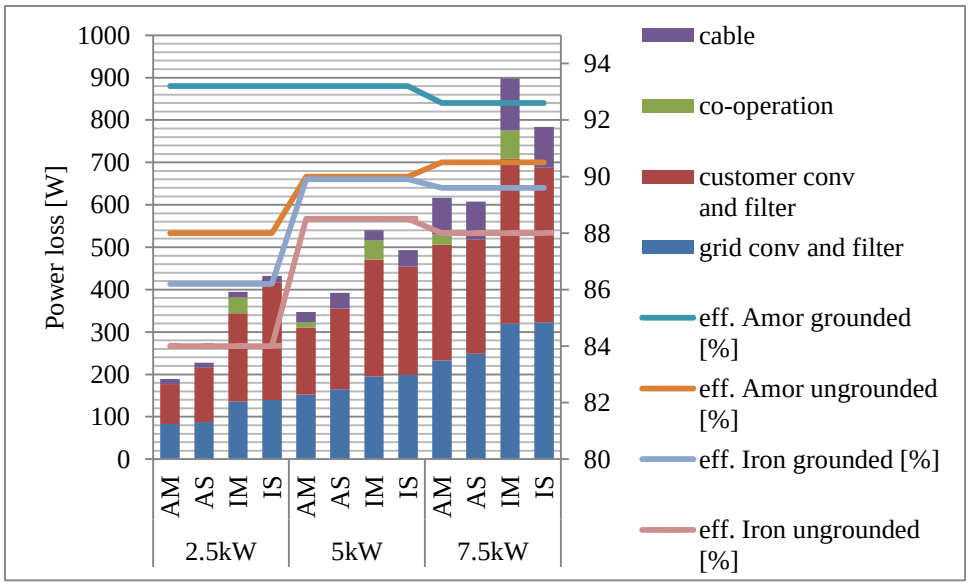


**Fig. 3.9.** The measured (M) and simulated (S) power losses of the DC network by using amorphous core inductors (A, number 5 and 8) or iron core (I, number 2 and 7) AC-filters

The measurements indicate that the low frequency harmonics exist in the DC current because both of the converters do not operate at exactly 50 Hz frequency (co-operation in Fig. 3.9). The converters should be synchronized with each other to reduce the DC current harmonics. The harmonics caused by interferences between the two converters increase the total losses compared to the measurements with the single converter causing inaccuracy to the DC cable power loss measurements. The 3rd current harmonics occur in the DC currents and the value of the 3rd harmonic component varies with 0.25 Hz as shown in Fig. 3.10a. The frequency difference of 0.08 Hz (1/3*0.25 Hz) between the grid and customer converters occur because of inaccuracy in the synchronization of the laboratory prototype converters. The same phenomena can be seen in DC voltages presented in Fig. 3.10c.

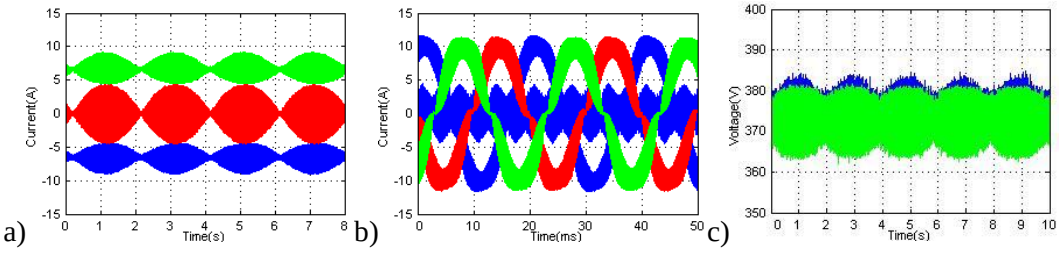


**Fig. 3.10.** Measured a) DC currents and b) current in the neutral conductor (blue) and the currents of $L_{cust}$ and c) DC voltages with 5 kW load, with the iron core LC-filter (2.2 mH and 5µF)

The largest current harmonics exist in the neutral conductor, because the harmonics of the positive and negative conductor are added to the neutral conductor as shown in Fig. 3.10b. Power losses caused by current harmonics are almost constant in spite of the loading condition but resistive losses of the DC cable are proportional to the transferred power.

The switching losses of the IGBTs and diodes are not possible to model accurately in the simulation model with a very low load, because the switching energy curves begins from 20 A in the datasheets. In addition, the high frequency current harmonics cause inaccuracy to the electrical measurements. The measured converter power loss results would be more accurate if the converter losses were measured by using the calorimeter instead of the power analyzers. The switching loss curves would be possible to fit to the measured power loss results if the measured results would be more accurate.

An inaccuracy exists between the measured and calculated filter inductor power losses, because accurate power losses caused by high frequency current harmonics are difficult to estimate. The current harmonics are supposed to be located at two frequencies, 10 kHz and 20 kHz. The current spectrum is spread to wider frequency area in reality. The filter loss simulation model would be more accurate but also more complex if all frequencies were taken into account. The Steinmetz equation assumes purely sinusoidal flux densities (Li et al., 2001; Krings et al., 2010; Mühlethaler et al., 2012; Akiror et al., 2012). The more sophisticated inductor core loss calculation methods, modified Steinmetz equation (MSE) or improved generalized Steinmetz equation (iGSE) or hysteresis loss model, guarantee higher accuracy also with non-sinusoidal current waveform (Li et al., 2001; Krings et al., 2010; Mühlethaler et al., 2012; Akiror et al., 2012). However, these equations are more complex. The parameters determined by fitting the model for the measured data are still used hence the equations are also valid only in a limited flux density and frequency range.

## 3.6 Conclusions

The power loss calculation methods for the converters, AC filters, balancing circuit, DC capacitors, DC cable and isolation transformer in the LVDC distribution are presented. The maximum error between the measured and simulated or analytically calculated power losses is 10 % when the inductor design is realistic i.e. the current harmonics are in a realistic level and the inductor do not saturate. The accuracy of the simulated power loss models is slightly higher especially at partial load conditions compared to the analytical average power loss equations. It is possible to carry out a rough estimation of power losses accurately enough for the converter and network topology comparison with the created simulation and calculation models but for the very detailed efficiency analyze, more complex models would be needed.

# 4 Influence of power electronic converter to the energy efficiency of the LVDC distribution network

## 4.1 Introduction

This chapter studies the effect of the power converter topology and AC-filter design to the energy efficiency of the LVDC distribution network. The analyses are based on the power loss models presented in Chapter 3. The outline of the chapter is following: in Section 4.2, the effect of the converter topology on the energy efficiency is analyzed. The influence of AC filter inductor design and core material to the power losses of the converter are studied in Sections 4.3 and 4.4. The influence of the converter switching components to the energy efficiency is discussed in Section 4.5. The impact of converter modulation frequency to the power losses is analyzed in Section 4.6. The influence of power quality limitations to the power losses is analyzed in Section 4.7. Finally, the effect of the customer load power factor to the power losses of the converters is discussed in Section 4.8 followed by conclusions in Section 4.9.

## 4.2 Converter topology

The power losses of the grid and customer converters by using different converter topologies with iron core AC-filter inductors are shown in (Rekola et al., 2012). However, it was concluded in the previous chapter that the power losses are significantly lower when the amorphous inductor cores are used. Therefore, the power losses of the grid converters and their amorphous core AC-filters are calculated and shown in Fig. 4.1. The used IGBTs and diodes are shown in Table 4.1 (Semikron, 2015a-e). The DC distribution network is supposed to be ungrounded. The used LCL-

filter values are shown in Fig. 2.17a. The required voltage rating of IGBTs used in three-level converter is half of that compared to two-level converter.

**Table 4.1.** The used power switching devices

| Converter | $u_{dc}$ [V] | $I_{ref}$ [A] | IGBT | Clamping diodes | IGBT max voltage [V] |
|---|---|---|---|---|---|
| NPC, Vienna | 750 | 100 | SKM75GB063D | SKKD40F | 600 |
| NPC, Vienna | 1500 | 50 | SKM75GB123D | SKKD40F | 1200 |
| 2-level | 750 | 50 | SKM75GB123D | | 1200 |
| 2-level | 1500 | 50 | SKM75GB176D | | 1700 |
| 12-pulse half-controlled | 1500 | 50 | SKKH27 | | 1200 |

The nominal power of the grid converters producing 750 VDC is 10 kVA and purely resistive load is used. The nominal power of the grid converters producing 1500 VDC is 20 kVA and purely resistive load is used. The required inductance value is reduced by half and the capacitance value is doubled in the LCL-filter when the nominal power is doubled to achieve the same current harmonics compared to AC-filter inductor parameters in Fig. 2.17a. The modulation frequency is 10 kHz.

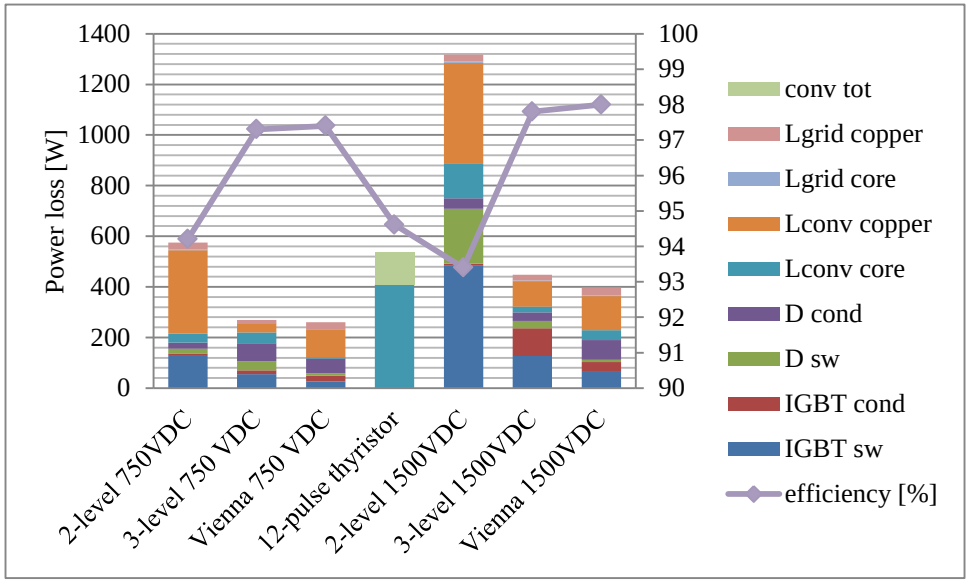


**Fig. 4.1.** Power losses and efficiency of the grid converters and their LCL-filter

The power losses of the 12-pulse half-controlled thyristor rectifier are lower compared to VSCs as shown in Fig. 4.1 but the filter inductor power losses (1 mH) are huge because of low frequency current harmonics. The converter power losses of two- and three-level converter connected to

750 VDC are almost the same. The IGBT switching losses of three-level converter are approximately 40 % of the switching losses of comparable two-level converter. Instead, the conduction losses of the IGBTs are higher in three-level converter, because there are two switching devices in the current path. Moreover, the diode switching and conduction losses are higher in three-level converters because of the clamping-diodes. However, the overall power losses of three-level converter are 47 % of the power losses of two-level converter because of using smaller AC filter inductors. The power losses of Vienna rectifier are slightly lower due to the lower number of power semiconductor switches.

The difference in IGBT switching losses of two- and three-level converters is significant when these are connected to 1500 VDC. The switching losses of three-level converter are approximately 25 % of the switching losses of two-level converter in spite of the increased number of power semiconductor switches. The overall efficiency is highest with Vienna-rectifier producing 1500 VDC and the efficiency of three-level converter is almost as high as that.

The power losses of the customer converters and their amorphous core AC-filter inductors are calculated and shown in Fig. 4.2 when the converters are connected to 750 VDC and in Fig. 4.3 when the converters are connected to 1500 VDC.

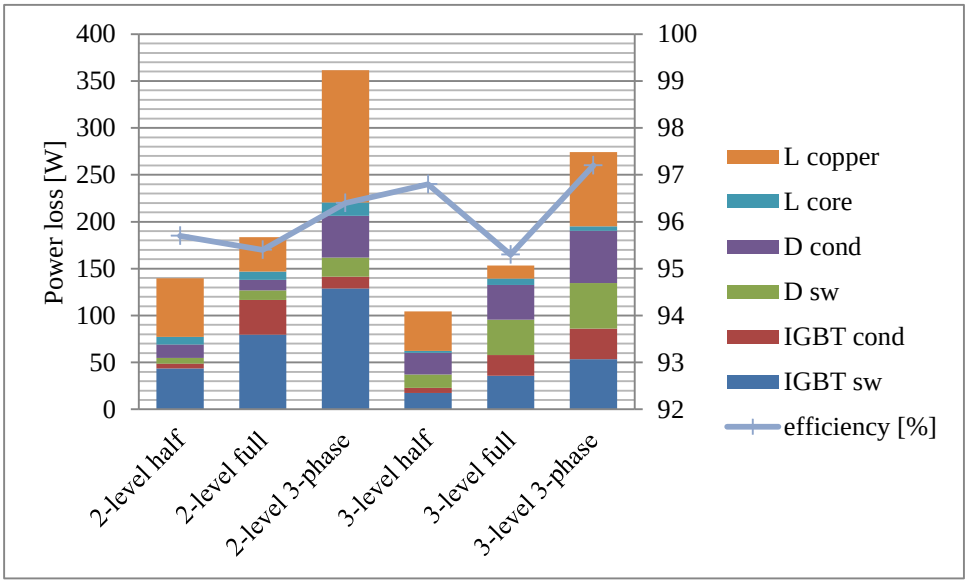


**Fig. 4.2.** The customer converters and their LC-filter power losses with 3.3 kW/phase resistive loads and efficiency for converter connected to 750 VDC

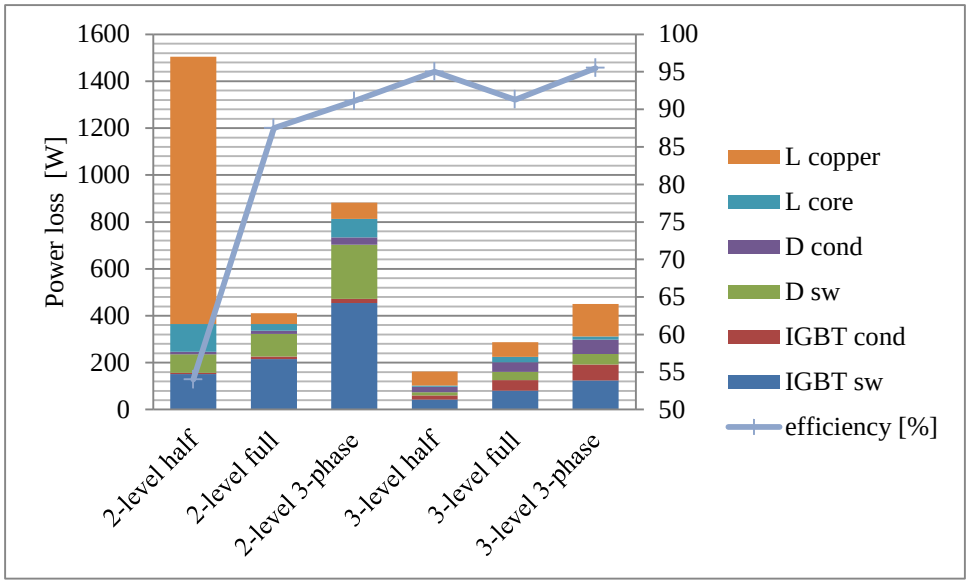


**Fig. 4.3.** The customer converters and their LC-filter power losses with 3.3 kW/phase resistive loads and efficiency for converter connected to 1500 VDC

The nominal power of the single-phase converters is supposed to be 3.3 kVA and nominal power of three-phase converters is 10 kVA. The same power semiconductor switches are used as with the grid converters, shown in Table 4.1. The used LC-filter values are shown in Fig. 2.17b-c. The modulation frequency of the converters is 10 kHz as with the grid converters. The energy efficiency of the three-level full-bridges is lower compared to half-bridges because of two converter-legs in spite of the lower filter inductor power losses as depicted in Figs. 4.2-4.3. The inductor copper losses are very large with the two-level half-bridge connected to 1500 VDC because of large required filter inductor.

The energy efficiency of the converters connected to 750 V DC is higher compared to the converters connected to 1500 VDC because of IGBTs with lower voltage capability. In addition, the modulation index of the converters connected to 750 VDC is higher compared to the converters connected to 1500 VDC if constant 230 Vrms phase voltage is produced to the customer. Therefore, smaller AC-filters are required when all the converter output voltage levels are used.

The power losses of the three-level converters are lower compared to the two-level converters similarly as with the grid converters in Fig. 4.1. The power losses of three-level converter are 76 % of the power losses of two-level converter connected to 750 VDC and 53 % of the power losses of two-level converter connected to 1500 VDC. It can be concluded that the energy efficiency is improved by using three-level converter instead of conventional two-level converter at 1500 VDC voltage level instead of 750 VDC in spite of the low modulation index.

## 4.3 AC-filter inductor design method

The AC-filter inductor can be designed according to multiple design methods as was discussed in Section 2.4.1. The inductor current harmonics needs to be limited to reduce the temperature rise and power losses of the inductor. The required inductance and capacitance values of LC-filter according to different design methods are calculated for three-level full-bridge customer converter (Fig. E.1 in Appendix E) and for three-level three-phase customer converter (Fig. E.2 in Appendix E). The amorphous inductor core power losses are calculated by using the LC-filter parameters shown in Fig. E.1-2. and presented in Fig. 4.4.

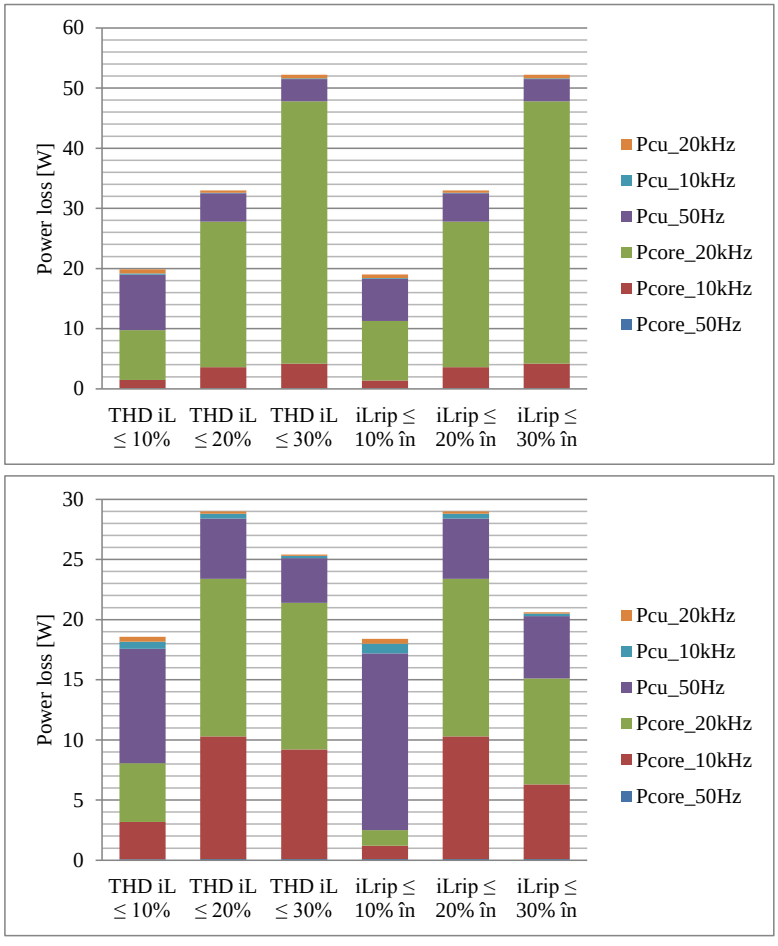


**Fig. 4.4.** The power losses of the LC-filter/phase with amorphous inductor cores connected after the three-level a) single-phase full-bridge and b) three-phase converter

THD of $u_{load}$ is ≤ 2% calculated up to 25 kHz. The nominal power of single-phase converter is 3.3 kVA and the nominal power of the three-level converter is 10 kVA. The modulation frequen-

cy is 10 kHz and the converters are connected to 750 V DC. The DC network is ungrounded. According to Fig. 4.4, the lowest power losses are achieved if the largest inductance value is chosen, i.e., $\Delta i_{L,conv,ripple} \leq 10\ \%\ \hat{\imath}_{nom1}$. The high frequency core losses are minimized when the large inductance value is used. It can be concluded that the inductor core losses are directly proportional to the inductor current harmonics. Instead, most of the copper losses are caused by fundamental frequency current, and therefore, the copper losses would increase when the load increases.

The required inductance and capacitance values of LCL-filter according to different design methods are calculated for three-level NPC grid converter and shown in Fig. E.3 in Appendix E. Same filter can be used also with the Vienna rectifier. THD of $i_{grid} \leq 2\%$ calculated up to 25 kHz. The nominal power of the converter is supposed to be 10 kVA, modulation frequency is 10 kHz and the converter produces 750 V DC. The amorphous inductor core power losses are calculated by using the inductance and capacitance values shown Fig. E.3 in Appendix E and presented in Fig. 4.5. According to Fig. 4.5, the lowest power losses of the LCL-filter are achieved by using the design methods THD $i_{Lconv} \leq 20\ \%$, $\Delta i_{Lconv,ripple} \leq 10\ \%$ or $\Delta i_{Lconv,ripple} \leq 30\ \%$. The differences in the power losses depending on the AC-filter design method are smaller with the grid converter compared to customer converters.

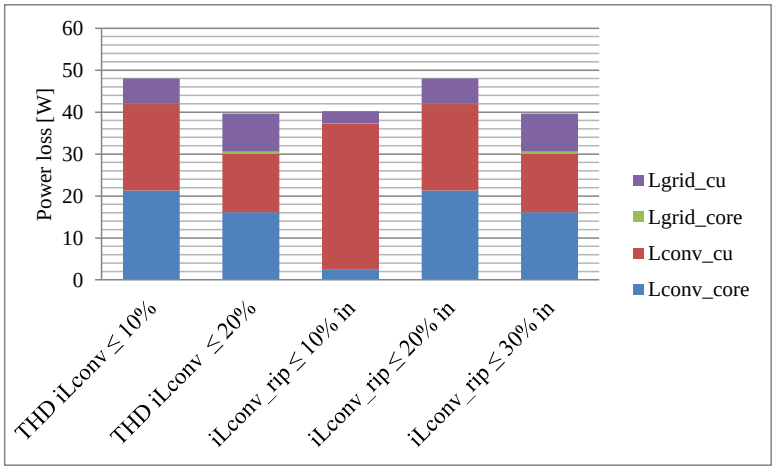


**Fig. 4.5.** The power losses of the LCL filter/phase with amorphous inductor core connected in front of the three-level grid converter or Vienna rectifier

The capacitance value of the LCL-filter in front of the grid converter would be increased from $0.05*C_b$ to $0.1*C_b$ without too large capacitive-current power losses. The required LCL-filter inductance values for the grid converters, which nominal power is 10 kVA are shown in Fig. E.4 in Appendix E. The achieved LCL-filter power losses are shown in Fig. 4.6.

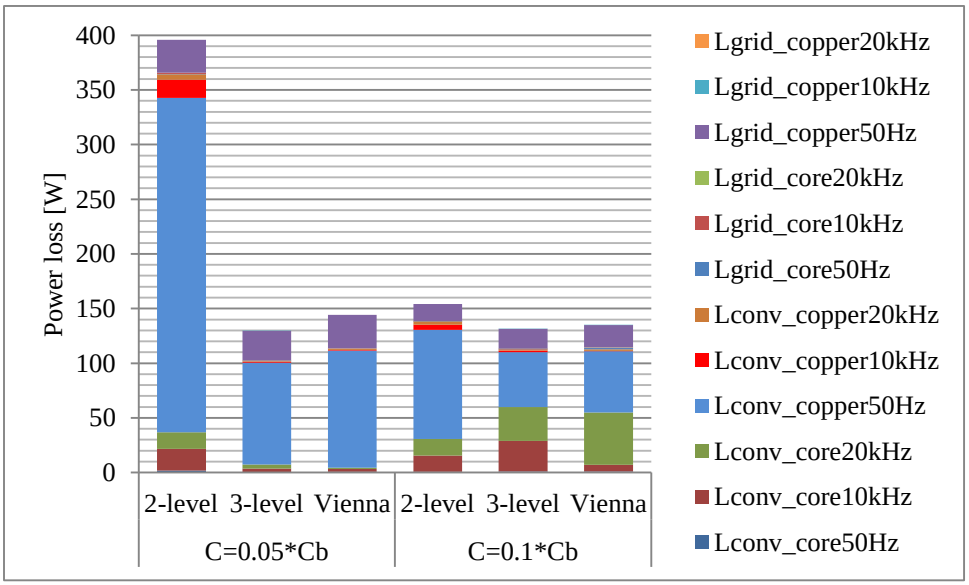


**Fig. 4.6.** The power losses of LCL-filter with the capacitance value of $C = 5\%*C_b$ or $C = 10\%*C_b$ and by using two-level converter, three-level NPC converter and Vienna rectifier

The LCL-filter power losses of three-level NPC converter and Vienna-rectifier are the same with both of the filter capacitance values. Instead, the LCL-filter power losses of two-level converter would be significantly lower if the capacitance value is increased. The inductor core losses at 50 Hz are negligible. The converter-side inductor $L_{conv}$ high frequency copper losses are almost zero with the three-level converters and couple of watts with the two-level converters. The grid-side inductor $L_{grid}$ high frequency copper losses are also negligible. Majority of the copper losses are caused by resistive losses at 50 Hz fundamental frequency. More than 70 % of the overall LCL-filter power losses are caused by fundamental frequency copper losses at the converter-side inductor when the capacitance is $C = 5\%*C_b$. The proportional part of the fundamental frequency copper losses decrease to 40 % of the overall power losses with three-level converters and to 65 % of the losses with two-level converter, respectively, when the capacitance is $C = 10\%*C_b$. Rest of the power losses are high frequency core losses of the converter side inductor $L_{conv}$.

## 4.4 AC-filter inductor core material

The customer loading varies on a large scale and most of the time the customer load is very low compared to the maximum load. Therefore, the energy efficiency of the converters is calculated not only at nominal load but also at partial load conditions. The efficiency of the grid converters and their iron core LCL-filters as well as the efficiency of the customer converters and their iron

core LC-filters as a function of resistive load are shown in Fig. 4.7 (Rekola et al., 2012). The nominal power of the grid converters producing 1500 VDC is supposed to be 20 kVA and the nominal power of grid converters producing 750 VDC is supposed to be 10 kVA. The nominal power of three-phase customer converters is 10 kVA and nominal power of single-phase customer converters is 3.3 kVA. The modulation frequency of the converters is 10 kHz. The DC network is supposed to be ungrounded. Single-phase half-bridges connected to 750 VDC are not taken into account due to lack of DC voltage balance.

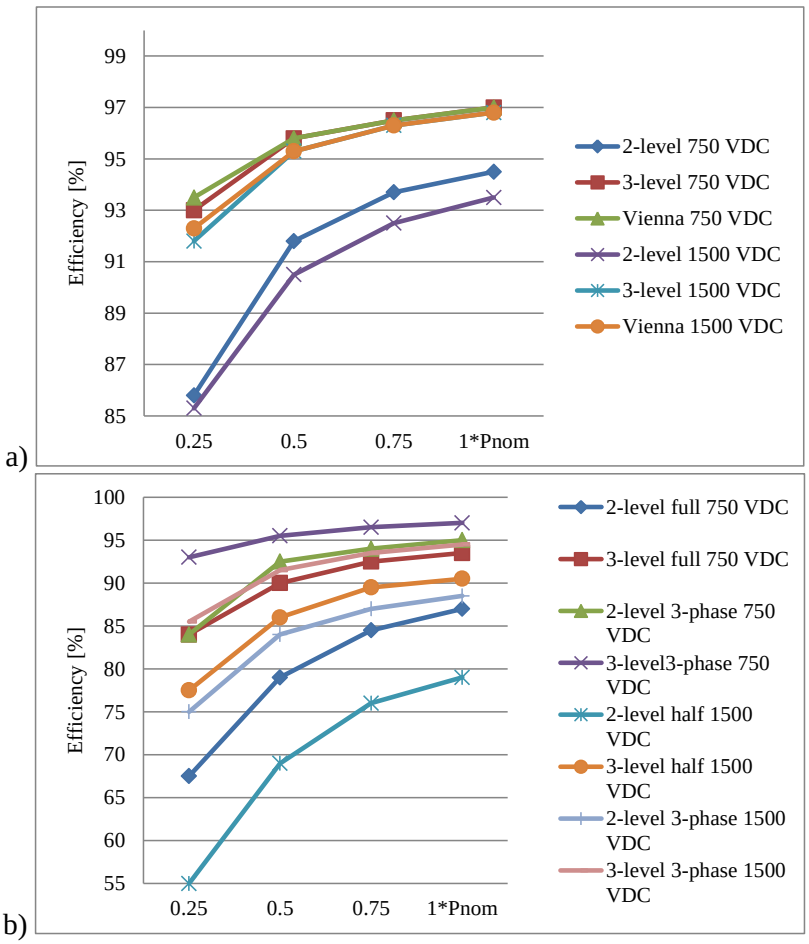


**Fig. 4.7.** Total efficiency of the a) grid converters and iron core LCL-filters, b) customer converters and iron core LC-filters

The efficiency of two-level grid converters is significantly lower compared to the efficiency of three-level grid converters as shown in Fig. 4.7a. The efficiency of the two-level converters decreases at partial loading conditions more severely than the efficiency of three-level converters because of the larger required filter inductors. Majority of the power losses are caused by high frequency current harmonics in the inductor core at partial load conditions. The most efficient grid converters are Vienna rectifier and the three-level NPC grid converter connected to 750 VDC. The efficiency of the grid converters connected to 1500 VDC is slightly lower. The highest cus-

tomer converter efficiency with the iron core filter inductors is achieved with three-level three-phase converter connected to 750 VDC. The main reason for the highest efficiency is the need of the smallest AC-filter inductance compared to other converters. It can be concluded that the converter efficiency is directly proportional to the required AC-filter inductance value when the iron core filter inductors are used.

The efficiency of the grid converters and their amorphous core LCL-filters and the efficiency of the customer converters and their amorphous core LC-filters as a function of resistive load are shown in Fig. 4.8. The two-level half-bridge connected to 1500 VDC is not taken into account because of very low energy efficiency compared to other converter topologies as was illustrated in Fig. 4.3.

a)

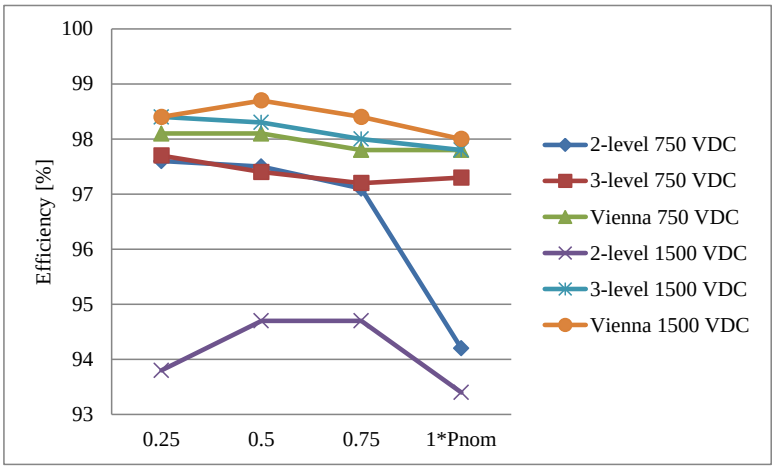


b)

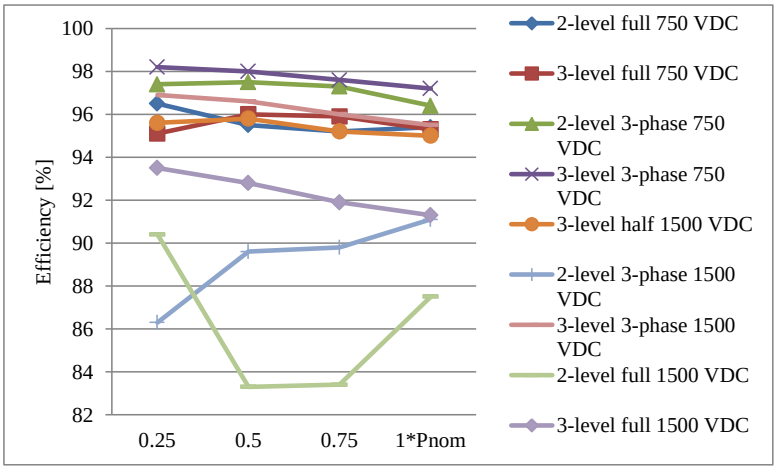


**Fig. 4.8.** Energy efficiency of a) the grid converters and amorphous inductor core LCL-filters, b) the customer converters and amorphous inductor core LC-filters

The no-load losses of amorphous alloy core are low and most of the inductor losses are caused by power losses in the copper windings, which are dependent on the fundamental power. The energy efficiency of the converters with amorphous inductor cores does not decrease in low loading conditions and the efficiency is significantly higher compared to the efficiency with the iron core inductors in the Fig. 4.7. The efficiency of the grid converters connected to 1500 VDC is higher compared to grid converters connected to 750 VDC due to smaller required AC-filter inductors as depicted in Fig. 4.8a. The three-level grid converter producing 1500 VDC have significantly lower power losses compared to power losses of two-level converters because of IGBTs with lower voltage rating. However, the power losses of two- and three-level grid converter producing 750 VDC are almost the same at partial load conditions.

The highest customer converter efficiencies are obtained by using the same topologies as with the iron core filter inductors. The highest efficiencies are achieved with the customer converters connected to 750 VDC because of higher modulation index compared to converters connected to 1500 VDC. The power losses of the single-phase full-bridges are significantly lower with amorphous alloy inductor cores compared to the power losses with iron core inductors. The current harmonics at twice the switching frequency do not cause high power losses in the amorphous inductor core contrary to the iron core. However, the energy efficiency of single-phase converters is lower compared to three-level converters.

## 4.5 Converter power semiconductor switches

Approximately 70 % of the three-level NPC converter power losses are caused by the converter and 30 % of the filter as shown in Fig. 4.2. Therefore, the effect of different power semiconductor switches (cf. Table 4.2) to the power losses of the converters are compared (Semikron, 2015a; Semikron, 2015f; Infineon, 2015; Vincotech, 2015).

**Table 4.2.** The parameters of the used IGBTs

| Component | $V_{CES}$ [V] | $I_C$ [A] | $V_t$ [V] | $V_f$ [V] | $R_{ce}$ [mΩ] | $R_f$ [mΩ] | $E_{on}$ [mJ] | $E_{off}$ [mJ] | $E_{rr}$ [mJ] |
|---|---|---|---|---|---|---|---|---|---|
| SKM75GB063D | 600 | 100 | 1.0 | 0.9 | 18.7 | 10 | 3 | 2.5 | 0.01 |
| SKM100MLI066T 3-level module | 600 | 105 | 0.7 | 0.9 | 9.5 | 6.3 | 2.5 | 4.2 | 1.9 |
| FS3L50R07W2H3F_B11 3-level module | 650 | 100 | 1.6 | 1.6 | 16.3 | 22.5 | 1.2 | 1.6 | 0.01 |
| 10-F106NIA 100SA-M135F 3-level module | 600 | 100 | 1.7 | 1.7 | 25 | 5.7 | 2.4 | 3.8 | 2.2 |

Power losses of three-level NPC customer converter with 10 kW load connected to 750 V DC by using the IGBTs shown in Table 4.2 are illustrated in Fig. 4.9. The differences in the power losses achieved with IGBTs by different manufacturers are negligible. The efficiency achieved with all components is approximately the same, 98 %, except the last one, which power losses are slightly higher.

Since significant differences in the converter power losses are not achieved by using different IGBTs, the power losses by using wide bandgap, silicon carbide (SiC) MOSFETs are calculated. The switching losses of SiC MOSFETS are significantly lower compared to conventional silicon IGBTs due to absence of tail current and fast recovery characteristics of the body diode (Hazra et al, 2015; Wang et al., 2013). In addition, the on-state resistance is lower compared to conventional silicon MOSFETs and the external freewheeling diode is not needed due to fast and robust intrinsic body diode (Hazra et al, 2015; Wang et al., 2013). The conduction losses of the MOSFET are calculated as follow hence there is not the zero-voltage drop as with the IGBTs

$$P_{cond,MOSFET} = \frac{1}{T}\int_0^T R_{ds,on} {i_{MOSFET}}^2 dt \tag{4.1}$$

where $R_{ds,on}$ is the drain-source on-state resistance and $i_{MOSFET}$ is the current flowing through the MOSFET.

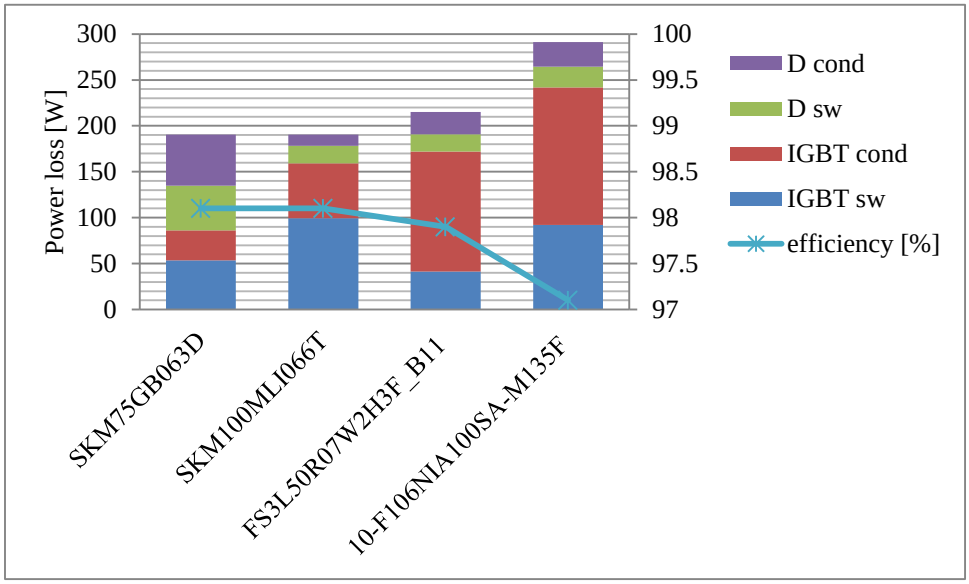


**Fig. 4.9.** Power losses of three-level NPC customer converter at nominal load with IGBTs

The power losses of the same three-level NPC customer converter with 10 kW load are calculated by using SiC MOSFETs shown in Table 4.3 (Microsemi, 2015; Microsemi, 2015a; Cree, 2015; Cree, 2015a; Cree, 2015b; Cree, 2015c). The current capability of all the analyzed SiC MOSFETs is not 100 A hence multiple components are connected in parallel to achieve the same current capability as with the IGBTs, marked as "number of comp" in Table 4.3. The current is supposed to be divided evenly between the parallel connected components.

**Table 4.3.** The parameters of the used SiC MOSFETs

| Component | Number of comp. | $V_{CES}$ [V] | $I_C$ [A] | $V_f$ [V] | $R_{ds,on}$ [mΩ] | $R_f$ [mΩ] | $E_{on}$ [mJ] | $E_{off}$ [mJ] | $E_{rr}$ [mJ] |
|---|---|---|---|---|---|---|---|---|---|
| APTMC60TL11CT3AG 3-level module | 5 | 600 | 21 | 2.0 | 150 | 0 | 0.45 | 0.25 | 0 |
| APTMC120AM20CT1AG | 1 | 1200 | 108 | 2.2 | 17 | 0 | 2.2 | 1.2 | 0 |
| CCS050M12CM2 | 2 | 1200 | 50 | 2.0 | 43 | 0 | 1.1 | 0.6 | 0 |
| CCS020M12CM2 | 5 | 1200 | 20 | 1.8 | 145 | 0 | 0.41 | 0.07 | 0 |
| CAS120M12BM2 | 1 | 1200 | 120 | 1.9 | 23 | 0 | 1.7 | 0.4 | 0 |
| CAS100H12AM1 | 1 | 1200 | 105 | 2.5 | 20 | 0 | 3.9 | 1.8 | 0.5 |

The power losses of the converter by using SiC MOSFETs are shown in Fig. 4.10.

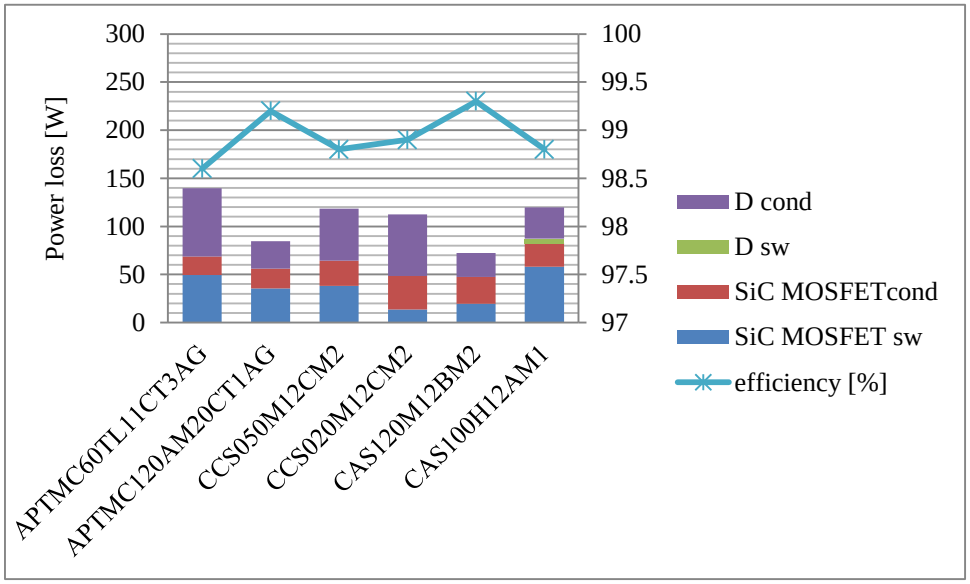


**Fig. 4.10.** Power losses of three-level NPC customer converter at nominal load with SiC MOSFETs

According to Fig. 4.10, the highest energy efficiency achieved with the conventional IGBTs is 98.1 % whereas with the SiC MOSFETs the highest efficiency is 99.3 %. The energy efficiency of the most suitable grid and customer converter topologies, evaluated in the previous Section 4.4, is calculated by using SiC MOSFETs instead of conventional IGBTs and shown in Fig. 4.11. The same SiC MOSFETs with 1200 V voltage capability are used both with the two- and three-level converters (CAS120M12BM2). The efficiency of two- and three-level converters increases approximately 1 % when conventional IGBTs are replaced by SiC MOSFETs according to Fig. 4.8 and Fig. 4.11.

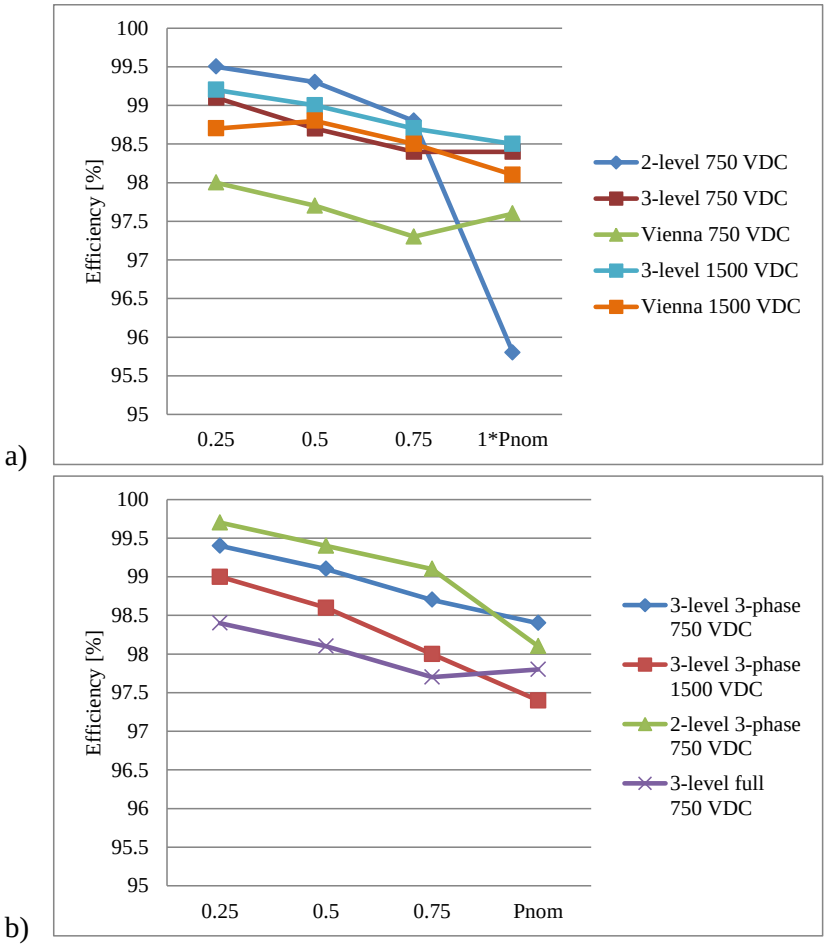


**Fig. 4.11.** Energy efficiency of a) the grid converters and amorphous inductor core LCL-filters, b) the customer converters and amorphous inductor core LC-filters with SiC MOSFETs

The efficiency of Vienna-rectifier does not increase, because it includes only three IGBTs or SiC MOSFETs. Therefore, majority of the power losses are conduction losses of diodes instead of switching and conduction losses of IGBTs or SiC MOSFETs. The efficiency of three-level NPC

grid converter is higher compared to Vienna rectifier when IGBTs are replaced by SiC MOSFETs because of low switching losses. It can be concluded that the efficiency increase achieved by replacing three-level NPC converter by Vienna rectifier is not relevant when SiC MOSFETs are used instead of IGBTs. Moreover, the energy efficiency of two-level converter connected to 750 VDC is higher compared to three-level NPC converter at low loading conditions because of lower number of switching devices when the voltage capability of the switching devices is the same in two- and three-level converters.

## 4.6 Converter modulation frequency

The modulation frequency of the power switching devices has an effect to the converter power losses as well as power losses and size of the AC filter. The power losses and efficiencies of the ungrounded three-level NPC grid and customer converters and their AC filters connected to 750 VDC with three different modulation frequencies at nominal resistive load and with one fourth of the nominal resistive load are presented in Fig. 4.12. The amorphous core inductors are used. The $THD_{40kHz}$ of grid current and customer load voltage are ≤ 2 % with nominal load. Both the conventional IGBTs as well as SiC MOSFETs are used.

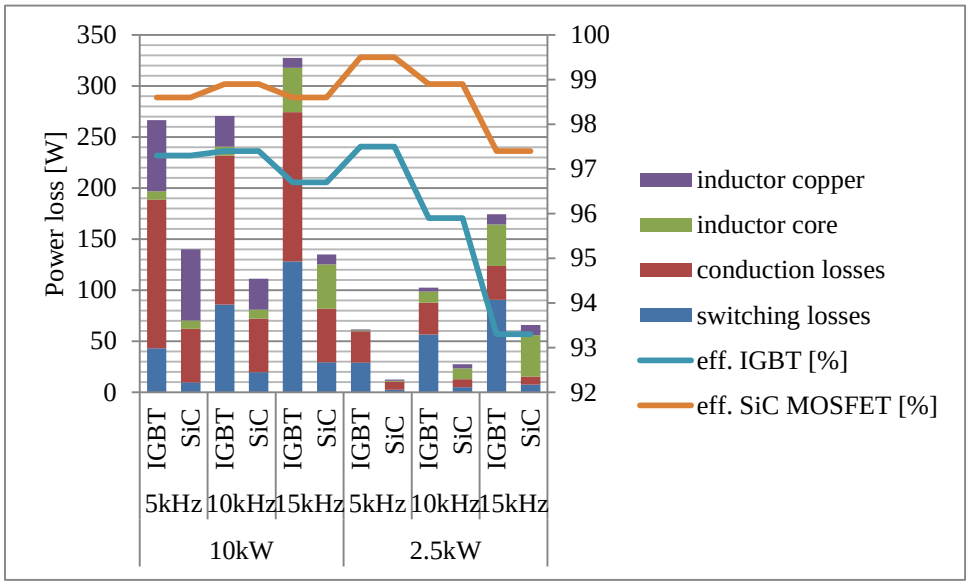


**Fig. 4.12.** Simulated losses of the three-level NPC customer converter with the modulation frequencies of 5 kHz, 10 kHz and 15 kHz wih the nominal load and with 0.25*$P_{nom}$ load by using IGBTs (SKM100MLI066T) and SiC MOSFETs (CAS120M12BM2)

The converter switching losses rise almost linearly as the switching frequency increases hence the switching losses are proportional to the modulation frequency. The conduction losses increase

along the increasing load ($P_{loss\_cond} \sim i^2$). The smaller AC-filter inductance value can be used if the modulation frequency is increased but it does not lead to lower total losses as shown in Fig. 4.12 because of increased converter switching losses as well as increased inductor core and copper high frequency power losses (Rekola and Tuusa, 2014b).

The power losses are the same in spite of the modulation frequency of 5 kHz or 10 kHz at nominal load when IGBTs are used. Instead, the energy efficiency increases when the modulation frequency increase from 5 kHz to 10 kHz at nominal load when SiC MOSFETs are used. The converter efficiency is substantially higher if IGBTs are replaced by SiC MOSFETs. The differences in the total efficiency are low at nominal load depending on the modulation frequency but the effect is significant at partial load conditions. The power losses would be lower if the modulation frequency is 5 kHz instead of 10 kHz at partial load conditions. Unfortunately, the switching frequencies below 10 kHz cause audible noise, and therefore, these are not possible to be used especially in the customer converter.

The highest efficiency at nominal load with IGBTs as well as with SiC MOSFETs is achieved by using 10 kHz switching frequency. The converter modulation frequency would be increased by using SiC MOSFETs without the significant increase of switching losses of the converter. However, the high frequency power losses of the AC filter inductor limits the increase of modulation frequency. The inductor core materials, which are designed to higher switching frequencies, such as ferrite, should be used if the modulation frequency will be increased. Unfortunately, the saturation flux density of the ferrite is approximately 1/3$^{rd}$ of that compared to amorphous alloy, and therefore, multiple ferrite core inductors should be connected in parallel to achieve the required power capability.

## 4.7 Power quality limitations

The standards about the power quality in the LVDC distribution are not yet totally established. The standards IEC 61727, IEC 61000-3-2, EN 60555 and IEEE Std 929-2000 limits the maximum grid current THD to 5 % whereas the standard EN 50160 limits the customer voltage THD $\leq$ 8 % up to 2 kHz frequency. The power losses of the ungrounded three-level NPC grid and customer converter with different THD limits are presented in Fig. 4.13. The converters are connected to 750 VDC. The amorphous core filter inductors are used. The customer voltage THD limit is set from 2 %, 4% or 8 % and the grid current THD limit is set from 2 % to 5 % calculated up to 25 kHz. The modulation frequency is 10 kHz and the nominal resistive load, 10 kW, is used.

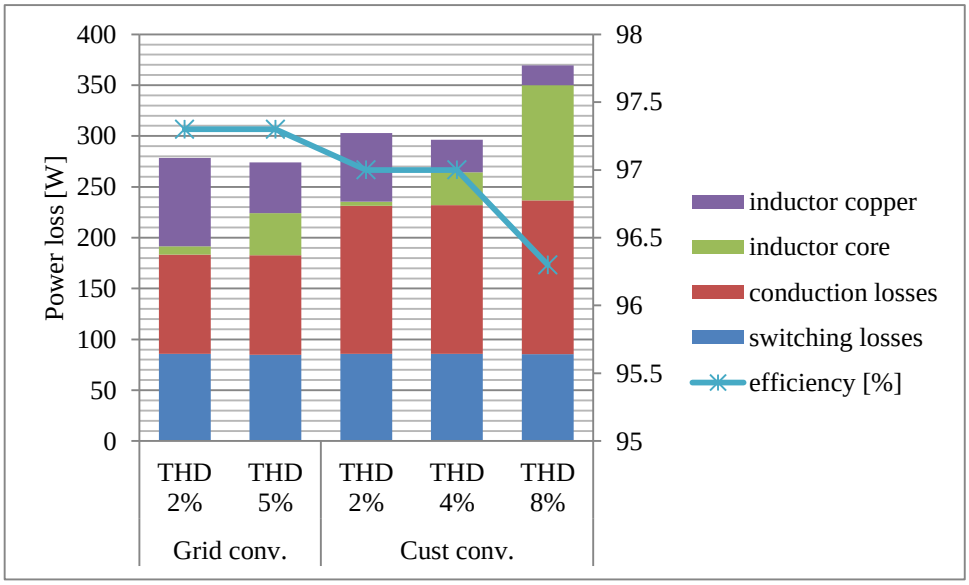


**Fig. 4.13.** Simulated three-level NPC converter power losses with the different THD limits of grid current and customer voltage

The converter power losses are almost constant in spite of the THD limit as depicted in Fig. 4.13. Instead, the THD limit has an effect to the size and power losses of the required AC filter. The required inductance value decreases hence the inductor copper losses decrease as the THD limit increases but at the same time, the inductor high frequency core losses increase. The efficiency of the grid converter decreases if the grid current allowed THD value is increased. The power losses of the customer filter decrease by half when the customer voltage THD limit is increased from 2 % to 4 % due to smaller required AC-filter inductance. However, the power losses are increased if the customer voltage THD limit is further increased to 8 %. It should be noted that the increased current harmonics increase also the power losses of the isolation transformer if it is required. It can be concluded that the power quality limitations has a significant effect to the power losses of the customer filter but the effect to the overall energy efficiency is not significant (Rekola and Tuusa, 2014b).

## 4.8 Customer power factor

The customer load is supposed to be purely resistive in the previous analysis. For instance heating and sauna stove are purely resistive loads but washing machine, lighting, dish washer and vacuum cleaner are inductive loads. The power losses of three-level three-phase converter with 10 kVA load and with variable power factor are shown in Fig. 4.14. The modulation frequency is assumed to be 10 kHz and the converter is connected to 750 VDC. Power semiconductor devices are defined in Figs. 2.3 and 2.7b.

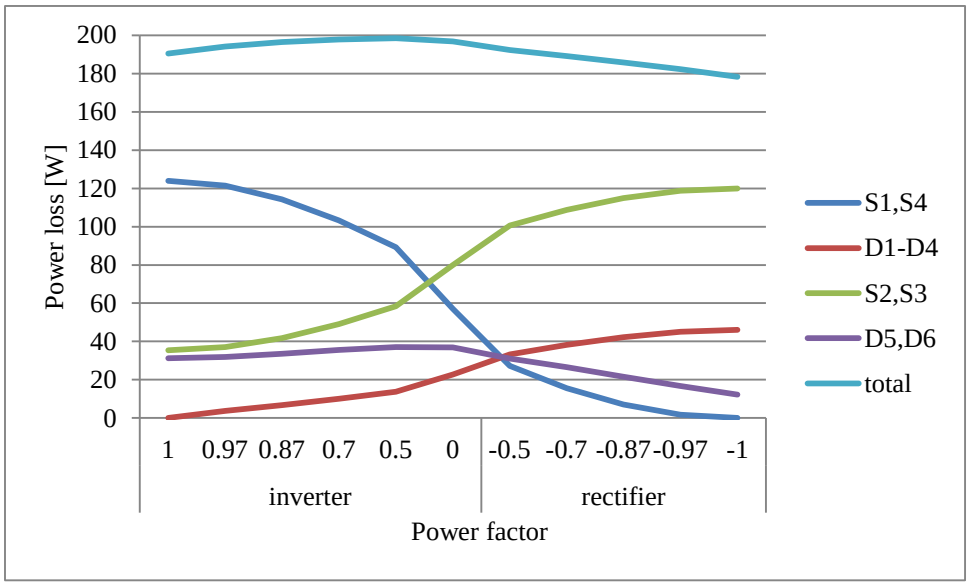


**Fig. 4.14.** The power losses of three-level three-phase converter with 10 kVA load and with variable power factor by using IGBT SKM100MLI066T

The difference in total converter power losses is not significant depending on the power factor as depicted in Fig. 4.14. However, the stresses of different switching components vary on a large scale. The analytical equations for the current rms and average values for the power semiconductors of three-level converter were given in (3.11) - (3.14) (Dieckerhoff et al., 2005; Moia et al., 2012). The current of outer IGBTs, $S_1$ and $S_4$ is zero in the rectifier mode and the current of anti-parallel diodes $D_1$-$D_4$ is zero in the inverter mode when the load is purely resistive (Rekola and Tuusa, 2011a). The maximum power losses of outer IGBTs are achieved at unity power factor in inverter mode and the maximum power losses of inner IGBTs are achieved at unity power factor in rectifier mode, respectively, as illustrated in Fig. 4.14 (Rekola and Tuusa, 2011a). IGBTs $S_2$ and $S_3$ are conducting during the whole positive or negative half cycle and the average current stresses of these IGBTs are constant in spite of the modulation index. It can be concluded that the average current stresses of IGBTs and diodes are not equal in three-level converter as in two-level converter. The uneven power loss distribution might lead to a decreased power capacity due to unsymmetrical temperature distribution of the semiconductor junction (Franquelo et al., 2008; Rodriguez et al., 2010). The unequal loss distribution limits the switching frequency of the three-level converter, because the semiconductor losses are linearly dependent on their temperature (Jing et al., 2013).

The active NPC-converter (ANPC) is created because of the problems caused by uneven power loss distribution in the conventional three-level NPC. The clamping diodes are replaced by similar

IGBTs as the other power semiconductor switches as shown in Fig. 4.15. The topology was introduced by Brückner and Bernet (2001). Four zero voltage states can be realized instead of two, and the distribution of conduction losses can be controlled during these zero states by selection of the upper or lower clamping IGBT and diode path (Brückner and Bernet, 2011). The conduction losses of the ANPC are lower compared to NPC because of lower on-state resistance $R_{ds,on}$ of the IGBTs compared to passive clamping diodes (Schöner et al., 2014). The switching losses of the ANPC might be lower compared to NPC with the properly designed, loss-balancing control scheme (Schöner et al., 2014). The efficiency of the ANPC is better compared to NPC with low load but the efficiency of NPC is higher with high power (Rodriguez et al., 2010; Schöner et al., 2014).

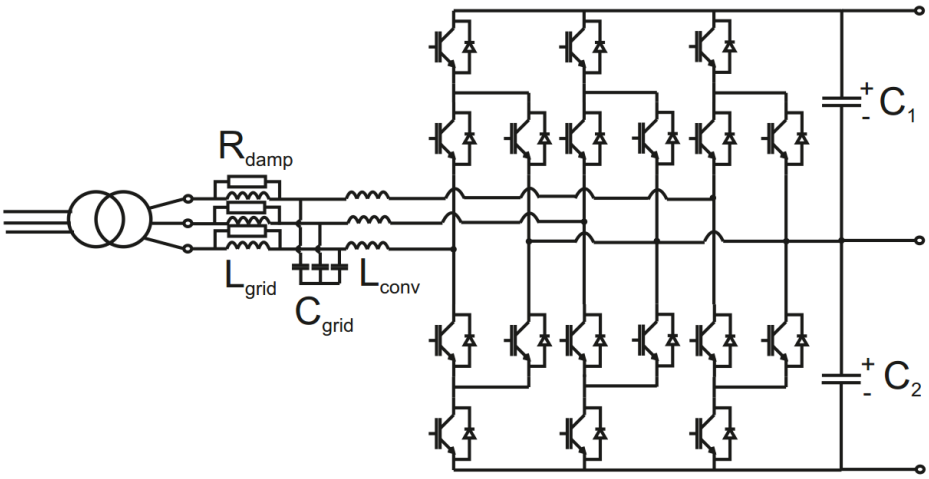


**Fig. 4.15.** Active NPC

## 4.9 Conclusions

The influence of converter topology, AC filter design method and filter inductor core material, used power switching devices, modulation frequency, power quality limitations and customer power factor to the energy efficiency of the converters in the LVDC distribution network is analyzed.

The size of the required AC-filter inductance is minimized if LCL-filter is connected in front of the grid converter but the LC-filter is adequate with the customer converter. The inductor current ripple should be ≤ 10 % of the current fundamental component amplitude to minimize the filter power losses. It can be concluded that the filter inductor core material has a significant effect to the power losses. The filter inductor core with low no-load losses, e.g. amorphous core, should be definitely used, because the customer load is most of the time very low compared to the momen-

tary maximum load. The energy efficiency of the converters is almost constant in spite of the loading conditions when amorphous core AC-filter inductors are used. Instead, the energy efficiency is low and decrease deeply as the load decreases if the conventional M400-50 laminated iron core filter inductors are used.

The highest grid converter energy efficiency is achieved with Vienna rectifier connected to 1500 VDC if conventional IGBTs and amorphous inductor cores are used. The current stresses are lower compared to the grid converter connected to 750 VDC and the voltage capability of the power semiconductors is half of that required with two-level converter. The energy efficiency of three-level NPC grid converter connected to 1500 VDC is almost as high as the efficiency of the Vienna rectifier. The highest energy efficiency is achieved if two- or three-level customer converters are connected to 750 VDC because the modulation index is maximized. The energy efficiency of three-level converter is higher at nominal load when conventional IGBTs are used. It can be concluded that the power loss difference between the IGBTs with voltage rating of 600 V or 1200 V is not so large that significant efficiency increase would be achieved by using three-level converter. Instead, the notable power loss increase is shown as the voltage capability of IGBTs increase from 1200 V. Therefore, the use of three-level converters is worthwhile especially at higher voltage levels.

The converter power losses do not change significantly depending on the use of IGBTs by different manufacturers. However, the energy efficiency of the converters is increased approximately by 1 % if the conventional silicon IGBTs are replaced by wide bandgap SiC MOSFETs. The highest energy efficiency is achieved with two-level grid converter connected to 750 VDC and with three-level NPC grid converter connected to 1500 VDC when conventional IGBTs are replaced by SiC MOSFETs. The efficiency of Vienna rectifier is lower compared to three-level NPC converters when IGBTS are replaced by SiC MOSFETs.

The decision of the use of two- and three-level customer converters connected to 750 VDC should be done according to the acquisition and maintenance costs. The three-level converter includes larger number of power semiconductor switches but voltage capability is half of that with the comparable two-level converter. In addition, the AC-filter inductors are half smaller. The drawback of three-level converters is unbalanced current stresses of the power semiconductor switches. The conventional three-level converter would be replaced by and ANPC topology enabling more equal power loss and lower power losses especially at partial load conditions.

The power losses of the converters and filters would be lower at low load if the modulation frequency of the converters would be lower than the used 10 kHz. Unfortunately, the modulation frequency decrease would lead to increased audible noise. The modulation frequency should not

increase from 10 kHz if conventional IGBTs are used due to increased switching losses, which are linearly proportional to modulation frequency. Instead, the switching frequency can be increased if SiC MOSFETs are used due to low switching losses. However, the increased high frequency power losses of the amorphous alloy inductor core limit the modulation frequency increase.

It can be concluded that the power quality limitations has an effect to the power losses and size of the customer filter but the effect to the overall energy efficiency is insignificant as long as the current and voltage THD is limited to be lower than 10 % calculated up to three times of the modulation frequency.

# 5 Effect of network configuration on energy efficiency of LVDC distribution network

## 5.1 Introduction

For facilitating the design of cost effective LVDC distribution networks, the total losses of the LVDC distribution network with different network configurations are evaluated and compared. The theoretical power loss analysis are based on assumption that the power losses of the LV network decreases with the use of DC, because resistive losses in cables are lower due to higher voltage level, lack of reactive power and skin effect (Nilsson et al., 2004; Engelen et al., 2006; Anand et al., 2010; Sannino et al., 2003; Kakigano et al., 2010; Kakigano et al., 2012; Shenai et al., 2011; Ali et al., 2012; Gwon et al., 2014). However, the amount of DC current harmonics depend on the used network configuration, converter topologies, customer behavior, exist of balancing circuit, control methods, control parameters and modulation methods of the converters. The target is to find the LVDC distribution network configuration with the lowest losses depending on the DC network length and identify the main power loss sources.

Section 5.2 describes influence of LVDC network grounding method to the power losses. The influence of DC network configuration including the used DC voltage level, DC cable length and the need of DC voltage balancing to the power losses are discussed in Section 5.3. The influence of converter topology depending on the used power semiconductor switches is discussed in Section 5.4. The influence of customer single-phase loads to the power losses are presented in Section 5.5. Finally, the influence of real Finnish customer loading behavior to the energy efficiency of LVDC distribution network is calculated and discussed in Section 5.6. The conclusions are drawn in Section 5.7.

## 5.2 Grounding method

The LVDC distribution network might be grounded or ungrounded as discussed in Section 2.5.1. The three-phase customer converter operates as three parallel-connected single-phase converters, when the whole LVDC distribution network is grounded thus increasing the current harmonics. The required filter parameters for three-level NPC grid and customer converters in the bipolar DC network, presented in Figs. 2.10a and 2.12, are shown in Table 5.1. Amorphous core filter inductors are used. The grid converter nominal load is 20 kVA producing 1500 VDC and the nominal load of the customer converter connected to 1500 VDC is 10 kVA. The modulation frequency of the converters is 10 kHz.

**Table 5.1.** Required AC-filter parameters in grounded and ungrounded DC network

| | Grid converter | | | Customer converter | |
|---|---|---|---|---|---|
| | $L_{grid}$ [mH] (pu) | $C_{grid}$ [μF] (pu) | $L_{conv}$ [mH] (pu) | $L_{cust}$ [mH] (pu) | $C_{cust}$ [μF] (pu) |
| Ungrounded | 0.3 (0.3 %) | 5 (5 %) | 1.1 (1 %) | 1.5 (3 %) | 4 (2 %) |
| Grounded | 0.4 (0.4 %) | 5 (5 %) | 1.6 (1.6 %) | 1.5 (3 %) | 6 (3 %) |

The simulated power losses of the grounded and ungrounded LVDC distribution network are shown in Fig. 5.1. The load is supposed to be purely resistive and it varies from 2.5 kW to 10 kW. Length of the DC cable is 1 km. The typical underground cable in LV distribution networks, AXMK 4*16mm$^2$, is used. The power losses of the supplying transformer, which decrease the AC voltage to at maximum 1kV AC, are not taken into account in the presented loss analysis.

The simplest way to realize the galvanic isolation in the ungrounded LVDC network is to install 10 kVA 50 Hz 400 V/400 V isolation transformer between the customer converter and the customer electrical installations, as shown in Fig. 2.10a. Unfortunately, the transformer is bulky and expensive. The isolation transformer causes 32 % of the total losses with the low load as shown in Fig. 5.1. The proportional part of the isolation transformer power losses decreases as the load increase. The transformer causes still 26 % of the overall power losses with nominal load. The customer converter power losses are large compared to grid converter power losses because of the low modulation index.

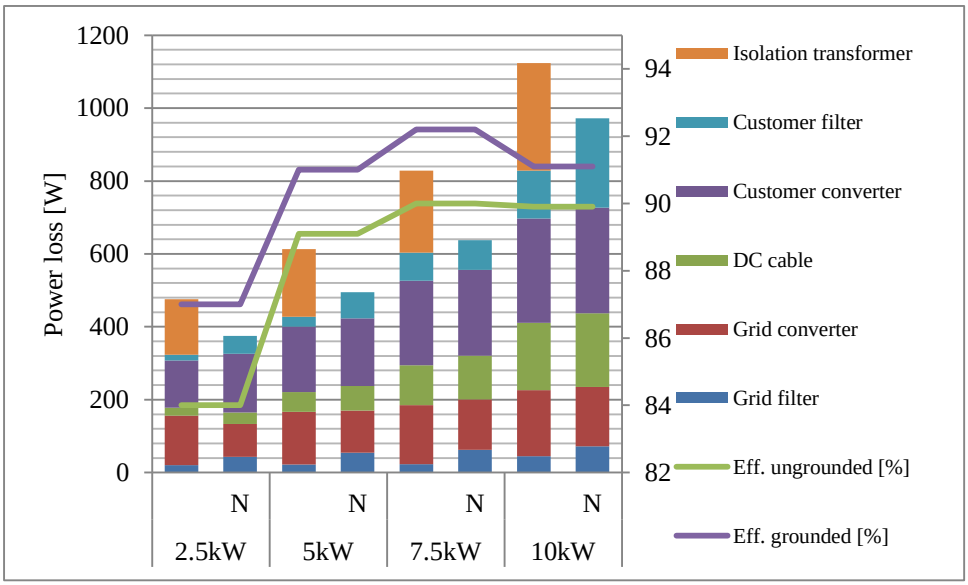


**Fig. 5.1.** Simulated power losses of ungrounded and grounded (marked as N) 1 km long LVDC distribution network with three-level three-phase grid and customer converters

The power losses of the grid converter are almost the same in the grounded and ungrounded networks. The grid filter losses are higher in the ungrounded network but the converter losses are slightly lower. The power losses of the customer filter are also higher in the grounded LVDC network because larger filters are needed to fulfill the power quality limitations. In addition, the power losses of the DC cable are approximately 10 % higher in the grounded network because of the additional grounding wire. In spite of these, the efficiency of the grounded DC network is approximately 3 % higher at partial load and 1 % higher at nominal load compared to the ungrounded network, because the isolation transformer is not needed.

## 5.3 LVDC distribution network configuration

The DC network might be unipolar consisting of one voltage level and the neutral or bipolar consisting of two voltage level and the neutral as shown in Section 2.5. Both halves of the bipolar DC distribution network can be loaded asymmetrically when the DC network is supplied by two grid converters without additional DC voltage balancing. Instead, the DC voltage balancing circuit is needed if the whole DC network is supplied by one grid converter.

The customer converter efficiency is better if the converter is connected to 750 VDC instead of 1500 VDC, because the modulation index of the converters is > 0.5 when 230 VAC phase voltage

is produced to the customer as shown in Section 4.2. The modulation index of the customer converter can be maintained high by using the isolation transformer with the voltage transformation ratio of 800 V/400 V instead of 400 V/400 V as shown in Fig. 5.2. Larger switching and conduction losses of the IGBTs rated at higher voltage increase the losses but on the contrary, the required current rating is reduced by half compared to converters connected to 750 VDC due to higher voltage level.

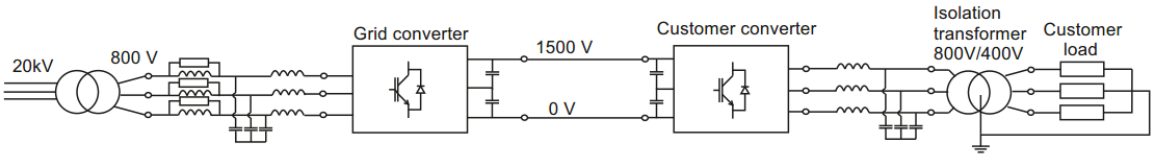


**Fig. 5.2.** A unipolar LVDC distribution network

The simulated DC voltages, DC currents, input current of the grid converter, and customer converter currents, are shown in Fig. 5.3. The converter load is 10 kW. The 3rd harmonic component occurs in the DC voltages but not in the DC currents because unipolar network without the neutral conductor is used.

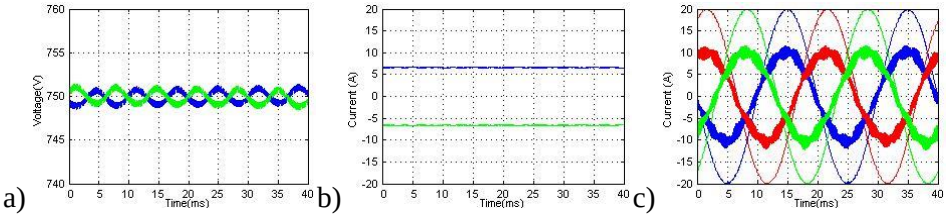


**Fig. 5.3.** Simulated a) DC voltages, b) DC currents, c) input current of the grid converter and customer converter currents when the load converter is connected to 1500 V DC

The total power losses and efficiencies of the LVDC distribution network supplied by one or two grid converters are illustrated in Fig. 5.4. Three-level NPC converters with 10 kHz modulation frequency and amorphous core filters are used. The power losses of the network configuration with 10 kW load connected between the negative pole and neutral, as in Fig. 2.10c, are marked as "400V/400V". The losses of the configuration presented in Fig. 2.10c, where 5 kW loads are connected to both halves of the DC link is marked as "400V/400V sym". The losses of the configuration presented in Fig. 5.2 with 10 kW load are marked as "800V/400V" in Fig. 5.3. The power losses are calculated by using two different lengths of the DC-cable: 200 m and 1 km.

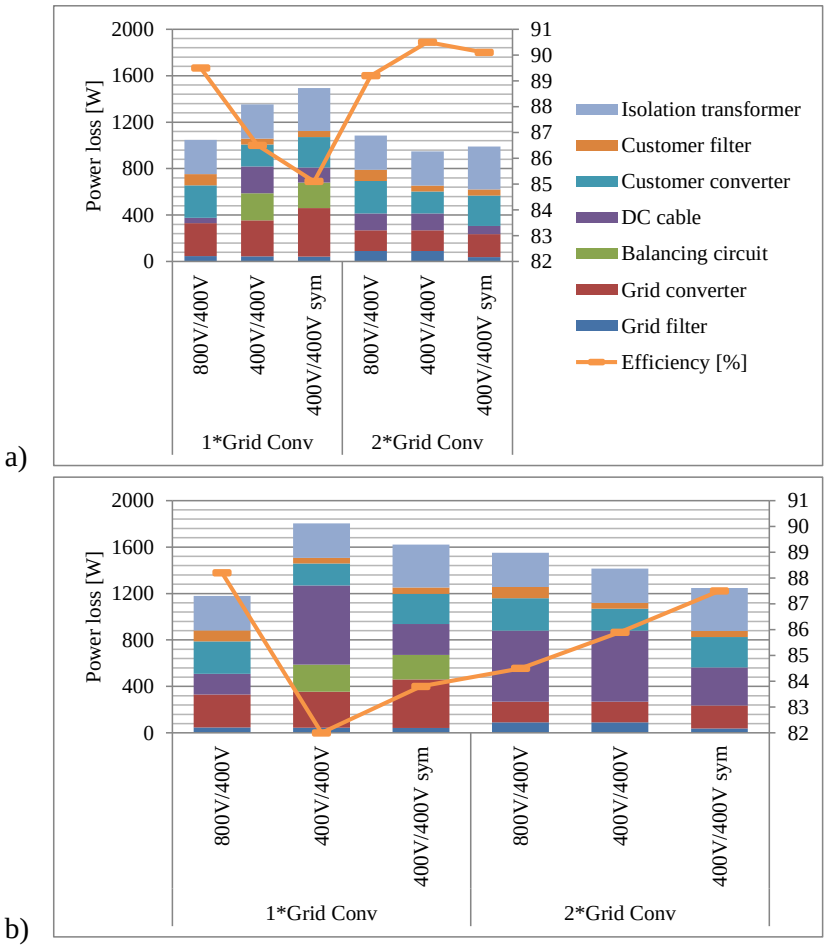


**Fig. 5.4.** Simulated total losses of the LVDC distribution network when the load converter is connected to 750 V DC or 1500 V DC with a) 200 m DC cable and b) 1 km DC cable

The power losses of two grid converters connected to 750 VDC are lower compared to one grid converter producing 1500 VDC. Instead, the power losses of the LCL-filter are lower due to lower current value when only one grid converter connected to 1500 VDC is used. The balancing circuit is needed when the DC network is supplied by one grid converter, causing additional power losses as shown in Fig. 5.4. The balancing circuit causes approximately 15 % of the total losses of the LVDC distribution network. The balancing inductor losses are insignificant, approximately 20 W, but the losses of IGBTs and diodes in the balancing leg are higher compared to power losses of the one converter leg due to lack of connection to the DC link midpoint. The power losses of the balancing circuit depend on balancing circuit configuration, used IGBTs and diodes and their modulation frequency as well as inductor core material and inductance value. The same semiconductors as in the grid converter are used with 10 kHz modulation frequency in the balancing circuit.

The power losses of the DC cable are lower if both the grid and customer converters are connected to 1500 VDC compared to 750 VDC. 3rd harmonic component do not exist in the DC current as shown in Fig. 5.3. However, the DC grid is more reliable if the grid is supplied by two grid converters instead of one. The other part of the bipolar DC grid might be used in spite of the fault in the other part (Lago et al., 2011).

The highest energy efficiency of the ungrounded LVDC distribution network is achieved, when both the grid converter and customer converter are connected to 750 VDC if the length of the bipolar DC network is 600 m at maximum. The total power losses are minimized especially due to low losses of the customer converters. The isolation transformer causes approximately 20 % of the total losses. The increased DC cable losses decrease the efficiency when the bipolar LVDC network is longer than that. Slightly higher energy efficiency is achieved by using the unipolar network configuration, i.e. the network is supplied by one grid converter and the customer converter is connected to 1500 VDC and by using the isolation transformer having a voltage transformation ratio of 800V/400V as shown in Fig. 5.4b if the DC cable is longer than 600 m. The total losses are minimized in spite of the increased customer converter power losses due to decreased DC cable power losses.

## 5.4 Converter topology depending on the used power semiconductor switches

The customer converter bridge power losses of two- and three-level converters with amorphous core AC filter inductors are almost the same when these are connected to 750 VDC as shown in Fig. 4.8. Therefore, the overall power losses of the ungrounded bipolar LVDC distribution network shown in Fig. 2.10b by using two- and three-level grid and customer converters are calculated and presented in Fig. 5.5. The IGBTs with lowest power losses (SKM100MLI066T) are used (Semikron, 2015f). The DC cable length is supposed to be 1 km. The typical underground cable in LV distribution networks, AXMK 4*16mm$^2$, is used.

The energy efficiency with 2.5 kW and 5 kW loads is same with two- and three-level converters. Instead, as the load increases to be higher than half of the nominal load, the efficiency of the LVDC network is higher when three-level converters are used. The power losses of two- and three-level converter power semiconductor switches, the power losses of the DC cable and the power losses of the isolation transformer are almost the same. However, the power losses of the AC filters are lower when three-level converters are because of smaller required filter inductors. The efficiency increase is approximately 1 % with 7.5 kW load and 2 % with the nominal load compared to the efficiency of the LVDC distribution network with two-level converters.

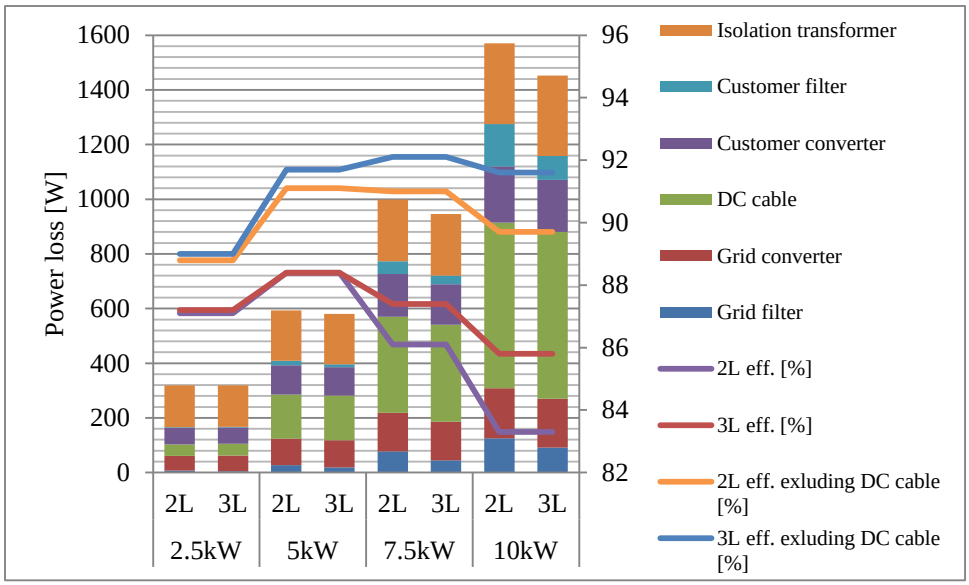


**Fig. 5.5.** Simulated total power losses of 1km long ungrounded LVDC distribution network with two- and three-level grid and customer converters with conventional IGBTs

The power losses of the ungrounded LVDC distribution network, which length is 1km, with two- and three-level converters are shown in Fig. 5.6 when the IGBTs are replaced by SiC MOSFETs. The SiC MOSFET with lowest power losses are used (CAS120M12BM2) (Cree, 2015b).

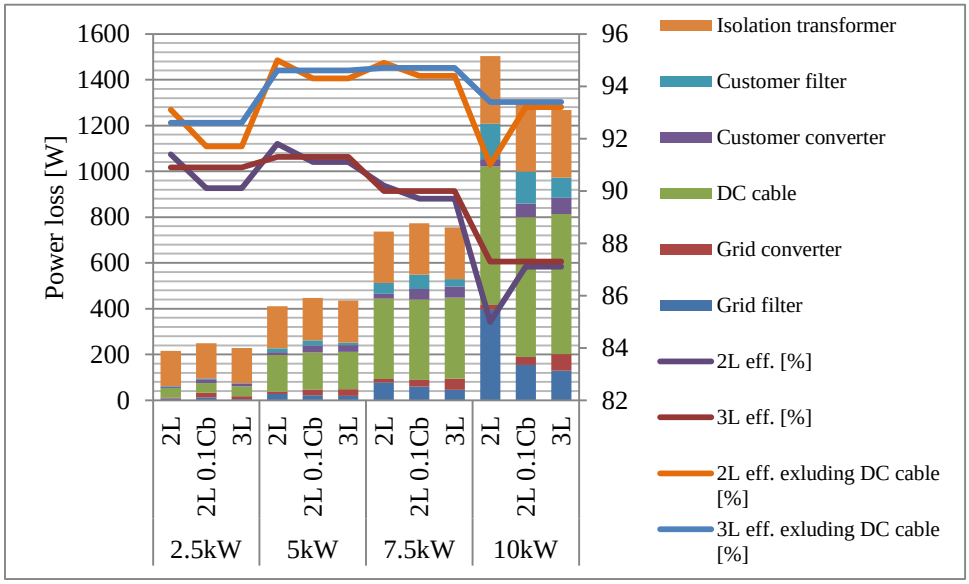


**Fig. 5.6.** Simulated total power losses of 1km long ungrounded LVDC distribution network with two- and three-level grid and customer converters with SiC MOSFETs

The energy efficiency of two-level grid converter with the LCL-filter, which capacitance value is $0.1*C_b$ instead of $0.05*C_b$ is shown to have the same efficiency as the three-level grid converter at nominal load in Fig. 4.6. Therefore the power losses of two-level converter are calculated by using the LCL-filter with the capacitance value of $0.05*C_b$ as well as $0.1*C_b$ and illustrated in Fig. 5.6. The capacitance value of the LCL-filter has a significant effect to the power losses at nominal load but the effect to the power losses at partial load conditions is negligible as depicted in Fig. 5.6. The power loss difference between two- and three-level converters connected to 750 VDC is negligible, when the conventional IGBTs are replaced by SiC MOSFETs. The voltage capability of the SiC MOSFETs used with both of the converters is the same. The overall energy efficiency with three-level NPC converters is approximately 2 % higher if the conventional IGBTs would be replaced by SiC MOSFETs and the energy efficiency of two-level converters is 4 % higher.

## 5.5 Single-phase loads

The single-phase customer loads cause 2nd harmonic to the DC current and voltage increasing DC cable power losses (Lago et al., 2011). The control of the phase-angle between the sinusoidal control signals of the PWM-modulators of the single-phase converters might have an effect on the DC cable power losses. The ungrounded bipolar LVDC distribution network, supplied by two grid converters, is presented in Fig. 5.7. Both of the grid converters are controlled to produce constant 750 VDC. In Fig. 5.7, three three-level single-phase full-bridge converters are connected to the bipolar LVDC distribution network between the positive pole and the neutral. The load of the single-phase converters is symmetrical 3.3 kW each or asymmetrical, when the first converter load is 5 kW, second 4 kW and the third converter load is 1 kW.

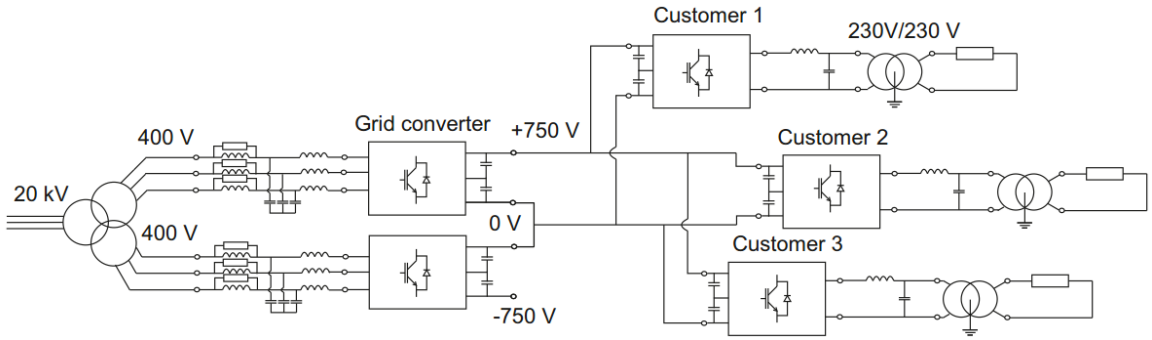


**Fig. 5.7.** A bipolar LVDC distribution network with single phase customer converter

The other option is that the same total power is supplied by one three-phase converter instead of three-single-phase converters as in Fig. 2.10b. The load is phase-symmetric 10 kW load (3.3 kW/phase) or phase-asymmetric, when the load in phase A is 5 kW, in phase B 4 kW and in phase

C 1 kW. The phase angle between the sinusoidal control signals of the PWM-modulators in three single-phase converters are selected as 0° or 120° since it might be possible to decrease the low frequency harmonics, which occur in the DC current and DC voltage by optimizing the phase angels of the sinusoidal control signals. The single-phase converters, having load of 3.3 kW each, with the phase-angle of 0° cause 2nd harmonic component to DC currents and DC voltages as shown in Figs. 5.8a-b. Instead, three single-phase converters with the phase-angle of 120° behaves as one three-phase converter, and therefore, these do not cause the 100 Hz component to the DC currents as shown in Figs. 5.8c and d. However, both three single-phase converters with the phase-angle of 120° and one three-phase converter produce 3rd harmonic component to the DC voltages due to three-level topology as shown in Figs. 5.8d and f. (Rekola et al., 2014a)

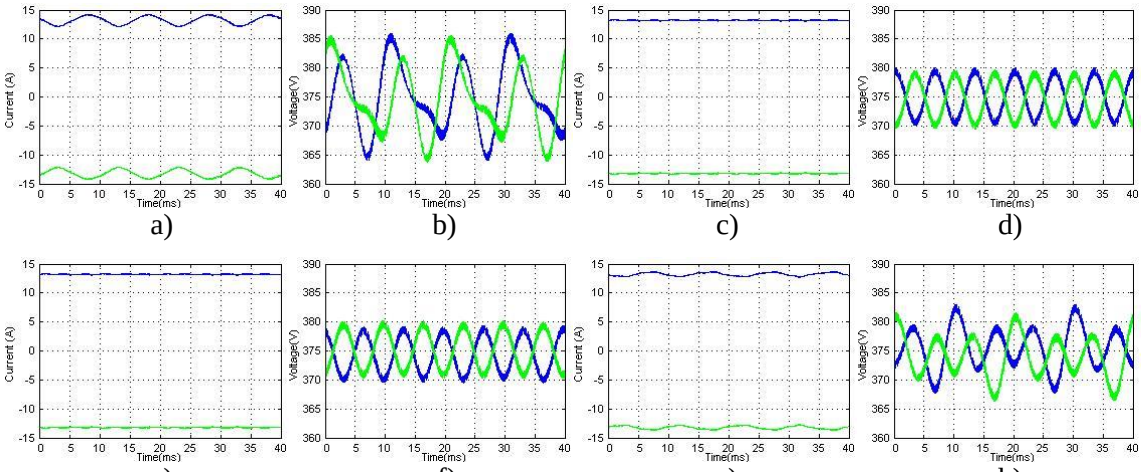


**Fig. 5.8.** Simulated DC currents and DC voltages with a-b) single-phase converters with 0° phase shift, c-d) single-phase converters with 120° phase shift, e-f) three-phase converter, g-h) asymmetrically loaded single-phase converters with 120° phase-shift

The optimized phase angle is shown to be 120° to minimize the DC current harmonics caused by the single-phase converters when the load of all three converters is the same. However, when the three single-phase converters are loaded asymmetrically, the 120° phase-angle do not minimize the DC current and DC voltage fluctuation as shown in Figs. 5.8g-h. The phase angle of single-phase converters as well as the phase angle between the phases in three-level converters needs to be changed if the load is asymmetrical to minimize the DC current and DC voltage fluctuation. The method to decrease the 2nd harmonic component in the DC currents is proposed by Lana et al. (2011). The DC voltage harmonics would be decreased also by increasing the DC capacitance value but it increases the acquisition costs of the converters as discussed in (Lana et al., 2011a). According to the standard, the maximum DC voltage fluctuation is allowed to be 10 %, i.e. 75 V,

but from the energy efficiency point of view, the DC voltage fluctuation should be limited to lower level (IEC Standard 60364).

The total power losses and efficiencies of the LVDC network with symmetrically and asymmetrically loaded (marked as "asym" in Fig. 5.9) single-phase and three-phase customer converters with 1 km long DC cable are presented in Fig. 5.9. The network is supposed to be ungrounded except the case "asym 3-phase 4-wire", in which the whole LVDC network is grounded hence the isolation transformer is not needed. According to the results illustrated in Fig. 5.9, the overall power losses of the LVDC network with the single-phase converters, which PWM-modulation reference signals phase shift is 0° or 120° are almost the same. The converter bridge power losses decrease approximately 20 W and the LC-filter power losses 70 W when the phase shift is 120° instead of 0°. It can be concluded that the achieved energy efficiency increase by optimizing the reference signal phase shift is not significant.

The power losses of the LCL-filter, grid converter, and DC cable are almost the same in spite of the use of three single-phase customer converters or one three-phase customer converter. However, the losses of the customer converter, LC-filter and isolation transformer are certainly lower when the load is supplied by only one converter instead of three converters. It can be concluded that the higher efficiency of the LVDC distribution network is achieved when one three-phase customer converter is used instead of multiple single-phase converters. Most of the current harmonics occur at 10 kHz, i.e., at the modulation frequency when the three-phase converter is used, whereas most of the current harmonics occur at twice of the modulation frequency, 20 kHz, when the single-phase full-bridge converters with the unipolar modulation scheme are used. The current harmonics at higher frequency cause increased losses in the LC-filter as shown in Section 3.3.

The grid converter and filter cause 20 % of the overall power losses as illustrated in Fig. 5.9. The DC cable power losses are almost the same in spite of the used customer converters and loading asymmetry. The DC cable power losses are 35% to 50 % of the overall power losses. The symmetrically loaded three-phase customer converter and filter causes 15 % of the power losses and the asymmetrically loaded converter causes 20 % of the overall power losses. Otherwise the customer converter and LC-filter cause approximately one third of the overall power losses. The isolation transformer power losses are approximately 20 % of the total power losses.

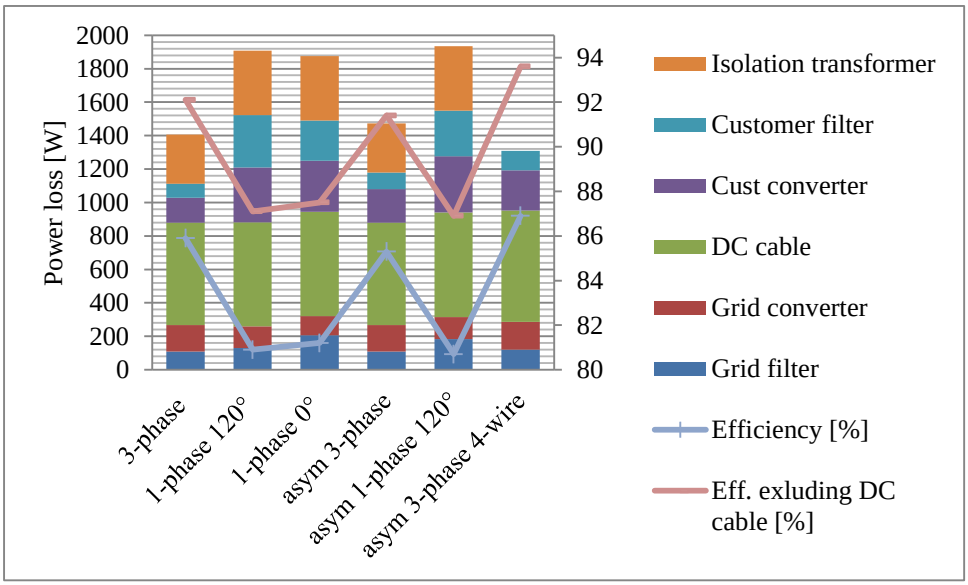


**Fig. 5.9.** Simulated total losses of the bipolar LVDC distribution network with three single-phase or one three-phase load converters with 1 km DC cable

The low frequency harmonics occur in the AC grid currents when the load is phase-asymmetric in the ungrounded LVDC distribution network increasing the power losses of grid converter and LCL-filter as shown in Fig. 5.9. Moreover, the 50 Hz isolation transformer has difficulties to supply distorted or unbalanced loads. Highly distorted load current can lead to transformer overloading or cause hotspots in the windings and result in a reduction of the expected lifetime of the transformer. The AC grid currents are sinusoidal in spite of the phase-asymmetrical load if the LVDC network is grounded as shown in Fig. 5.10. The power losses of the converters and AC-filters are higher when the DC network is grounded. However, the isolation transformer is not needed hence the energy efficiency is higher compared to ungrounded network.

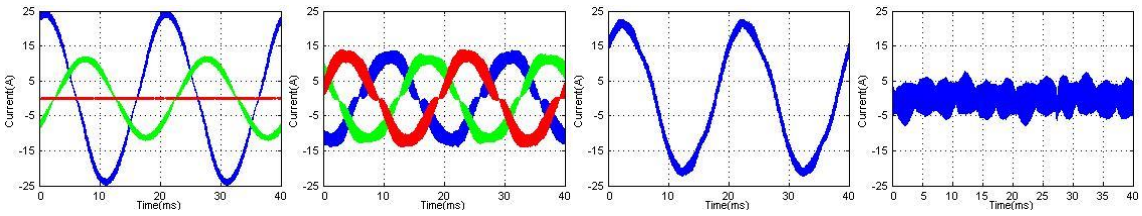


a) b) c) d)

**Fig. 5.10.** Measured a) customer load currents, b) grid converter input currents, c) current in the grounding wire in the customer converter and e) current in the grounding wire in the grid converter when the load in phase A is 4 kW (blue), in phase B 2 kW (green) and in phase C 0 kW (red)

## 5.6 Customer behavior

The total power loss of the LVDC distribution network during one year is analyzed with the aid of typical load characteristic of Finnish customer. The customer has electric storage heating, which causes a high electric load at winter nights but most of the time the load is under 10 % of the maximum load as shown in Fig. 5.11. The total consumed energy is 10.2 MWh/year. The customer load is assumed to be resistive operating at unity power factor.

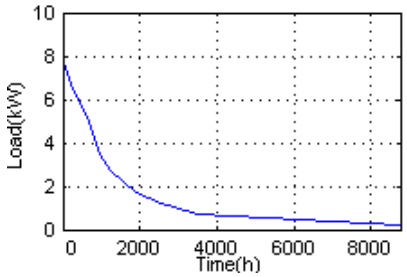


**Fig. 5.11**. Duration curve of customer with electric storage heating

The bipolar, ungrounded, ± 750 VDC distribution network (Fig. 2.10b) as well as unipolar ungrounded network with 800V/400V isolation transformer (Fig. 5.2) and unipolar grounded network (Fig. 2.12) are used. The length of the DC cable is supposed to be 2.5 km. Three-level three-phase grid and customer converters with the modulation frequency of 10 kHz are used. The nominal power or the converters producing 750 VDC is 10 kVA and the nominal power of the converters, which produce 1500 VDC, is 20 kVA, respectively. Both conventional silicon IGBTs and SiC MOSFETs are used as power semiconductor switches in the converter bridges and both iron and amorphous core AC filter inductors are used (Semikron, 2015f; Cree, 2015b). The power losses and energy efficiency of the whole LVDC distribution network during one year is shown in Fig. 5.12.

The high frequency inductor core losses cause 40 % of the overall power losses if the iron core filter inductors are used. Instead, the high frequency inductor core losses are only 3 % of the overall power losses when the iron core inductors are replaced by the amorphous core filter inductors. The majority of the filter losses are high frequency core losses also with the amorphous core when the load is lower than one quarter of the nominal load. The fundamental frequency core losses are insignificant in both iron and amorphous core inductor. More than half of the overall power losses are caused by isolation transformer because of high no-load losses. The energy efficiency of the grounded network is substantially higher compared to the ungrounded network due to lack of isolation transformer in spite of increased converter power losses. The energy efficiency of the grounded LVDC distribution network can be further increased from 82.2 % to 88.2 % by replacing conventional silicon IGBTs with SiC MOSFETs.

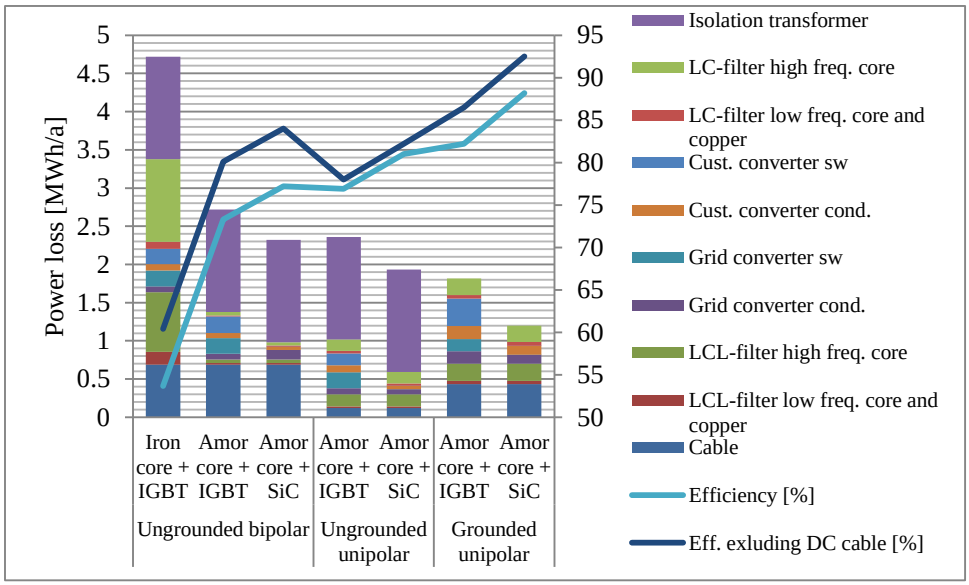


**Fig. 5.12**. Total power losses of a customer with electrical heating during one year

The previous energy efficiency analysis of the LVDC distribution network is concentrated mainly to the power losses of the DC cable. For example, the energy efficiency of the rural Finnish LVAC network, which length is 17km, would increase from 94 % to 96.5 % by using LVDC if only the cable conduction losses are taken into account (Lana et al., 2015). However, it should be noted that only one quarter of the overall power losses is caused by the DC cable in the ungrounded bipolar DC network, 5 % of the overall power losses in the ungrounded unipolar DC network and 35 % in the grounded unipolar DC network as illustrated in Fig. 5.12. Therefore, the optimization of the energy efficiency of the power converter in the LVDC distribution network is crucial to optimize the energy efficiency of the whole network.

## 5.7 Use of isolated DC/DC converter instead of isolating line-frequency transformer

The major part of the overall power losses of the ungrounded LVDC distribution network occur in the isolating line-frequency (50 Hz) transformer as presented in the previous chapter. The transformer could be replaced by isolated, high power density, bidirectional DC/DC converter, including a high-frequency isolation transformer with amorphous core. Isolated DC/DC converter topologies which are suitable to PV, electric vehicle (EV), energy storage, traction auxiliary power and data center applications are widely studied during the last years (Pavlovsky et al., 2009; Wang et. al. 2011a; Du et al., 2011; Kim et al., 2013).

Two-level full-bridge DC/DC converter topologies are preferred in high-power applications instead of half-bridge topologies, because of lower voltage and current stresses and lower current harmonics (Tan et al., 2011; Mattsson et al., 2014). The energy efficiency of the DC/DC converters is further increased by using soft-switching methods, such as zero-voltage switching and zero-current switching, instead of hard switching (LaBella et al., 2014; Tan et al., 2011; Pavlovsky et al., 2009; Wang et al., 2012; Mattsson et al., 2014). High switching frequency, at least 20 kHz, is used to minimize the converter volume (Wang et al., 2011a; Pavlovsky et al., 2009; Simanjorang, 2010).

The four-wire customer converter topology needs to be used if the line-frequency isolation transformer is replaced by isolated, bidirectional DC/DC converter as shown in Fig. 5.13. Therefore, the power losses of the customer converter and the customer LC-filter increase.

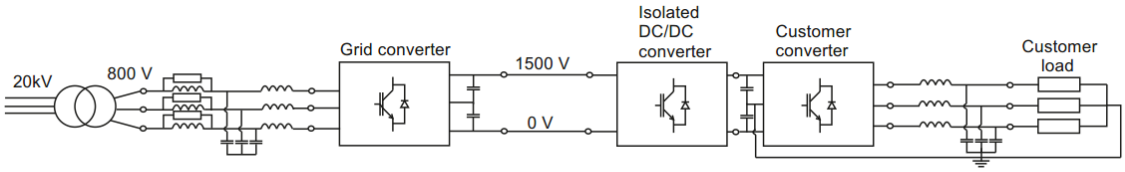


**Fig. 5.13.** Four-wire customer converter with isolated DC/DC converter

The minimum required energy efficiency of the isolated DC/DC converter is calculated to achieve as high efficiency of the LVDC distribution network as in the calculations presented in Fig. 5.12. The energy efficiency of the isolated DC/DC converter should be at least 88 % at the whole operating area if the bipolar LVDC distribution network structure is used. However, the energy efficiency of the DC/DC converter should be at least 97 % to achieve as high overall energy efficiency with the bipolar LVDC distribution network as with the unipolar LVDC distribution network. The energy efficiency of the 750 V/400 V two-level bidirectional, isolated DC/DC converter with 1200V Si IGBTs or MOSFETs with soft switching method is approximately 97 % in broad load range (Pavlovsky, 2009; Inoue and Akagi, 2007; Tan et al., 2011; Du et al., 2011; Kim et al., 2013).

The energy efficiency of the DC/DC converter decreases if the power devices with the voltage capability of higher than 1200 V are needed. Therefore multilevel DC/DC converter topologies need to be used. The voltage stress of the primary-side switches would be $U_{in}/n$ and current stresses of the secondary-side inductors and diodes would reduce to be $I_{out}/n$ by using $n$-level converter (Wang et al., 2011a). In the unipolar network, shown in Fig. 5.13, the energy efficiency of the isolated DC/DC converter needs to be at least 94 % to achieve as high energy efficiency as with the line-frequency transformer. Furthermore, the energy efficiency of the DC/DC converter

needs to be at least 96 % at the whole operating area to achieve as high energy efficiency as with the grounded unipolar LVDC distribution network.

The measured energy efficiency of 1500V/48V, 2kW multilevel DC/DC-converter including four switch pairs was shown to be 93 % when the output power is at least half of the nominal (Wang et al., 2012). However, the energy efficiency decreases to be as low as 79 % with the very low load (Wang et al., 2012). Instead of multilevel DC/DC converter, also the modular converter structure can be used, meaning that multiple low-power converters are connected in series and parallel (Fan and Li, 2011). The efficiency of hundred Si IGBT DC/DC converters with the nominal power of 10 kW, meaning the total power of 1 MW, is 97 % with the switching frequency of 20 kHz (Biela et al., 2008). 65 converter modules based on GaN-FET devices of 300 W 48 V-48 V are connected in series and parallel achieving 19.2 kW total nominal power in the studies by Hayashi (2013). The maximum efficiency was 97 % with the switching frequency of 2 MHz and 95 % with the switching frequency of 20 kHz (Hayashi, 2013).

It can be concluded that the energy efficiency will not be improved or it is only insignificant by using isolated DC/DC converter instead of line-frequency isolated transformer, because the customer load is most of the time very low compared to the nominal power of the converters.

## 5.8 Conclusions

According to theoretical analysis presented so far, the high efficiency of the LVDC network is mainly attributed to the low losses in the DC cable (Nilsson et al., 2004; Engelen et al., 2006; Anand et al., 2010; Sannino et al., 2003; Kakigano et al., 2010; Kakigano et al., 2012; Shenai et al., 2011). The theoretical loss analysis does not take into account that the converters produce low frequency harmonics to the DC currents and voltages causing additional losses in the DC cable, in the converters and their AC-filters.

The LVDC distribution network configuration with the lowest losses is determined depending on the length of the network and the main power loss sources are identified. According to the results, the highest efficiency is achieved when LVDC distribution network is grounded and three-level NPC converters are connected to 1500 VDC. If the network needs to be ungrounded, two- or three-level converters should be connected to 750 VDC when the length of the bipolar network is 600 m at maximum. The total losses are minimized especially due to low losses in the customer converters. When the bipolar LVDC network is longer than that, the increased DC cable losses decrease the efficiency. Therefore, the maximum energy efficiency is achieved when the unipolar

network configuration is used by connecting the three-level grid and customer converters to 1500 VDC and by using the voltage transformation ratio of 800 V/400 V instead of 400 V/400 V in the isolation transformer. The DC cable power losses are minimized due to reduced number of DC current harmonics and no need of the balancing circuit.

The energy efficiency of two- and three-level converters, connected to 750 VDC, are the same when the filter inductor cores with low no-load losses, e.g. amorphous alloy core and SiC MOSFETs are used. However, when the converters are connected to 1500 VDC, the power losses of three-level NPC converter are significantly lower compared to two-level converter.

Many of the home electronic devices use single-phase supply. It can be concluded that the highest efficiency of the LVDC distribution network is achieved when three-phase customer converter is loaded phase-asymmetrically instead of the use of multiple single-phase converters. In the ungrounded LVDC distribution network, low frequency harmonics occur in the AC grid currents increasing the power losses when the load is phase-asymmetric. Instead, the asymmetrical load does not cause additional harmonics to the AC currents in the grounded network. Therefore, the energy efficiency of the grounded network is higher compared to ungrounded network also with phase asymmetrical load.

The total power loss of the LVDC distribution network during one year is analyzed with the aid of typical load characteristic of Finnish customer. It can be concluded that more than half of the overall power losses are caused by isolation transformer because of high no-load losses in the ungrounded LVDC distribution network. The line-frequency isolation transformer would be replaced by isolated DC/DC converter. However, significant energy efficiency increase is not achieved by using isolated DC/DC converter because the customer load is most of the time very low compared to the nominal power of the converters.

The energy efficiency of the grounded network is substantially higher due to lack of isolation transformer in spite of increased converter power losses. The energy efficiency can be optimized by using amorphous core AC filter inductors instead of iron core inductors and by using SiC MOSFETs instead of conventional IGBTs. It should be noted that only 35 % of the overall power losses is caused by DC cable losses in the grounded bipolar DC network. Therefore, the optimization of the energy efficiency of the power converter in the LVDC distribution network is crucial to optimize the energy efficiency of the whole network.

# 6 Conclusions

The conventional LVAC distribution network will be changed towards the future Smart Grid due to tightened environmental regulation. Therefore, increased number of renewable power generation units will be installed to the network. Both the energy production and consumption will vary on a large scale but, at the same time, the customers are highly dependent on high quality and uninterruptable power supply. One option to realize the future Smart Grid would be to replace the present LVAC distribution network by LVDC. The control methods and stability of both the AC and DC microgrids are intensively studied during the last years. It can be concluded based on the studies that the control might be simpler and the grid operation more reliable if the conventional AC grid would be replaced by DC grid. However, the detailed energy efficiency analysis of the DC grid is not thoroughly studied. The energy efficiency and total lifetime costs are the key parameters when the network owners consider the future grid structure. Therefore, the energy efficiency of the LVDC distribution network is analyzed in this study, especially, from the power electronics perspective.

## 6.1 Final conclusions

In this study, simulation and calculation models are developed to assessing LVDC distribution network power losses. According to theoretical analysis presented so far, the high efficiency of the LVDC network is mainly attributed to the low losses in the DC cable (Nilsson et al., 2004; Engelen et al., 2006; Anand et al., 2010; Sannino et al., 2003; Kakigano et al., 2010; Kakigano et al., 2012; Shenai et al., 2011; Ali et al., 2012; Gwon et al., 2014). The theoretical loss analysis does not consider the power losses of the converters, AC filter and transformers. The target of the

created power loss simulation models is to be fast and general hence these are based on the datasheets of the power semiconductor switches and the inductor core materials.

The power loss results furnished by the developed models are compared against measurements obtained by electric and calorimetric tests. The maximum error between the measured and simulated power losses is 10 % when the inductor design is realistic, i.e., the current harmonics are limited to realistic level. The accuracy of the simulated power loss models is slightly higher, especially, at partial load conditions compared to the accuracy of the analytical average power loss models. Based on the results given by the models, it is possible to compare different components and network parameters on the energy efficiency point of view. However, for the more detailed efficiency analysis, more complex models would be needed.

The converter topologies are compared by taking into account the controllability of AC current and DC voltage and size of the required AC filter. The voltage source grid converters should be used instead of LCCs, because the DC voltage and the power factor of PCC can be controlled, and furthermore, the bidirectional power flow is possible.

The AC filter design methods and filter inductor core materials are compared. The required filter inductance value is minimized if LCL-filter is connected in front of the grid converter and the LC-filter after the customer converter. The inductor current ripple should be limited to be $\leq 10$ % of the current fundamental component amplitude to minimize the filter power losses. The modulation frequency of the customer converter should be at least 10 kHz to limit the audible noise, and therefore, the use of large inductance minimizes the high frequency inductor core losses. Moreover, the filter inductor core material with low losses caused by high-frequency current should be used. The energy efficiency of the converters is almost constant in spite of the loading conditions when amorphous core inductors are used. Instead, the energy efficiency is low and decrease considerably as the load decreases if the conventional M400-50 laminated iron core filter inductors are used. This is important, because the customer load varies on a large scale.

The converter power losses are not changed significantly depending on the use of IGBTs by different manufacturers. However, the energy efficiency of the converters increases if the conventional IGBTs are replaced by SiC MOSFETs. The modulation frequency is not possible to increase higher than 10 kHz if conventional IGBTs are used due to increased switching losses. Instead, the modulation frequency would be increased without the increase of switching losses if SiC MOSFETs are used. However, the increased high frequency power losses of the amorphous alloy inductor core limit the modulation frequency increase.

The energy efficiency of two- and three-level converters connected to 750 VDC is almost the same when the filter inductor cores with low no-load losses, e.g. amorphous alloy core and SiC MOSFETs are used. However, when the converters are connected to 1500 VDC, the power losses

of three-level NPC converter are significantly lower compared to two-level converter. It can be concluded that the notable power loss increase is shown as the voltage capability of the power semiconductor switching devices increase from 1200 V. Therefore, the use of three-level NPC converters is worthwhile especially at higher voltage levels. The drawback of three-level converters is unbalanced current stresses of the power semiconductor switches. The conventional NPC three-level converter would be replaced by ANPC topology enabling more equal power loss distribution.

The LVDC distribution network configuration with the lowest losses is determined depending on the length of the network and the main power loss sources are identified. The LVDC distribution network should be grounded to minimize the overall power losses if it is possible according to local safety standardization and grounding conditions. The energy efficiency of the grounded network is substantially higher due to lack of isolation transformer in spite of increased converter power losses. The three-level NPC converters with SiC MOSFETs and amorphous core AC filter inductors should be used and connect to 1500 VDC to minimize the power losses of the LVDC distribution network.

The 50 Hz isolation transformer is the main power loss source if the galvanic isolation is needed to isolate the ungrounded LVDC distribution network and the grounded customer electrical installations. The highest energy efficiency is achieved by using two- or three-level converters with SiC MOSFETs and amorphous core AC filter inductors and by connecting the converters to 750 VDC if the length of the DC cable is less than 600 m. Otherwise, slightly higher energy efficiency is achieved by using three-level converters with SiC MOSFETs and amorphous core AC filter inductors and by connecting the converters to 1500 VDC. Moreover, the voltage transformation ratio of 800 V/400 V must be used instead of 400 V/400 V in the isolation transformer.

The power losses are minimized, if the three-phase customer converter is loaded phase-asymmetrically instead of the use of multiple single-phase converters. In the ungrounded LVDC distribution network, low frequency harmonics occur in the AC grid currents increasing the power losses when the load is phase-asymmetric. Instead, asymmetrical load does not caused additional harmonics to the AC currents and the isolation transformer is not needed in the grounded network and therefore, the energy efficiency is higher.

## 6.2 Suggested future research topics

The research carried out as a part of this thesis elucidated various questions that could be the potential future research topics. Some of the most interesting problems and research questions are highlighted below:

It was concluded that the 50 Hz isolation transformer is the main power loss source if the galvanic isolation is needed between the LVDC distribution network and the customer electrical installations. The line-frequency isolation transformer would be replaced by isolated DC/DC converter but the achieved energy efficiency increase is not significant. However, an isolated DC/DC converter would enable the fed of large variable loads like electrical heating, saunas and EV charging station directly from DC. Moreover, the modulation index of the customer DC/AC converter would be optimized by setting the DC voltage level to the desired value by DC/DC converter.

The centralized customer converter operates most of the time at very low load compared to the maximum power of the converter. If large customer loads would be fed directly by DC, the nominal power of the customer AC/DC converter might be lower and it can operate most of the time near its nominal power. Moreover, the modular converter structure might be useful, meaning, that the customer converter consists of multiple smaller converters. The converters can be designed to low power level increasing the scalability and reliability. Ferrite would be used as a filter inductor core material in the modular converter designed to lower nominal power achieving lower power losses also at higher modulation frequencies.

The efficiency of the DC distribution network is not higher compared to present AC distribution network according to the results presented in this thesis. However, the energy efficiency comparison should be done in the future by taking into account the decreased number of DC/AC and AC/DC conversion stages of renewable energy generation and energy storages.

**References**


Agustoni A., Borioli E., Brenna M., Simioli G., Tironi E. and Ubezio G. (2005). LVDC distribution network with distributed energy resources: analysis of possible structures, 18th International Conference and Exhibition on Electricity Distribution (CIRED), pp. 1-5.

Ahmadi R. and Ferdowsi M. (2014). Improving the performance of a line regulating converter in a converter-dominated DC microgrid system, IEEE Trans. on Smart Grid **5**(5): 2553-2563

Ali S. Q., Babar M. S., Maqbool S. D. and Al- Ammar E. A.(2012). Comparative analysis of AC DC microgrids for the Saudi Arabian distribution System, IEEE PES Transmission and Distribution Conference and Exposition, pp.1-8.

AlLee G. and Tschudi W. (2012). Edison redux: 380Vdc brings reliability and efficiency to sustainable data centers, IEEE Power Energy Mag. **10**(6):50-59.

Anand S. and Fernandes B. G. (2010). Optimal voltage level for DC microgrids, 36th Annual Conference on IEEE Industrial Electronics Society (IECON), pp.3034-3039.

Akiror J.C. and P. Pillay. (2012). On the coefficients of core loss formulas for electrical machines, 38th Annual Conference on IEEE Industrial Electronics Society (IECON), pp. 1927-1933.

Bendre A., Cuzner R. and Krstic S. (2009).Three-level converter system – design guidelines for a neutral point clamped converter, IEEE Ind. Appl. Mag. **15**(2):12-23.

Bertotti G. (1988). General properties of power losses in soft ferromagnetic material, IEEE Trans. Magn. **24**(1):621-630.

Biela J., Aggeler D., Inoue S., Akagi H. and Kolar J. W (2008). Bi-directional isolated DC-DC converter for next-generation power distribution - comparison of converters using Si and SiC devices, Power Conversion Conference (PCC'07), pp. 510-517.

Bose B. K..(2013). Global energy scenario and impact of power electronics in 21st century, IEEE Trans. Ind. Electron. **60**(7):2638-2650.

Bose S., Pal S., Natarajan B., Scoglio C.M., Das S. and Schulz N.N.(2012). Analysis of optimal reconfiguration of shipboard power systems, IEEE Trans. Power Syst. **27**(1): 189-197.

Brenna M., Lazaroiu G. C., Superti-Furga G. and Tironi E. (2009). Premium power quality with DG integrated DC systems, IEEE PowerTech, pp. 1-6.

Brenna M., Bulac C., Lazaroiu G.C., Superti-Furga G. and Tironi E. (2008). DC power delivery in distributed generation systems, 13th International Conference on Harmonics and Quality of Power (ICHQP), pp. 1-6.

Brückner T. and Holmes D. G. (2005). Optimal pulse-width modulation for three-level inverters, IEEE Trans. Power Electron. **20**(1):82-89.

Brückner T. and Bernet S. (2001). Loss balancing in three-level voltage source inverters applying active NPC switches, IEEE 32nd Annual Power Electronics Specialists Conference (PESC), pp. 1135-1140.

Byeon G., Yoon T., Oh S., Jang G. (2013). Energy management strategy of the DC distribution system in buildings using the EV service model, IEEE Trans. Power Electron. **28**(4):1544-1554

Chen D., Xu L. and Yao L. (2013). DC voltage variation based autonomous control of DC microgrids, IEEE Trans. Power Del. **28**(2): 637-648.

Cree, "CCS050M12CM2" http://www.cree.com/Power/Products/SiC-Power-Modules/SiC-Modules/CCS050M12CM2, datasheet, 2015.

Cree, "CCS020M12CM2" http://www.cree.com/Power/Products/SiC-Power-Modules/SiC-Modules/CCS020M12CM2, datasheet, 2015.

Cree, "CAS120M12BM2" http://www.cree.com/Power/Products/SiC-Power-Modules/SiC-Modules/CAS120M12BM2, datasheet, 2015.

Cree, "CAS100H12AM1" http://www.cree.com/Power/Products/SiC-Power-Modules/SiC-Modules/CAS100H12AM1, datasheet, 2015.

Dieckerhoff S., Bernet S. and Krug D. (2005). Power loss-oriented evaluation of high voltage IGBTs and multilevel converters in transformerless traction applications, IEEE Trans. on Power Electron. **20**(6): 1328-1336.

Dong D., Luo F., Zhang X., Boroyevich D., Mattavelli P. (2013).Grid-interface bidirectional converter for residential DC distribution systems- part 2: AC and DC interface design with passive components minimization, IEEE Trans. on Power Electron. **28**(4):1667-1679.

Dowell P.L. (1966). Effects of eddy currents in transformer windings, Proc. IEEE. **113**(8): 1387-1394.

Dragicevic T., Vasquez J.C., Guerrero J. M. and Skrlec D. (2014). Advanced LVDC electrical power architectures and microgrids - a step towards a new generation of power distribution networks, IEEE Electrification Mag. **2**(1):54-65.

Du Y.,Lukic S., Jakobson B. and Huang A. (2011). Review of high power isolated bi-directional DC-DC converters for PHEV/EV DC charging infrastructure, IEEE Energy Conversion Congress and Exposition (ECCE), pp. 553-560.

Eaton, Low voltage dry-type distribution transformers for general purpose, http://www.eaton.com/Eaton/ProductsServices/Electrical/ProductsandServices/ElectricalDistribution/Transformers/LowVoltageDry-TypeDistribution/GeneralPurpose/index.htm, datasheet, 2015.

Engelen K., Leung Shun E., Vermeyen P., Pardon I., D'hulst R., Driesen J. and Belmans R. (2006). The feasibility of small-scale residential DC distribution systems, 32nd Annual Conference on IEEE Industrial Electronics Society (IECON), pp. 2618-2323.

Enslin J.H and Heskes P.J. (2004). Harmonic interaction between a large number of distributed power inverters and the distribution network, IEEE Trans. Power Electron. **19**(6): 1586-1893.

Erickson R. W. and Maksimovic D. (2001). Fundamentals of power electronics, 2nd edition, Kluwer Academic Publishers.

European Commission, Low Voltage Directive, LVD 2006/95/EC, European Union Directive, Brussels, 2006

European Standard EN 50160, Voltage Characteristics of Electricity Supplied by Public Electricity Networks, CENELEC: European Committee for Electrotechnical Standardization, 2010.

Fan H. and Li H. (2011). High-frequency transformer isolated bidirectional DC-DC converter modules with high efficiency over wide load range for 20kVA solid-state transformer, IEEE Trans. Power Electron. **26**(12):3599-3608.

Flourenzou N., Agelidis V. G. and Demetriades G. D. (2009). VSC-based HVDC power transmission systems: an overview, IEEE Trans. Power Electron. **24**(3):592-602.

Franquelo L., Rodriquez J., Leon J., Kouro S., Portillo R. and Prats M. (2008). The age of multilevel converters arrives, IEEE Ind. Electron. Mag. **2**(2):28-39.

Friedrich K. (2010). Modern HVDC PLUS application of VSC in modular multilevel converter topology, IEEE International Symposium on Industrial Electronics (ISIE), pp. 3807-3810

Guarnieri M. (2013). The alternating evolution of DC power transmission, IEEE Ind. Electron. Mag. **7**(3):60-63.

Guerrero J. M., Vasquez J. C., Matas J., de Vicuña L. G. and Castilla M. (2011). Hierarchical control of droop-controlled AC and DC microgrids—a general approach toward standardization, IEEE Trans. Ind. Electron. **58**(1):158-172.

Guerrero J.M., Loh P.C., Lee T.L. and Chandorkar M. (2013). Advanced control architectures for intelligent microgrids—Part II: Power quality, energy storage, and AC/DC microgrids," IEEE Trans. Ind. Electron. **60**(4):1263-1270.

Günes I., Üstüntepe B. and Hava A. (2009). Modern transformerless uninterruptible power supply (UPS) systems, International Conference on Electrical and Electronics Engineering (ELECO), pp. 316-320.

Gu Y., Xiang X., Li W., He X. (2014). Mode-adaptive decentralized control for renewable DC microgrid with enhanced reliability and flexibility, IEEE Trans. Power Electron. **29**(9): 5072-5080.

Gwon G.-H., Kim D.-U., Oh Y.-S., Han J. and Kim C.-H. (2014). Analysis of efficiency for AC and DC load in LVDC distribution system, 12th IET International Conference on Developments in Power System Protection (DPSP), pp.1-5.

Hakala T., Järventausta P., Lähdeaho T. (2013). The utilization potential of LVDC distribution, 22th International Conference and Exhibition on Electricity Distribution (CIRED), pp.1-4.

Hakala T., Lähdeaho T. and Järventausta P. (2015). Low voltage DC distribution – utilization potential in a large distribution network company, IEEE Trans. Power Del. **99**:1.

Hakala T., Lähdeaho T. and Komsi R. (2015a). LVDC pilot implementation in public distribution network, 23rd International Conference and Exhibition on Electricity Distribution (CIRED), pp.1-4.

Hasegawa R. (2004). Applications of amorphous magnetic alloys, Materials Science and Engineering **375-377**:90-97.

Hasegawa R. and Azuma D. (2008). Impacts of amorphous metal-based transformers on energy efficiency and environment, Journal on Magnetism and Magnetic Materials **320**(20):2451-2456.

Hayashi Y. (2013). Power density design of SiC and GaN DC–DC converters for 380 V DC distribution system based on series-parallel circuit topology, 28th Annual Applied Power Electronics Conference and Exposition (APEC), pp. 1601-1606.

Hazra S., De A., Cheng L., Palmour J., Schupbach M., Hull B.A., Allen S. and Bhattacharya S. (2015). High switching performance of 1700V, 50A SiC power MOSFET over Si IGBT/BiMOSFET for advanced power conversion applications, IEEE Trans. Power Electron. **99**, pp. 1

Hitachi (2015) Powerlite® Inductor Cores Technical Bulletin http://www.hitachimetals.com/product/amorphous/powerliteinductorcores/documents/POWERLITE_C_opt.pdf

Ide P., Froehleke N. and Grotstollen H. (1997). Investigation of low cost control schemes for a selected 3-level switched mode rectifier, 19th International Telecommunications Energy Conference (INTELEC'97), pp. 413-418.

International Energy Agency IEA (2015) http://www.iea.org/

IEC 61000-3-2 Electromagnetic compatibility (EMC), Part 3-2: Limits- Limits for harmonic current emissions (equipment input current ≤ 16A per phase), 2014.

IEC 61727 Ed. 2, Photovoltaic (PV) Systems – Characteristics of the Utility Interface, 2004.

IEEE Std 519-1993, IEEE recommended practices and requirements for harmonic control in electrical power systems, 1993

IEEE Std 1547-2003, IEEE standard for interconnecting distributed resources with electric power systems, 2003.

IEC Standard 60364, Low Voltage Electrical Installations, IEC: Internationale Electrotehnical Commission, 2006.

Infineon (2015) FS3L50R07W2H3F_B11 Datasheet http://www.infineon.com/dgdl/Infineon-FS3L50R07W2H3F_B11-DS-v3_1-en_de.pdf?fileId=db3a30433fe811c7013fec12b85d3c49

Inoue S. and Akagi H. (2007). A bidirectional isolated DC-DC converter as a core circuit of the next-generation medium voltage power conversion system, IEEE Trans. Power Electron. **22**(2):535-542.

Jing X., He J. and Demerdash N. A. O. (2013). Application and losses analysis of ANPC converters in doubly-fed induction generator wind energy conversion system, IEEE International Electri Machines & Drives Conference (IEMDC), pp. 131-138.

Justo J.J., Mwasilu F., Lee J. and Jung J-W. (2013). AC-microgrids versus DC-microgrids with distributed energy resources: a review, Renewable and Sustainable Energy Reviews, **24**:387-405.

Kakigano H., Nomurra M. and Ise T., Van Roy J. and Driesen J. (2012). Basic sensitivity analysis of conversion losses in a DC microgrid, International Conference on Renewable Energy Research and Applications (ICRERA), pp. 1-6.

Kakigano H., Nomurra M. and Ise T.(2010). Loss evaluation of DC distribution for residential houses compared with AC system, International Power Electronics Conference (IPEC), pp. 480-486.

Kakigano H., Miura Y. and Ise T. (2010a). Low-voltage bipolar-type DC microgrid for super high quality distribution, IEEE Trans. Power Electron. **25**(12):3066-3075.

Kakigano H., Miura Y. and Ise T. (2009). Configuration and control of a DC microgrid for residential houses, Transmission & Distribution Conference & Exposition: Asia and Pacific, pp.1-4.

Karabiber A., Keles C., Kaygusuz A. and Alagoz B. B. (2013). An approach for the integration of renewable distributed generation in hybrid DC/AC microgrids, Renewable energy **52**: 251-259.

Kim H-S., Ryu M-H., Baek J-W and Jung J-H. (2013) High-efficiency isolated bidirectional AC-DC converter for a DC distribution system, IEEE Trans. Power Electron. **28**(4):1642-1654.

Kolar J.W. and Round S. D. (2006) Analytical calculation of the RMS current stress on the DC-link capacitor of voltage-PWM converter systems, IEE Proceedings – Electric Power Applications **153**(4):535-543.

Kolar J.W., Ertl H. and Zach F. C.(1996). Design and experimental investigation of a three-phase high power density high efficiency unity power factor PWM (VIENNA) rectifier employing a novel integrated power semiconductor module, 11th Annual Applied Power Electronics Conference and Exposition (APEC), pp. 514-523.

Kolar J. W. and Zach F.C. (1994). A novel three-phase utility interface minimizing line current harmonics of high-power telecommunications rectifier modules, Telecommunications Energy Conference (INTELEC'94), pp. 367-374

Krings A. and Soulard J. (2010). Overview and comparison of iron loss models for electric machines, International Conference on Ecological Vehicles and Renewable Energies, pp.1-10.

LaBella T., Yu W., Lai J-S., Senesky M. and Anderson D. (2014). A bidirectional-switch-based wide-input range high-efficiency isolated resonant converter for photovoltaic applications, IEEE Trans. Power Electron. **29**(7):3473-3484.

Lago J. and Heldwein M. L. (2011) Operation and control-oriented modeling of a power converter for current balancing and stability improvement of DC active distribution networks, IEEE Trans. Power Electron. **26**(3):877-885.

Lana A., Mattsson A., Nuutinen P., Peltoniemi P., Kaipia T., Kosonen A., Aarniovuori L. and Partanen J. (2014). On low-voltage DC network customer-end inverter energy efficiency, IEEE Trans. Smart Grid **5**(6):2709-2717.

Lana A., Lindh T., Kaipia T. and Partanen J. (2011). Minimization of the harmonic current content and power losses in DC transmission link of LVDC distribution system by phase angle regulation of inverter loads, International Exhibition & Conference for Power Electronics, Intelligent Motion and Power Quality (PCIM Europe), pp.1266-1271.

Lana A., Kaipia T., Nuutinen P., Lindh T. and Partanen J. (2011a). On dimensioning LVDC network capacitancies and impact on power losses, 21st International Conference on Electricity Distribution (CIRED), pp. 1-4.

Lassila J., Partanen J., Kaipia T., Haakana J. and Koivuranta K. (2009). Potential and strategic role of power electronics in electricity distribution systems, 20th International Conference on Electricity Distribution (CIRED), pp. 1-4.

de Leon F. and Semlyen A. (1993). Time domain modeling of eddy current effects for tranformer transients, IEEE Tans. Power Del. **8**(1):271-280.

Liserre M., Blaabjerg F. and Hansen S. (2005). Design and control of an LCL-filter-based three-phase active rectifier, IEEE Trans. Ind. Appl. **41**(5):1281-1290.

Li J., Abdallah T. and Sullivan C. R. (2001). Improved calculation of core loss with nonsinusoidal waveforms, IEEE Industry Applications Society Annual Meeting, pp. 2203-2210.

Loh P.C., Li D., Chai Y. K. and Blaabjerg F. (2013). Hybrid AC-DC microgrids with energy storages and progressive energy flow tuning, IEEE Trans. Power Electron. **28**(4):1533-1543

Madduri P. A., Rosa J., Sanders S. R., Brewer E. A. and Podolsky M. (2013). Design and verification of smart and scalable DC microgrids for emerging regions, IEEE Energy Conversion Congress and Exposition (ECCE), pp. 73-79.

Mahmoodi M., Gharehpetian G.B., Abedi M. and Noroozian R.(2006) Control systems for independent operation of parallel DG units in DC distribution systems, IEEE International Power and Energy Conference (PECON), pp. 220-224.

Mattsson A., Väisänen V., Nuutinen P., Kaipia T., Lana A., Peltoniemi P., Silventoinen P. and Partanen J. (2014). Implementation design of the converter-based galvanic isolation for low voltage DC distribution, International Power Electronics Conference (IPEC-ECCE-ASIA), pp.587-594.

Microsemi (2015) APTMC60TL11CT3AG Datasheet http://www.microsemi.com/product-directory/modules-a-hybrids/index.php?option=com_microsemi&view=pmsearch&layout=flash&tmpl=component&catid=1347

Microsemi (2015b) APTMC120AM20CT1AG Datasheet http://www.microsemi.com/product-directory/modules-a-hybrids/index.php?option=com_microsemi&view=pmsearch&layout=flash&tmpl=component&catid=1347

Mohan N., Undeland T. M and Robbins W. P. (2003). Power electronics – converters, applications, and design. 3rd edition. John Wiley & Sons, Inc.

Mohsenian-Rad H. and Davoudi A. (2014). Towards building an optimal demand response framework for DC distribution networks, IEEE Trans. on Smart Grid **5**(5):2626-2634

Moia J., Lago J., Perin A. J. and Heldwein M. L. (2012) Comparison of three-phase PWM rectifiers to interface AC grids and bipolar DC active distribution networks, 3rd IEEE International Symposium on Power Electronics for Distributed Generation Systems (PEDG), pp. 221-228.

Mühlethaler J, Biela J., Kolar J. W. and Ecklebe A. (2012). Improved core-loss calculation for magnetic components employed in power electronic systems, IEEE Trans. Power Electron. **27**(2):964-973.

Nabae A., Takahashi I. and Akagi H. (1981) A new neutral point clamped PWM inverter, IEEE Trans. Ind. Appl. **17**(5):509-517.

Nilsson D. and Sannino A. (2004). Efficiency analysis of low- and medium-voltage dc distribution systems, IEEE Power Engineering Society General Meeting, pp. 2315-2321.

Nuutinen P., Mattsson A., Kaipia T., Peltoniemi P., Pinomaa A., Lana A., Karppanen J. and Silventoinen P. (2014). Power electronic losses of a customer-end inverter in low-voltage direct current distribution, 16th European Conference on Power Electronics and Applications, EPE'14-ECCE Europe, pp.1-10.

Nuutinen P., Peltoniemi P. and Silventoinen P.(2013). Short-circuit protection in a converter-fed low-voltage distribution network, IEEE Trans. Power Electron. **28**(4):1587-1597.

Patterson B.T. (2012) DC, come home: DC microgrids and the birth of the "Enernet", IEEE Power Energy Mag. **10**(6):60-69.

Pavlovsky M., de Haan S. W. H. and Ferreira J. A. (2009). Reaching high power density in multikilowatt DC-DC converters with galvanic isolation, IEEE Trans. Power Electron., **24**(3):603-612.

Peltoniemi P., Nuutinen P. and Pyrhönen J. (2012). LQG-based voltage control using load adaptive controller, 15th International Power Electronics and Motion Control Conference (EPE/PEMC), pp. 1-8.

Peltoniemi P., Nuutinen P. and Pyrhönen J. (2012a). Tuning of the Load Adaptive Controller for DC/AC Converter in LVDC Power Distribution, IEEE Energy Conversion Congress and Exposition (ECCE), pp. 3795-3802.

Peltoniemi P., Nuutinen P., Pyrhönen J.(2013) Observer-based output voltage control for DC power distribution purposes, IEEE Trans. Power Electron. **28** (4):1914-1926.

Perso (2015) http://perso.uclouvain.be/ernest.matagne/ELEC2311/T2006/NOFP.pdf

Pysmian (2015)
http://fi.prysmiangroup.com/en/business_markets/markets/pd/downloads/datasheets/AXMK-PLUS_4joht.pdf

Radwan A. A. A. and Mohamed Y. A-R. I. (2012) Linear active stabilization of converter-dominated DC microgrids, IEEE Trans. Smart Grid, **3**(1):203-216.

Reed G.: DC technologies- solutions to electric power system advancements, IEEE Power and Energy Mag. **10**(6):10-17.

Rekola J., Jokipii J. and Suntio T. (2014). Losses of converters with iron and amorphous core AC-filter inductors in LVDC distribution, 40th Annual Conference of IEEE Industrial Electronics Society (IECON), pp.1587-1593.

Rekola J., Jokipii J. and Suntio T. (2014a). Effect of network configuration and load profile on efficiency of LVDC distribution network, 16th European Conference on Power Electronics and Applications (EPE'14-ECCE Europe), pp.1-10.

Rekola J. and Tuusa H. (2014b). Efficiency of converters and amorphous core AC-filters in an LVDC distribution, 29th Annual IEEE Applied Power Electronics Conference and Exposition (APEC), pp. 1827-1834.

Rekola J., Virtanen A., Jokipii J. and Tuusa H. (2012). Comparison of converter losses in an LVDC Distribution, 38th Annual Conference of IEEE Industrial Electronics Society (IECON), pp. 1240-1245.

Rekola J. and Tuusa H. (2011). Comparison of line and load converter topologies in a bipolar LVDC distribution, 14th European Conference on Power Electronics and Applications (EPE), pp. 1-10

Rekola J. and Tuusa H. (2011a). Comparison of load inverter topologies in a bipolar LVDC-distribution, International Conference on Renewable Energies and Power Quality (ICREPQ'11), pp.1-6.

Rivera S., Wu B., Kouro S., Yaramasu V. and Wang J. (2015) Electric vehicle charging station using a neutral point clamped converter with bipolar DC bus, IEEE Trans. Ind. Electron., vol. 62, pp. 1999-2009, April 2015

Rodriguez J., Bernet S., Steimer P. K. and Lizama I. E. (2010). A survey on neutral-point-clamped inverters, IEEE Trans. Ind. Electron., **57**(7):2219-2230.

Rodriguez J., Lai J-S., Peng F. Z. (2002). Multilevel inverters: a survey of topologies, controls and applications, IEEE Trans. Ind. Electron. **49**(4):724-738.

Roggia L., Rech C., Schuch L., Baggio J. E., Hey H. L. and Pinheiro J. R.(2011) Design of a sustainable residential microgrid system including PHEV and energy storage device, European Conference on Power Electronics and Applications (EPE), pp. 1-9.

Sannino A., Postiglione G. and Bollen M. H.J. (2003) Feasibility of a dc network for commercial facilities, IEEE Trans. Ind. Appl., **39**(5):1499-1507.

Sarker M. J., Asare-Bediako B., Slootweg J. G., Kling W.L. and Alipuria B. (2012). DC micro-grid with distributed generation for rural electrification, 47th International Universities Power Engineering Conference (UPEC), pp. 1-6.

Schneider D. (2008). Edison's final revenge, American Scientist **96**(2):107-108.

Schöner C., Derix D. and Hensel A. (2014). Comparison and evaluation of different three-level inverter topologies for PV systems, 16th European Conference on Power Electronics and Applications (EPE-ECCE Europe), pp. 1-10.

Shenai K. and Shah K. (2011). Smart DC micro-grid for efficient utilization of distributed renewable energy, IEEE Energytech, pp.1-6.

Semikron (2015) Application Note AN-11001 http://www.semikron.com/dl/service-support/downloads/download/semikron-application-note-an-11001-3l-npc-tnpc-topology-en

Semikron (2015a) SKM75GB063D Datasheet http://www.semikron.com/dl/service-support/downloads/download/semikron-datasheet-skm75gb063d-22890050

Semikron (2015b) SKM75GB123D Datasheet
http://www.semikron.com/download/assets/gecont/40.pdf

Semikron (2015c) SKM75GB176D Datasheet http://www.semikron.com/dl/service-support/downloads/download/semikron-datasheet-skm75gb176d-22890850

Semikron (2015d) SKKH27 Datasheet http://www.semikron.com/dl/service-support/downloads/download/semikron-datasheet-skkt-27-07897231

Semikron (2015e) SKKD40F Datasheet http://www.alldatasheet.com/datasheet-pdf/pdf/206285/SEMIKRON/SKKD40F.html

Semikron (2015f) SKM100MLI066T Datasheet http://www.semikron.com/dl/service-support/downloads/download/semikron-datasheet-sk-100-mli-066-t-24914470

Simanjorang R., Yamaguchi H., Ohashi H., Takeda T., Yamazaki M. and Murai H. (2010). A high output power density 400/400V isolated DC/DC converter with hybrid pair of SJ-MOSFET and SiC-SBD for power supply of data center, 25th Annual Applied Power Electronics Conference and Exposition (APEC), pp. 6487-653.

Staudt I., Wintrich A., Haddad K. and Cardi V. (2011) Numerical loss calculation and simulation tool for 3L NPC Converter design, International Exhibition & Conference for Power Electronics, Intelligent Motion and Power Quality (PCIM Europe), pp.483-488.

Steinmetz C. P. (1984). On the law of hysteresis. Proc. IEEE **72**(2):196-221.

Tan N. M. L., Abe T. and Akagi H. (2011). Topology and application of bidirectional isolated DC-DC converters, 8th IEEE International Conference on Power Electronics (ICPE & ECCE Asia), pp. 1039-1046.

Techakittiroj K. and Wongpaibool V. (2009). Co-existence between AC-distribution and DC-distibution: in the view of appliances, 2nd International Conference on Computer and Electrical Engineering (ICCEE), pp.421-425

Teichmann R. and Bernet S. (2005). A comparison of three-level converters versus two-level converters for low-voltage drives, traction, and utility applications, IEEE Trans. Ind. Appl. **41**(3):855-865.

Teodorescu R., Liserre M. and Rodriguez P. (2011). Grid Converters for Photovoltaic and Wind Power Systems, ISBN 9780470667057

von Jouanne A., Dai S. and Zhang H. (2001) A simple method for balancing the DC-link voltage of three-level inverters, IEEE 32nd Annual Power Electronics Specialists Conference (PESC), pp. 1341-1345.

Wang X., Blaabjerg F. and Wu W. (2014). Modeling and analysis of harmonic stability in an AC power-electronics-based power system, IEEE Trans. Power Electron., **29**(12):6421-6432.

Wang G., Wang F., Magai G., Lei Y., Huang A. and Das M. (2013). Performance comparison of 1200V 100A SiC MOSFET and 1200V 100A silicon IGBT, IEEE Energy Conversion Congress and Exposition (ECCE), pp. 3230-3234.

Wang H., Chung H. and Ioinovici A. (2012). A new concept of high-voltage DC-DC conversion using asymmetric voltage distribution on the switch pairs and hybrid ZVS-ZCS scheme, IEEE Trans. Power Electron. **27**(5):2242-2259.

Wang F., Duarte J. L., Hendrix M. A. M. and Ribeiro P. F. (2011). Modeling and analysis of grid harmonic distortion impact of aggregated DG inverters, IEEE Trans. Power Electron. **26**(3):786-797.

Wang H., Chung H. and Ioinovici A. (2011a). A class of high-input low-output voltage single-step converters with low voltage stress on the primary side switches and high output current capacity, IEEE Trans. Power Electron. **26**(6):1659-1672.

Wang Y., Xing W., Zhang G., Niu W. and Han D. (2010) Experimental study of testing models for low noise amorphous alloy core power transformers, International Conference on Electrical and Control Engineeering (ICECE), pp. 3725-3728.

Wang F., Pei Y., Boroyevich D., Burgos R. and Ngo K. (2008) Ac vs. Dc Distribution for Off-Shore Power Delivery, 34th Annual Conference of IEEE Industial Electronics (IECON), pp. 2113-2118.

Wang Q., Chen Q., Jiang W., Hu C. (2007). Analysis and comparison of conduction losses in neutral-point-clamped three-level inverter with pwm control, International Conference on Electrical Machines and Systems (ICEMS), pp. 143-148.

Wang T., Ye Z., Sinha G. and Yuan X. (2003). Output filter design for a grid-interconnected three-phase inverter, IEEE 34th Annual Power Electronics Specialists Conference (PESC), pp. 779-784.

Wang F. (2002). Sine-triangle versus space-vector modulation for three-level PWM voltage-source inverters, IEEE Trans. Ind. Appl., **38**(2):500-506.

Wei X., Xiao L., Yao Z. and Gong C. (2010). Design of LCL filter for wind power inverter, World Non-Grid-Connected Wind Power and Energy Conference (WNWEC), pp.1-6.

Vincotech (2015) 10-F106NIA100SA-M135F Datasheet
http://www.vincotech.com/uploads/tx_st9products/10-xx06NIA100SA-M135Fxx-D3-14.pdf

Virtanen A. and Tuusa H. (2012). Performance comparison of conventional STATCOM and STATCOM with energy storage in a low voltage induction motor application, IEEE Energy Conversion Congress and Exposition (ECCE), pp. 4719-4726.

Virtanen A., Jokipii J., Rekola J. and Tuusa H. (2013). Influence of network voltage level, converter topology and integration of energy storage on the power losses of STATCOM devices, 28th Annual IEEE Applied Power Electronics Conference and Exposition (APEC), pp. 1615-1622.

Xiao C., Chen G. and Odendaal W. (2007) Overview of power loss measurement techniques in power electronic systems, IEEE Trans. Ind. Appl. **43**(3):657-664.

Xu L., Williams B.W. and Yao L. (2008). Multi-terminal DC transmission systems for connecting large offshore wind farms, IEEE Power and Energy Society General Meeting – conversion and delivery of electrical energy in the 21st century, pp. 1-7.

Xu L. and Chen D. (2011). Control and operation of a DC Microgrid with variable generation and energy storage, IEEE Trans. Power Del. **26**(4): 2513-2522.

Yuan C., Haj-Ahmed M. A. and Illindala M. S. (2014) An MVDC microgrid for a remote area mine site: protection, operation and control, IEEE Industry Applications Society Annual Meeting, pp.1-9.

Zhang L., Sun K., Xing Y., Feng L. and Ge H. (2011). A modular grid-connected photovoltaic generation system based on DC bus, IEEE Trans. Power Electron. **26**(2): 523-531.

Zhang X., Gong C. and Yao Z. (2015). Three-level DC converter for balancing DC 800-V voltage, IEEE Trans. Power Electron. **30**(7):3499-3507.

# APPENDIX A: Laboratory setup

The laboratory LVDC distribution network prototype consists of two tree-level, three-phase, four-wire converters and 200 m long AXMK 4*16mm² underground cable connected between these as shown in Fig. A.1. SKM 75GB123D IGBT-modules and SKKD 40F10 diode modules as clamping diodes are used. The nominal power of the converters is 10 kVA. The converters use space vector modulation with the modulation frequency of 10 kHz. The LCL-filter is connected in front of the grid converter and LC-filter after the customer converter. Size of the electrolytic DC-capacitors in both converters and in both halves of the DC link is 1100 μF. The balancing circuit is added to the grid converter and the balancing inductance value is 5 mH.

The control of the converters is implemented on Freescale's 32-bit MPC563MZP66 microcontrollers. The microcontroller board contains current and voltage measurements, overcurrent and overvoltage protection and logic circuits to create the modulation signals. LEM LA55-P current transformers are used in the current measurements. The control of the IGBTs is realized by Concept SCALE control circuits. The microcontroller is controlled through RS-232 series cable from the computer.

The DC voltages, converter side inductor currents and grid voltages are measured to control the grid converter. The startup of the grid converter is realized by using charging resistors and the converter operates as a diode bridge to charge the DC capacitors without high current spikes. The final value of the DC voltage is peak-to-peak value of the grid phase voltage (650 VDC) if the neutral-wire is connected hence the converter operates as a four-wire converter. If the neutral conductor is not connected, the final DC voltage value is the peak value of the main grid voltage (565 VDC).

The current measurement equipment includes Tektronix AM503B current amplifiers with A6312 current probes, and all voltages are measured with Tektronix P5200 high voltage differential probes. The measured current and voltage waveforms are sampled and stored with a LeCroy LC334AM 500 MHz digital oscilloscope. The measured data is filtered using a seventh-order Butterworth digital filter with a cut-off frequency of 25 kHz.

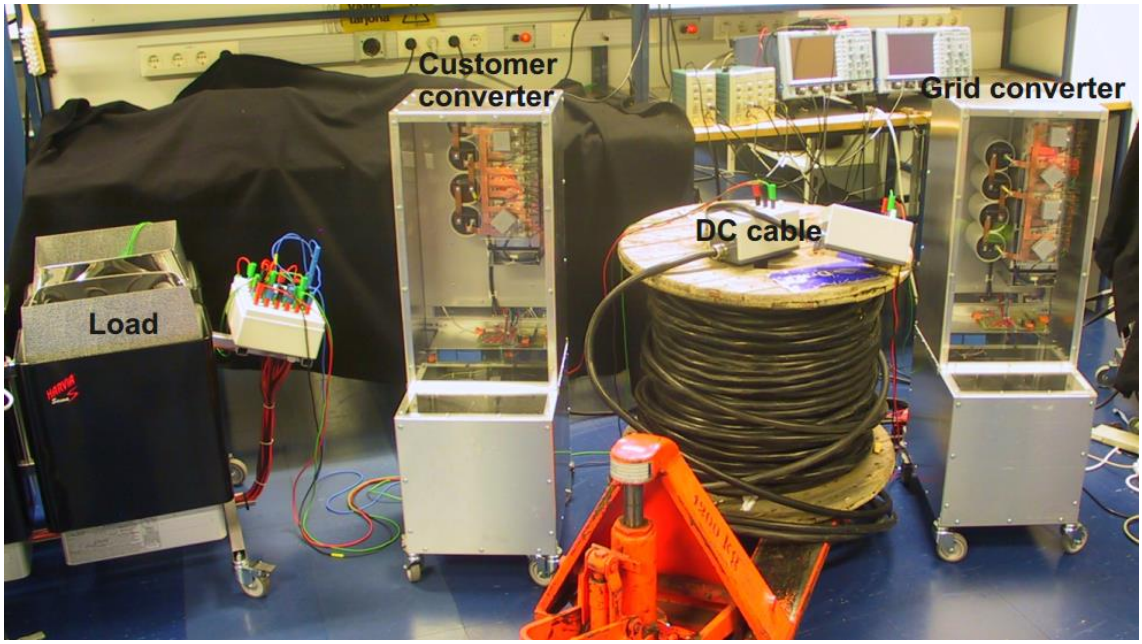


**Fig. A.1.** Laboratory prototype DC network

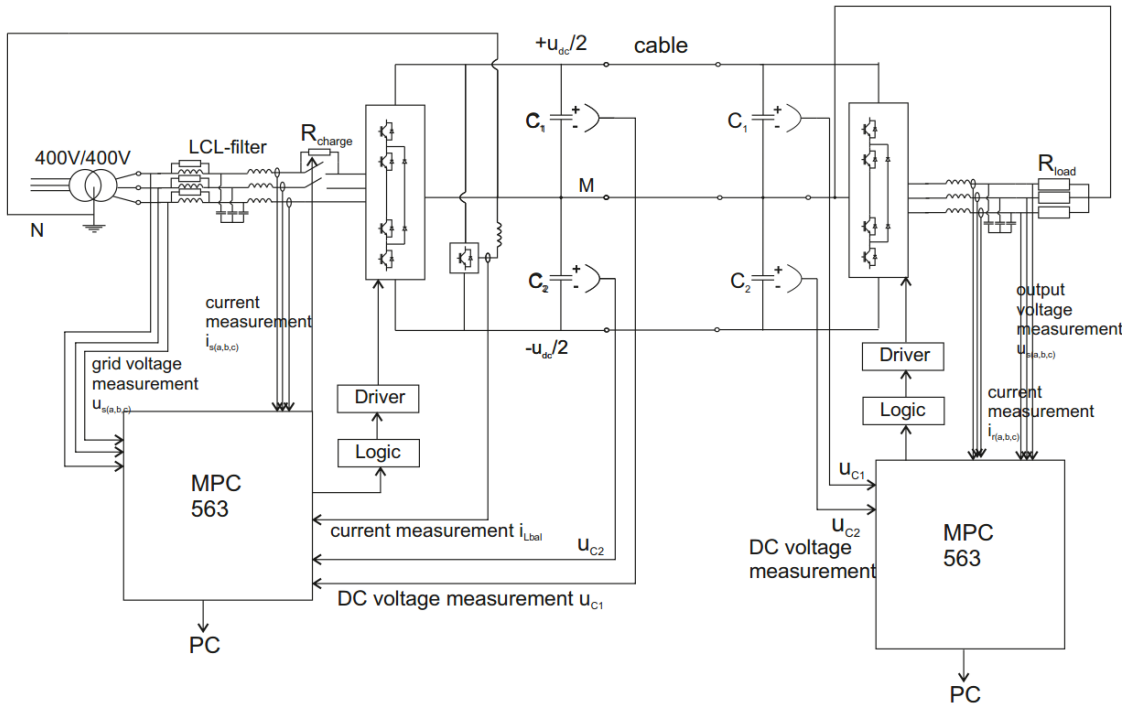


**Fig. A.2.** The circuit schematic of the DC network prototype

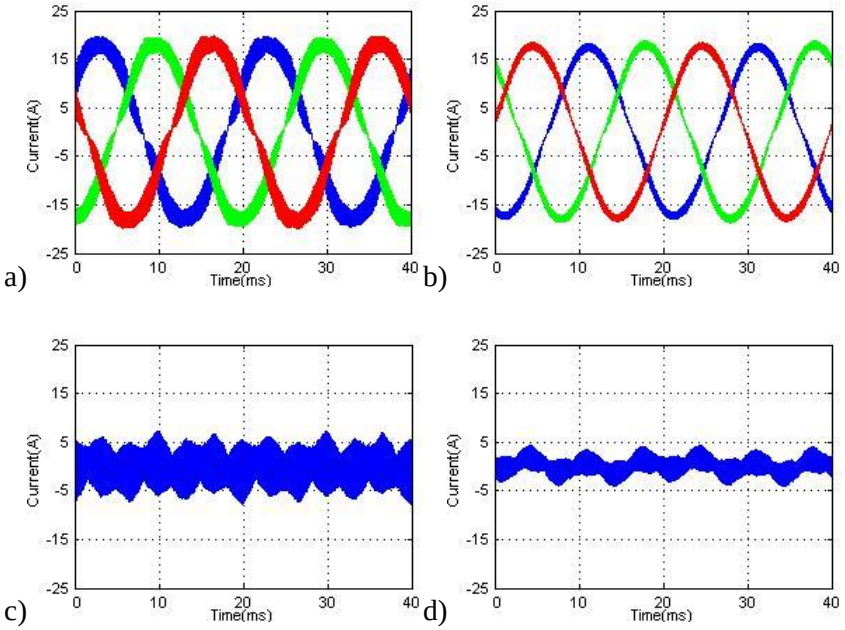


**Fig. A.3.** a) $L_{conv}$ currents in front of the grid converter, b) $L_{cust}$ currents after the customer converter, c) neutral wire current at customer converter and d) neutral wire current at grid converter with 10 kW resistive load in the grounded DC grid

# APPENDIX B: Power loss measurement setup

The power losses of the AC filters are measured by using the air-cooled open type balance calorimeter. Calorimetric method is based on direct loss measurement calculated from the generated heat and it is independent of electrical quantities of the device under test. Therefore, calorimetric methods are considered the most accurate power loss measurement techniques because the current or voltage harmonics generated by the device under test do not affect to the results unlike in the electrical measurements (Xiao et al., 2007). Accurate controls of the airflow, the temperature and the humidity are required during the whole test (Xiao et al., 2007). The drawback of the calorimetric measurements is that these are very time consuming.

The air-cooled open type balance calorimeter is presented in Fig. B.1a and the operational principle is illustrated in Fig. B.1b. A calorimeter is thermally insulated container used to measure power losses of electrical devices. The open-type calorimeter exchanges heat directly with the surrounding air. The calorimeter consists of a 200 mm thick aluminium coated polyurethane measurement chamber, two temperature transducers for measuring the inside and outside temperatures, a DC fan in the outlet and an air mass flew sensor in the inlet. The heat producing element is located in a thermally insulated container.

During the calorimeter use and calibration, a constant air flow was forced through the case by a fan, hence the output air mass flow $m_{air,o}$ is equal with the input air mass flow $m_{air,i}$, measured with the air mass flew sensor. The system is in operation until the temperature difference $T_{out}$-$T_{in}$ becomes steady. The temperature rise indicates the total power losses of the device if the heat is completely absorbed by air. The total power loss $P_{loss}$ can be calculated as follows

$$P_{loss} = m_{air,i} \cdot (T_{out} - T_{in}) \cdot c_{air} + P_{case} \quad \text{(B.1)}$$

where $c_{air}$ is the thermal capacity of the air ($c_{air}$ = 1.005 kJ/kgK) and $P_{case}$ is the conductive heat power leak through the case, which is determined with the calibration measurements (Xiao et al., 2007).

Power losses are determined in two steps namely, a main test and a calibration test. Prior to the actual measurements, the calorimeter is calibrated with known electrical power supplied to a heat resistor. The calorimeter degree of filling and the distribution of air flow and temperature have an effect on the calorimeter performance. Thus, two different calibration measurements are needed because the size of the LCL- and LC-filter boxes differs from each other. The resulting calibration curves for filters are presented in Fig. B.2. The equations for the calibration curves are B.2 and B.3.

$$P_{loss,LC-filter} = 13.96 \cdot (T_{out} - T_{in}) - 7.267(W) \quad \text{(B.2)}$$

$$P_{loss,LCL-filter} = 11.44 \cdot (T_{out} - T_{in}) - 20.65(W) \quad \text{(B.3)}$$

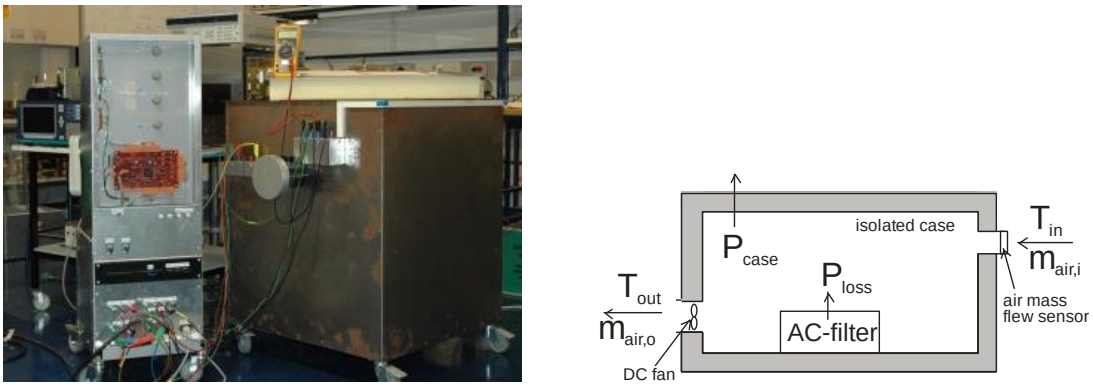


a) b)

**Fig. B.1.** a) Open-type balance calorimeter and b) operation principle of the calorimeter

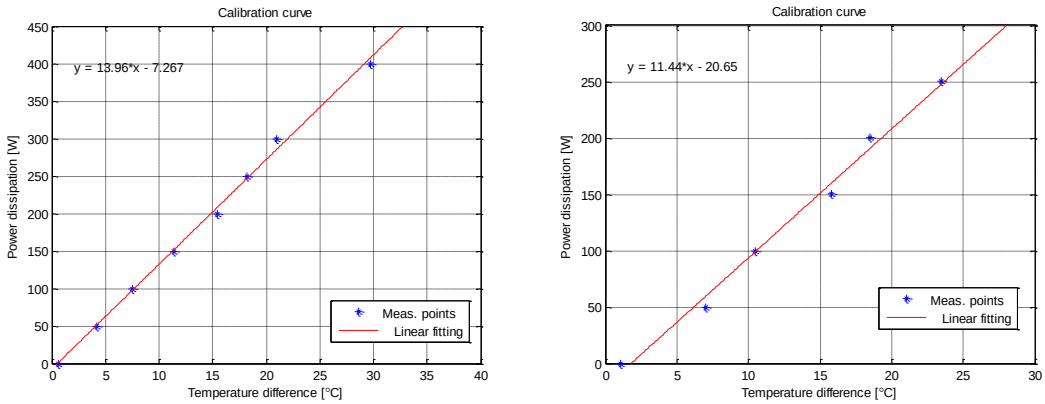


**Fig. B.2.** The calibration curves of a) LC-filter and b) LCL-filter

The electrical measurements are used in the converter power loss analysis. The losses of the converters were measured using two power analyzers: Yokogawa WT1030 digital power meter which can measure frequencies up to 500 kHz and LEM Norma D6100 wideband power analyzer which can measure frequencies up to 1 MHz. The power losses of the converters are defined as

$$P_{loss,conv} = P_s - P_l - P_{loss,filt} \quad \text{(B.4)}$$

where $P_s$ is the supplied power, $P_l$ is the power fed to the load, $P_{loss,filt}$ are the AC filter power losses and $P_{loss,conv}$ are the power loss of the converter.

# APPENDIX C: Simulated and measured voltage and current harmonics

The THD of the measured and simulated customer converter LC-filter inductor current and customer load voltage with resistive loads 2.5 kW, 5 kW, 7.5 kW and 10 kW are calculated up to 25 kHz and presented in Tables C.1-4. The measured and simulated current of the grid converter LCL-filter inductor $L_{conv}$ and grid current are shown in Table C.5. The measured current and voltage waveforms are sampled and stored with a digital oscilloscope and filtered using a seventh order Butterworth digital filter with a cutoff frequency of 25 kHz. The measurements are done by using the laboratory prototype presented in Appendix A. The used AC-filter inductors are presented in Table 3.1.

**Table C.1.** Customer converter with 2.5 kW resistive load

| AC-filter | Measured THD of $i_L$ [%] | Simulated THD of $i_L$ [%] | Measured THD of $u_{load}$ [%] | Simulated THD of $u_{load}$ [%] |
|---|---|---|---|---|
| 1 | 18.0 | 18.0 | 3.9 | 1.6 |
| 1N | 40.1 | 42.7 | 4.2 | 4.0 |
| 2 | 16.9 | 17.4 | 1.6 | 0.9 |
| 2N | 38.9 | 41.0 | 2.7 | 2.0 |
| 3 | 23.2 | 23.4 | 1.9 | 1.1 |
| 3N | 51.5 | 53.7 | 3.1 | 2.6 |
| 4N | 27.1 | 29.6 | 2.5 | 1.5 |
| 5 | 39.6 | 40.0 | 2.2 | 1.7 |
| 5N | 92.5 | 100.5 | 4.1 | 4.9 |
| 6N | 41.6 | 39.0 | 2.4 | 1.9 |

**Table C.2.** Customer converter with 5 kW resistive load

| AC-filter | Measured THD of $i_L$ [%] | Simulated THD of $i_L$ [%] | Measured THD of $u_{load}$ [%] | Simulated THD of $u_{load}$ [%] |
|---|---|---|---|---|
| 1 | 9.1 | 9.0 | 2.7 | 1.5 |
| 1N | 25.3 | 21.0 | 4.6 | 3.9 |
| 2 | 8.8 | 8.8 | 1.8 | 0.9 |
| 2N | 19.6 | 20.3 | 3.3 | 2.0 |
| 3 | 12.0 | 11.8 | 2.2 | 1.1 |
| 3N | 26.3 | 26.8 | 3.7 | 2.6 |
| 4N | 14.5 | 14.8 | 3.2 | 1.5 |
| 5 | 20.4 | 19.9 | 2.4 | 1.8 |
| 5N | 48.7 | 51.4 | 4.3 | 4.8 |
| 6N | 19.5 | 19.3 | 2.8 | 1.9 |

**Table C.3.** Customer converter with 7.5 kW resistive load

| AC-filter | Measured THD of $i_L$ [%] | Simulated THD of $i_L$ [%] | Measured THD of $u_{load}$ [%] | Simulated THD of $u_{load}$ [%] |
|---|---|---|---|---|
| 1 | 5.9 | 6.0 | 2.4 | 1.5 |
| 1N | 13.1 | 14.0 | 4.8 | 3.9 |
| 2 | 5.7 | 5.9 | 1.8 | 0.9 |
| 2N | 12.5 | 13.6 | 3.4 | 2.0 |
| 3 | 7.9 | 7.9 | 2.2 | 1.1 |
| 3N | 16.4 | 17.8 | 3.9 | 2.6 |
| 4N | 9.4 | 9.9 | 2.9 | 1.6 |
| 5 | 12.6 | 13.3 | 2.4 | 1.7 |
| 5N | 31.7 | 34.3 | 4.8 | 4.8 |
| 6N | 12.9 | 12.9 | 3.0 | 1.9 |

**Table C.4.** Customer converter with 10 kW resistive load

| AC-filter | Simulated THD of $i_L$ [%] | Simulated THD of $u_{load}$ [%] |
|---|---|---|
| 1 | 4.5 | 1.5 |
| 1N | 10.5 | 3.8 |
| 2 | 4.4 | 0.9 |
| 2N | 10.2 | 2.1 |
| 3 | 5.9 | 1.1 |
| 3N | 13.4 | 2.6 |
| 4N | 7.4 | 1.6 |
| 5 | 10.9 | 1.9 |
| 5N | 27.9 | 5.3 |
| 6N | 9.7 | 2.0 |

**Table C.5.** Grid converter

| Load | LCL-filter | Measured THD of $i_{Lconv}$ [%] | Simulated THD of $i_{Lconv}$ [%] | Measured THD of $i_{grid}$ [%] | Simulated THD of $i_{grid}$ [%] |
|---|---|---|---|---|---|
| 2.5 kW | 7 | 13.4 | 15.9 | 4.5 | 2.5 |
| | 8 | 19.9 | 22.1 | 7.0 | 3.8 |
| 5 kW | 7 | 7.9 | 8.0 | 4.6 | 1.3 |
| | 8 | 10.5 | 11.2 | 3.9 | 2.2 |
| 7.5 kW | 7 | 6.4 | 5.4 | 4.2 | 1.1 |
| | 8 | 8.5 | 7.6 | 3.7 | 1.8 |
| 10 kW | 7 | 5.4 | 4.0 | 3.9 | 0.8 |
| | 8 | | 5.8 | | 1.8 |

# APPENDIX D: Base values

The base values of the converters are shown in Table D.1. The fundamental frequency is 50 Hz.

**Table D.1.** The base values of the converters

| | Grid converter | Grid converter | Grid converter | 12-pulse thyristor bridge | Customer converter | Customer converter |
|---|---|---|---|---|---|---|
| Voltage $U_{dc}$ [V] | 750 | 1500 | 1500 | 1500 | 750 | 1500 |
| Voltage $U_{LL}$ [V] | 400 | 800 | 800 | 562 | 400 | 400 |
| Power $S_N = 3U_N I_B$ [kVA] | 10 | 10 | 20 | 10 | 10 | 10 |
| Impedance $Z_B = U_{LL}^2/S_N$ [Ω] | 32 | 64 | 32 | 63 | 16 | 16 |
| Capacitance $C_B = 1/Z_B\omega_B$ [μF] | 100 | 50 | 100 | 50 | 200 | 200 |
| Inductance $L_B = Z_B/\omega_B$ [mH] | 102 | 204 | 102 | 201 | 51 | 51 |

# APPENDIX E: Required AC filter parameters depending on the design method

The required inductance and capacitance values of LC-filter according to multiple different design methods are calculated for three-level single-phase full-bridge customer converter with unipolar modulation (Fig. E.1) and for three-level three-phase customer converter (Fig. E.2). THD of $u_{load} \leq 2\%$ calculated up to 25 kHz. The nominal power of converters is supposed to be 3.3 kVA/phase. The modulation frequency is 10 kHz. The converters are connected to 750 VDC and these produces 230 VAC rms phase voltage to the customer. The DC network is ungrounded.

The required inductance and capacitance values of LCL-filter according to multiple different design methods are calculated for three-level NPC grid converter and shown in Fig. E.3. The same filter can be used also with the Vienna rectifier. THD of $i_{grid} \leq 2\%$ calculated up to 25 kHz. The nominal power of the converter is supposed to be 10 kVA. The modulation frequency is 10 kHz and the converter produces 750 V DC. The current THD of the converter side inductor $L_{conv}$ is not possible to increase from 14 % in the LCL-filter design of the grid converter. Otherwise the grid current THD is not possible to keep ≤ 2 % when the capacitance value is limited to 5 % of $C_b$.

The capacitance value of the LCL-filter in front of the grid converter would be increased from $0.05*C_b$ to $0.1*C_b$ without too large capacitive current power losses. The required LCL-filter inductance values for the grid converters, which nominal power is 10 kVA are shown in Fig. E.4. The same filter inductor can be used with three-level NPC grid converter and with Vienna rectifier.

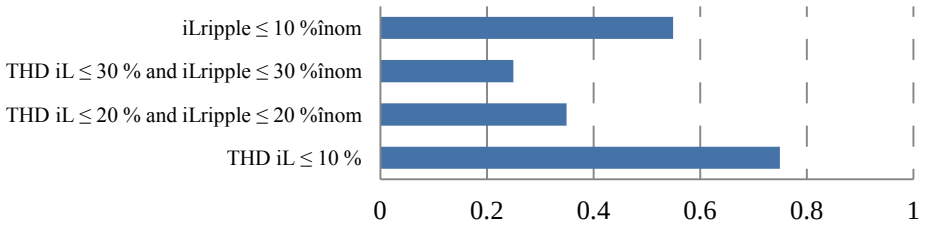


| | THD iL ≤ 10 % | THD iL ≤ 20 % and iLripple ≤ 20 %înom | THD iL ≤ 30 % and iLripple ≤ 30 %înom | iLripple ≤ 10 %înom |
|---|---|---|---|---|
| L [mH] | 0.75 | 0.35 | 0.25 | 0.55 |
| L [pu %] | 1.5 | 0.7 | 0.5 | 1 |
| C [µF] | 3 | 5 | 7 | 3 |
| C[pu %] | 1.5 | 2.5 | 3.5 | 1.5 |
| fres [kHz] | 3.3 | 3.8 | 3.8 | 3.9 |
| îripple [%] | 7.4 | 16 | 27 | 10 |
| THD iL [%] | 10 | 20 | 29 | 13 |

**Fig. E.1.** Required AC-filter parameters for three-level single-phase full bridge

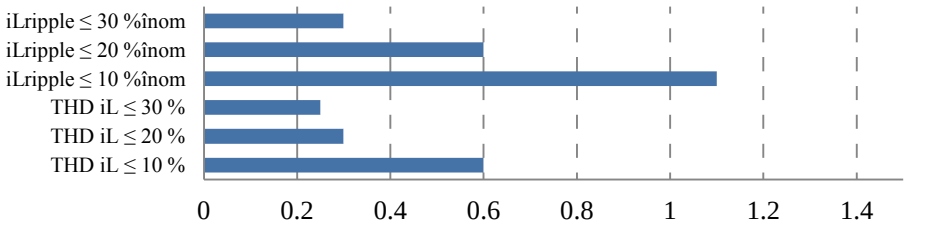


| | THD iL ≤ 10 % | THD iL ≤ 20 % | THD iL ≤ 30 % | iLripple ≤ 10 %înom | iLripple ≤ 20 %înom | iLripple ≤ 30 %înom |
|---|---|---|---|---|---|---|
| L [mH] | 0.6 | 0.3 | 0.25 | 1.1 | 0.6 | 0.3 |
| L [pu %] | 1 | 0.6 | 0.5 | 2 | 1 | 0.6 |
| C [µF] | 4 | 9 | 10 | 3 | 4 | 7 |
| C[pu %] | 2 | 5 | 5 | 1.5 | 2 | 3.5 |
| fres [kHz] | 3.2 | 3.1 | 3.2 | 2.8 | 3.2 | 4.9 |
| îripple [%] | 20 | 38 | 48 | 10 | 20 | 30 |
| THD iL [%] | 10 | 20 | 24 | 5 | 10 | 15 |

**Fig. E.2.** Required AC-filter parameters for three-level three-phase customer converter

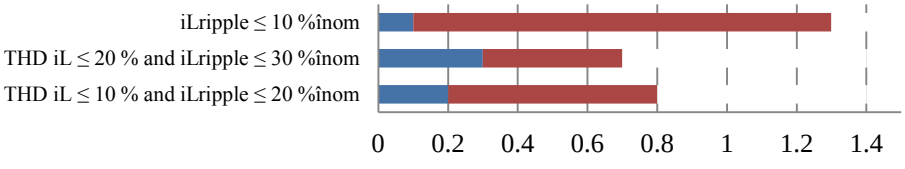


| | THD iL ≤ 10 % and iLripple ≤ 20 %înom | THD iL ≤ 20 % and iLripple ≤ 30 %înom | iLripple ≤ 10 %înom |
|---|---|---|---|
| Lgrid [mH] | 0.2 | 0.3 | 0.1 |
| Lconv [mH] | 0.6 | 0.4 | 1.2 |
| Lconv [pu %] | 0.6 | 0.4 | 1.2 |
| Lgrid [pu %] | 0.2 | 0.3 | 0.1 |
| C [µF] | 10 | 10 | 10 |
| C[pu %] | 10 | 10 | 10 |
| fres [kHz] | 4.1 | 3.8 | 5.2 |
| îripple [%] | 18 | 27 | 9 |
| THD iL [%] | 10 | 14 | 5 |

**Fig. E.3** Required LCL-filter parameters for three-level NPC grid converter and Vienna rectifier

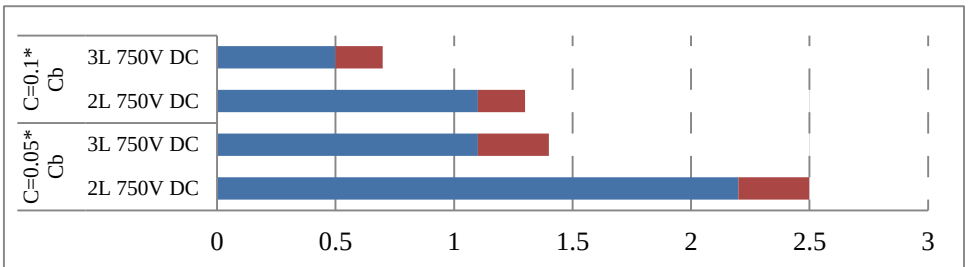


| | C=0.05*Cb | | C=0.1* Cb | |
|---|---|---|---|---|
| | 2L 750V DC | 3L 750V DC | 2L 750V DC | 3L 750V DC |
| Lconv[mH] | 2.2 | 1.1 | 1.1 | 0.5 |
| Lgrid [mH] | 0.3 | 0.3 | 0.2 | 0.2 |
| Lconv [pu %] | 2.3 | 1.1 | 1 | 0.5 |
| Lgrid[pu %] | 0.3 | 0.3 | 0.2 | 0.2 |
| Cgrid [µF] | 5 | 5 | 10 | 10 |
| Cgrid [pu %] | 5 | 5 | 10 | 10 |
| fres [kHz] | 4.3 | 4.9 | 4.4 | 4.8 |

**Fig. E.4.** Required LCL-filter parameters when $C = 5\%*C_b$ and $C = 10\%*C_b$ for two- and three-level grid converters

Tampereen teknillinen yliopisto
PL 527
33101 Tampere

Tampere University of Technology
P.O.B. 527
FI-33101 Tampere, Finland

ISBN 978-952-15-3606-9
ISSN 1459-2045